The role of Nrf2 in skeletal muscle phenotype and mitochondrial function

Matthew J. Crilly

A thesis submitted to the Faculty of Graduate Studies in partial fulfillment of the requirements for the degree of

Master of Science

Graduate Program in Kinesiology and Health Science

York University
Toronto, Ontario, Canada

December 2015

Abstract

Nuclear erythroid 2 p45-related factor 2 (Nrf2) is a master regulator of oxidative defence, by controlling the expression of a battery of antioxidant enzyme proteins during stressful stimuli. Although Nrf2 is widely expressed, its role in regulating skeletal muscle phenotype remains to be elucidated. We sought to investigate the impact of Nrf2 on exercise-induced mitochondrial adaptations and aging using wild-type (WT) and knockout (KO) mice at 3 and 12 months of age. Basally, our results indicate that Nrf2 is important for mitochondrial respiration and skeletal muscle performance. Although Nrf2 did not impact mitochondrial content under quiescent conditions, it was necessary for mitochondrial content adaptations that occur in response to training. However, we also showed that exercise was capable of rescuing the initial deficits in respiration and muscle performance in animals lacking Nrf2, highlighting the broad cellular signaling benefits of exercise training beneficial effects of exercise training.

Acknowledgements

I would like to express my special appreciation and thanks to my supervisor Dr. David Hood. Your guidance and mentorship facilitated my growth and development, allowing me to step outside of my comfort zone and successfully complete the work herein. For that, I am forever grateful. Of course, this work was also made possible thanks to the love and support from a huge cast of family and friends. I truly consider myself lucky to have each and every one of you in my life. Thank you.

Table of Contents

List of Tables

Chapter 2: Manuscript

Appendix A: Data Tables and Statistical Analysis

List of Figures

List of Abbreviations

ADP	Adenosine diphosphate
AMP	Adenosine monophosphate
AMPK	AMP-activated protein kinase
ANOVA	Analysis of Variance
ARE	Antioxidant Response Element
ATP	Adenosine triphosphate
BACH1	BTB and CNC homology 1, basic leucine zipper transcription factor 1
BTB	Broad complex, tramtrack, bric-a-brac
C. elegans	Caenorhabditis elegans
Ca^{2+}	Calcium
CBP	CREB-binding protein
CCA	Chronic contractile activity
CLK1	CDC-Like Kinase 1
CNC	Cap 'n' Collar
CO	Carbon monoxide
Complex III	Cytochrome bc1
CoQ	Coenzyme Q
COX	Cytochrome Oxidase
COXI/ IV	Cytochrome Oxidase I/ IV
CS	Citrate synthase
CUL3	Cullin-3
Cyt c	Cytochrome c
DAF-16	FOXO orthologue
daf-2	IGF-1 orthologue
DNA	Deoxyribonucleic acid
Drp1	Dynamin-related protein 1
eIF-3f	eukaryotic translation initiation factor 3, subunit f
ETC	Electron Transport Chain
FOXO3	Forkhead Box O3
G6PD	Glucose-6-Phosphate Dehydrogenase
GFP	Green Fluorescent Protein
GPx1/ 4/ 5	Glutathione Peroxidase 1/4/5
GSH	Glutathione
H_2O_2	Hydrogen Peroxide
HO-1	Heme Oxygenase-1
HRP	Horseradish Peroxidase
IMF	Intermyofibrillar
IMM	Inner mitochondrial membrane
$\Delta\Psi$	Membrane Potential
JNK	c-Jun N-terminal Kinase
K^+	Potassium

Keap1	Kelch-like ECH-associated protein 1
KO	Knockout
LC3	Microtubule-associated protein light chain 3
MAFbx	Atrogin-1
Mfn1/-2	Mitofusin 1/ -2
MHC	Myosin Heavy Chain
MnSOD	Manganese Superoxide Dismutase
Prx3/ 5	Peroxiredoxin 3/ 5
RNA	Ribonucleic Acid
mRNA	messenger RNA
mtDNA	Mitochondrial DNA
MuRF1	Muscle RING-finger protein 1
MyoD	Myogenic Differentiation 1
Na^+	Sodium
NADH	Nicotinamide Adenine Dinucleotide
NADH dehydrogenase	Complex I
NADPH	Nicotinamide Adenine Dinucleotide Phosphate
Neh1-7	Nrf2-ECH homology 1-7
NF-κB	Nuclear Factor-kappa B
NLS	Nuclear Localization Signal
NES	Nuclear Exporting Signal
NQO1	NADPH quinone oxidoreductase 1
NRF-1/-2	Nuclear Respiratory Factor-1/ -2
Nrf2	Nuclear erythroid 2 p45-related factor 2
NUGEMPS	Nuclear Genes Encoding Mitochondrial Proteins
OMM	Outer Mitochondrial Membrane
OPA1	Optic Atrophy 1
p38	p38 mitogen-activated protein kinase
p53	Tumor Suppressor protein 53
p62/SQSTM1	p62/ Sequestosome 1
PGC-1α	Peroxisome proliferator-activated receptor gamma coactivator 1-alpha
PINK1	PTEN-induced kinase 1
ROS	Reactive Oxygen Species
Runx1	Runt-related transcription factor 1
SDH	Succinate Dehydrogenase
SDS-PAGE	Sodium Dodecyl Sulfate Polyacrylamide Gel Electrophoresis
SOD2	Superoxide Dismutase 2
SS	Subsarcolemmal
Tfam	Mitochondrial transcription factor A
TPS	Trains Per Second

TRAF6	TNF receptor-associated factor 6
Trx	Thioredoxin
UCP2/-3	Uncoupling Protein 2/ -3
UPS	Ubiquitin Proteasome System
WT	Wild-type

Chapter 1: Review of Literature

1.1.0 Skeletal muscle structure and function

In humans, muscle comprises the largest group of tissues in the body, accounting for approximately half of the body's weight. Skeletal muscle alone comprises ~40% of body weight with smooth and cardiac muscle making up the other 10% of the total weight. Since skeletal muscle accounts for such a large proportion of total body mass it is not surprising that it has a significant contribution to several bodily functions. From a mechanical point of view, the primary function of skeletal muscle is to convert chemical energy, in the form of adenosine triphosphate (ATP), into mechanical energy to generate force, maintain posture and produce movement. From a metabolic perspective, skeletal muscle is essential for energy storage, maintenance of blood glucose homeostasis, fatty acid oxidation and temperature regulation.

The architecture of skeletal muscle is characterized by a very particular and quite sophisticated arrangement of muscle fibres. Each individual muscle fibre is comprised of specialized contractile elements called myofibrils. Furthermore, each myofibril consists of a regular arrangement of highly organized cytoskeletal elements – the thick filament, myosin and the thin filament, actin. Despite its unique shape and organization, muscle contains many of the same organelles that are present in other cell types. However, there is heterogeneity in human skeletal muscle that is characterized by differences in the biochemical, mechanical and metabolic phenotypes of individual fibres. The most frequently used classification system includes three fibre types: type I (slow, oxidative, fatigue-resistant), type IIA (fast, oxidative, intermediate metabolic properties) and type IId/x (fastest, glycolytic, fatigable) (123). The oxidative capacity of a fibre is determined by the number of mitochondria, the number of capillaries and the amount of myoglobin it

contains. Whereas the oxidative capacity of the muscle coincides with the metabolic profile of the muscle fibre, the maximum velocity of muscle shortening (fast vs. slow) is dependent on the type of myosin heavy chain (MHC) ATPase isoform it possesses (123).

A unique feature of skeletal muscle fibres is that they are multinucleated. In general, each nucleus within a muscle fibre controls the type of proteins synthesized within a specific region of the cell. These regions are commonly referred to as nuclear domains, which are highly regulated but not constant in size (6, 138). Furthermore, since skeletal muscle is a post-mitotic tissue it cannot be replicated by mitosis when destroyed or injured. As such, skeletal muscle contains a group of myogenic precursor cells, called satellite cells. These cells reside between the sarcolemma and the basal lamina and contribute to muscle growth, repair and regeneration (93, 151).

1.1.1 Skeletal muscle plasticity and adaptation

Skeletal muscle is a highly malleable tissue exhibiting remarkable capabilities in its ability to adapt to a number of physiological and pathological conditions. For instance, changes in contractile activity induced by alterations in physical activity, muscle disuse or aging can have a pronounced effect on the metabolic and morphological characteristics of the muscle.

Exercise is a potent stimulus and powerful metabolic stressor. Each bout of exercise initiates signaling events that alter the expression of a variety of nuclear DNA and mitochondrial DNA (mtDNA) gene products, resulting in phenotypic adaptations. One of the most dramatic examples of this phenotypic adaptation is the increase in mitochondrial volume, which coincides with fatigue-resistance and improvements in endurance performance. However, muscle responds to exercise in a training-specific

manner. That is, endurance training leads to an increase in oxidative capacity, which is mediated by expansion of the mitochondrial reticulum (181), whereas, resistance training induces the hypertrophy of muscle fibres to enhance force production (125).

In contrast to the beneficial effects elicited with exercise, chronic muscle disuse results in marked reductions in mitochondrial content (2, 156) and muscle mass (2, 156). Muscle wasting of this nature is largely due to accelerated protein degradation with concomitant reductions in protein synthesis (124). Although it has been demonstrated that disuse atrophy is largely mediated by the proteasomal (28, 184) and lysosomal systems (95), there is also evidence to suggest that apoptosis (2) is another contributing factor. Similarly, atrophy is also a defining feature of aging skeletal muscle that contributes to progressive weakness and increased frailty. Additionally, aging also provokes phenotypic changes in mitochondria, which are attributed to both inactivity and inherent, aging-induced changes in mitochondrial synthesis and degradation pathways.

1.1.1.1 Mitochondrial biogenesis

Mitochondrial adaptations that occur in response to exercise training are commonly referred to as “mitochondrial biogenesis”. This process is typically characterized by an increase in mitochondrial content and alterations to the mitochondrial ultrastructure. Although this phenomenon has long been established (52) the regulatory mechanisms governing this process have only recently been investigated. For instance, a current study utilizing a model of chronic contractile activity (CCA) demonstrated significant increases in the mitochondrial fusion proteins, Mfn2 and OPA1, with concomitant reductions in Drp1, a critical protein involved in mitochondrial fission (60). Furthermore, there is evidence to suggest that signaling events promoting mitochondrial

remodelling are one of the earliest events to occur in response to an acute bout of exercise. For instance, it was shown that a single bout of exercise promoted an increase in the membrane interactions between skeletal muscle mitochondria in both the subsarcolemmal (SS) and intermyofibrillar (IMF) subfractions (127). Additionally, Cartoni et al. (20) revealed that the mRNA expression of Mfn1 and Mfn2 were significantly increased 24 hours following an acute bout of exercise. Collectively, these results provide a molecular basis for the observed changes in mitochondrial morphology and indicate that these alterations are likely initiated following a single bout of exercise.

Although mitochondrial biogenesis begins with the putative signaling brought about by acute muscle contractions, the final phenotypic adaptation is the cumulative result of a complex series of molecular events. These include signaling events to initiate biogenesis, the transcription of nuclear and mitochondrial genes, the import of nuclear genes into the mitochondria and the assembly of proteins into functional multi-subunit complexes (55).

1.1.1.1.1 PGC-1α

Peroxisome proliferator-activated receptor gamma coactivator 1-alpha (PGC-1α) is a transcriptional coactivator that is often regarded as the most significant regulator of mitochondrial biogenesis and function. Evidence for this has been supported by gain of function experiments in both cultured cells (170, 180) and transgenic mice (84). Since PGC-1α is a transcriptional coactivator, it lacks the capacity to bind nuclear DNA directly. Rather, it functions by augmenting the activity of transcription factors, such as nuclear respiratory factors 1/2 (NRF-1 and NRF-2) (146, 180), and facilitating the recruitment of histone-modifying proteins. This in turn, allows for greater accessibility of

the transcriptional machinery to DNA for transcription (174). Coactivation of NRF-1 on the Tfam promoter (180), a required factor for the transcription of mtDNA, illustrates the importance of PGC-1α in the coordinated expression of mitochondrial genes derived from both nuclear and mitochondrial genomes. Thus, there is strong evidence to suggest that PGC-1α sits at the crux of the regulation of mitochondrial content and function.

It is known that a single bout of exercise can elicit changes in the expression of factors involved in mitochondrial biogenesis, including PGC-1α. However, repeated bouts of exercise over a given period of time results in the progressive increase in PGC-1α, NRF-1 and Tfam protein expression (11, 45, 61) . These results indicate that these factors are not only crucial for the constitutive maintenance of mitochondrial content and function but are also critical for mediating the mitochondrial adaptations to exercise. In support of this, skeletal muscle-specific overexpression of PGC-1α is sufficient to enhance basal mitochondrial content and endurance performance (19). In contrast, PGC-1α KO mice exhibit impairments in mitochondrial content and function (4). Furthermore, skeletal muscle-specific ablation of PGC-1α results in impaired endurance performance, which is likely due to alterations in mitochondrial structure and function, as well as reduced expression of oxidative fibres (50). Although it is evident that PGC-1α is essential for the maintenance of a healthy mitochondrial network, its absolute necessity for mediating exercise-induced adaptations is still being questioned. The question arises because it has been shown that PGC-1α is not mandatory for training-induced increases in mitochondrial proteins, suggesting that other factors other than PGC-1α can exert these adaptations (85). However, in contrast to the previous findings, skeletal muscle-specific deletion of PGC-1α attenuated the expression of mitochondrial proteins following an

endurance training program, demonstrating an impaired adaptive response (40). This suggests that there is perhaps a specific role for PGC-1α in mediating the adaptations of skeletal muscle to exercise.

1.1.1.1.2 AMPK

As previously mentioned, mitochondrial biogenesis occurs as a result of enhanced intracellular signaling that is generated by muscular contraction. Among these signals is the increased activation of the metabolic energy sensor AMP-activated protein kinase (AMPK). Exercise increases ATP turnover within muscle cells resulting in a decrease in the ATP-to-ADP ratio. Consequently, there is also a rise in the formation of AMP which is an allosteric activator of AMPK. The enhanced expression of factors favoring oxidative metabolism, including PGC-1α, uncoupling protein 3 (UCP3), cytochrome c, succinate dehydrogenase and citrate synthase, have been linked with increased AMPK activation (13, 62, 68, 179). Moreover, these effects appear to be mediated by AMPK regulation of PGC-1α at both the gene and protein levels. For instance, Garcia-Roves et al. (39) demonstrated that genetically or pharmacologically enhancing AMPK activation resulted in an increase in both PGC-1α mRNA and protein expression. This is likely attributed to AMPK augmenting the binding of critical transcription factors to the PGC-1α promoter (62). Furthermore, AMPK activation increases the phosphorylation of PGC-1α, a post-translational modification that is important for the induction of PGC-1α regulated genes (68). The necessity of AMPK in the regulation of mitochondrial content has been bolstered by studies documenting that knocking out the β-subunits of AMPK results in reduced mitochondrial content and muscle function, consequently impairing

endurance performance (116). Collectively, these findings highlight the importance of AMPK in regulating mitochondrial content.

1.1.1.1.3 p38 MAPK

Map kinases, such as p38, can be activated by a number of stressful stimuli, which include cytokines, growth factors, and exercise (23). Through its ability to phosphorylate target protein substrates, p38 has the capacity to regulate multiple cellular processes. In particular, p38 has been implicated in regulating exercise-induced changes in gene expression. For instance, Akimoto et al. (5) demonstrated that an acute bout of exercise increased p38 activity which resulted in an increase in PGC-1α mRNA content. The increase in PGC-1α transcript is likely attributed to increased gene transcription, since overexpression of p38 has been shown to increase PGC-1α promoter activity. Furthermore, contractile activity-induced increases in PGC-1α promoter and protein activity were attenuated with inhibition of p38 (183). In addition to its ability to regulate PGC-1α at the level of transcription, it has also been demonstrated that p38 can phosphorylate PGC-1α, thereby augmenting its ability to regulate the expression of nuclear genes-encoding mitochondrial proteins (NUGEMPS) (132). Taken together, these findings suggest that p38 is highly sensitive to contractile activity-evoked activation, and that it is an important signaling kinase for exercise-induced mitochondrial biogenesis.

1.1.1.1.4 Voluntary running wheel

The running wheel is a crucial instrument for the measurement of physical activity in laboratory rodents. Since most rodents readily run in wheels, it provides an uncomplicated and easily quantifiable measure of physical activity. However, like humans, the tendency for rodents to be more or less active is shaped by both genetic and

environmental factors. Although the use of the running wheel is often employed to research the effects of exercise on metabolism and obesity, it can also be used to induce and study physiological adaptations like mitochondrial biogenesis (143). This is made possible by the fact that voluntary wheel running can be a prodigious activity. For instance, within a 24-hour time-frame it has been demonstrated that rats and mice can run a distance of up to 43 and 16 km, respectively (153). Evidently, this is analogous to a long slow-distance run performed by a human. Ultimately, voluntary wheel running serves as a simplistic model of physical activity which provides researchers with the opportunity to study the health benefits associated with moderate exercise.

1.1.2 Skeletal muscle disuse atrophy

Skeletal muscle mass and fibre size vary according to both physiological and pathological conditions. An increase in muscle mass, or hypertrophy, is commonly observed in response to mechanical overload (synergistic ablation, strength training) or anabolic hormonal stimulation. In contrast, a decrease in muscle mass, or atrophy, results from aging, starvation, cancer, diabetes, bed rest, loss of neural input or catabolic hormonal stimulation. Ultimately, the regulation of skeletal muscle mass is determined by protein turnover. That is, the balance between protein synthesis and degradation. Although the exact mechanisms mediating muscle atrophy are not completely understood, experiments from both human and animal models have concluded that disuse-induced muscle atrophy occurs due to both reductions in protein synthesis and accelerated rates of protein breakdown (42, 43, 152). This increase in proteolysis is largely reflected by the activation of the ubiquitin proteasome and autophagy systems (15, 28, 82, 144). Although muscle atrophy is characterized by the net loss of myofibrillar

and sarcoplasmic proteins, a preferential loss of myofibrillar proteins is a hallmark of disuse-induced muscle wasting (108).

1.1.2.1 Ubiquitin-Proteasome System

In the ubiquitin-proteasome system (UPS), proteins are targeted for degradation by the 26S proteasome. This is accomplished by the covalent attachment of ubiquitin molecules onto the target protein. The E3 ubiquitin ligase enzymes are the rate-limiting step in the ubiquitination process since they bind the protein substrate and catalyze the movement of the ubiquitin from the E2 enzyme onto the substrate. Thus, this step is crucial and necessary for the subsequent proteasomal-dependent degradation. Among the many E3 ubiquitin ligases, only a few have been found to regulate the atrophy process and to be markedly induced under conditions promoting atrophy.

The pioneering studies by Goldberg (44) and Glass (16) had a significant impact on our understanding of muscle atrophy and the associated profiling of gene expression. They were the first to identify Atrogin-1/MAFbx and MuRF1, two E3's that are specifically expressed in smooth and striated muscle that are markedly induced in response to an atrophy-inducing stressor. Mice deficient for either MuRF1 or MAFbx genes were more resistant to disuse-related atrophy. This was exhibited by a 56% and 36% muscle sparing effect in the MAFbx and MuRF1 KO mice, respectively, following 14 days of denervation (16). Interestingly, these two enzymes appear to exert their effects differently. Currently, it has been demonstrated that MuRF1 targets several structural proteins, including troponin I (73), myosin heavy chains (26), actin (129), myosin binding protein C and myosin light chains 1 and 2 (28). In contrast, the substrates identified for MAFbx are largely involved in growth-related processes or survival

pathways. For instance MAFbx promotes the degradation of MyoD (167), a key muscle transcription factor, and eIF3-f, an important activator of protein synthesis.

Another E3 ligase that has attracted some attention in mediating disuse atrophy is TRAF6. Notably, TRAF6 KO mice are more resistant to muscle loss that is induced by denervation (121) and starvation (120). These protective effects may be partially explained by the reduced expression of both MuRF1 and MAFbx with TRAF6 inhibition. Moreover, it appears that the optimal activation of JNK, AMPK, FOXO3 and NF-κB pathways are partially dependent on the presence of TRAF6 (120). Therefore, the effects on both FOXO3 and NF-κB signaling may explain where there is a reduction in MuRF1 and MAFbx expression in the KO animals. Collectively, these findings provide evidence for the critical role of the UPS in mediating skeletal muscle atrophy.

1.1.2.2 Autophagy-Lysosome System

Autophagy mediates the bulk degradation of cytoplasmic components, accounting for the degradation of most long-lived proteins, including organelles. Ultimately, these are sequestered by double-membrane vesicles, called autophagosomes, to the lysosome for cellular digestion. Several years ago it was demonstrated that autophagy is active in muscle cells during catabolic conditions (32, 148). Moreover, using transgenic mice expressing LC3 fused with GFP; Mizushima et al. (103) documented the activation of the autophagy system during fasting in skeletal muscle. Furthermore, electron microscopic and biochemical studies have also demonstrated that autophagy is induced in response to denervation (38). However, this effect appears to be partially dependent on the presence of PGC-1α since animals lacking PGC-1α were shown to have an attenuation in the induction of autophagy in response to denervation (168).

The regulation of autophagy is not only organ-dependent (103) but also appears to differ between stimuli. That is, denervation-induced atrophy shows a slower pace of autophagy when compared with fasting-mediated atrophy. It is thought that this discrepancy is partially mediated by Runx1, which is upregulated during denervation. Furthermore, the importance of Runx1 for the preservation of muscle mass is highlighted by the myofibrillar disorganization and excessive autophagy that occurs with denervation in response to Runx1 inhibition (177). These results indicate that Runx1 is crucial for preventing excessive muscle wasting due to hyperactivation of autophagy.

Although it is understood that the autophagy-lysosome and ubiquitin proteasome systems are coordinately regulated (95, 184), their relative contribution to organelle remodelling, protein breakdown and muscle atrophy remains to be determined.

1.1.3 Aging

Loss of strength and mass, or sarcopenia, is a defining feature of aging skeletal muscle and is thought to be the precipitating factor contributing to impairments in mobility, increased risk of frailty, disability and even death (30). Although the etiology of sarcopenia is multifactorial, several studies have found evidence for reductions in mitochondrial content and function in aging muscle (21, 47, 128). Aberrant mitochondrial function can be detrimental since this can potentially result in ROS-induced oxidative damage to macromolecules, including those within the mitochondrion (i.e. mtDNA and ETC complexes). This in turn, can lead to additional mitochondrial dysfunction and further elevations in ROS resulting in a "vicious cycle" scenario that can ultimately contribute to cell death and sarcopenia (18, 37)**.** Typically increases in ROS are mitigated by an intracellular antioxidant response that is largely controlled by the transcription

factor Nrf2. However, it has been reported that there is a significant reduction in Nrf2 nuclear expression in elderly humans leading a sedentary lifestyle (141). Moreover, disruption of Nrf2 appears to induce oxidative stress resulting in greater ubiquitination, lipid peroxidation and pro-apoptotic signaling in the aged skeletal muscle of Nrf2 KO animals (101). These results indicate that the loss of Nrf2 can exacerbate the aging phenotype and augment the signaling of skeletal muscle degradation pathways upon aging.

Previously, it has been shown that autophagy is required for the maintenance of muscle mass (97). However, there are several studies indicating that this process is impaired with aging (70, 82), which likely contributes to the sarcopenic phenotype. Compounding this issue further is the reduced capacity for generation of new mitochondria. Specifically, aged animals have a compromised ability to augment mitochondrial biogenesis in response to both endurance training (14) and chronic electrical stimulation (90, 91) . This impairment likely coincides with the reduced expression (21) and attenuated induction of PGC-1α (14), in addition to increased degradation of precursor proteins destined for import into the mitochondria (58).

In addition to its role in maintaining mitochondrial content and health, several lines of evidence have also linked PGC-1α with muscle maintenance. For instance, Brault et al. (17) demonstrated that overexpression of PGC-1α inhibited muscle atrophy induced by denervation. Moreover, in the context of aging, Wenz et al. (178) demonstrated that muscle-specific overexpression of PGC-1α protected aging animals from sarcopenia and metabolic disease.

Although the loss in muscle mass observed with aging culminates from a number of combined factors, there is certainly strong evidence to indicate that mitochondria and its associated machinery serve as a nexus point for modulating a wide range of cellular functions and signaling pathways that affect the aging phenotype. Understanding these mechanisms is important for the development of therapeutic strategies designed to increase the health and vitality of the elderly.

1.2.0 Structure and function of mitochondria

Mitochondria are dynamic organelles that consist of a double membrane and are involved in producing large amounts of adenosine triphosphate (ATP), which serves as the cell's energy currency. For this reason, mitochondria are regarded as the "powerhouses" of the cell. Each mitochondrion is completely enclosed by an outer membrane, while the second inner membrane forms a series of convoluted folds, termed cristae. Located within these cristae are the protein complexes that are collectively referred to as the electron transport chain (ETC). According to the chemiosmotic theory, respiratory complexes within the ETC pump protons across the inner mitochondrial membrane (IMM), generating an electrochemical gradient, with the free energy being used to synthesize ATP (150).

Electron microscopy of skeletal muscle fibres has demonstrated that mitochondria form a reticulated network with interconnected mitochondria concentrated under the sarcolemma, termed the subsarcolemmal mitochondria (SS) and interspersed amongst the myofibrils, designated the intermyofibrillar mitochondria (IMF). Due to the strategic arrangement of the SS mitochondria to the peripherally-localized myonuclei, it has been postulated that this particular population provides the ATP that is necessary for

membrane and nuclear functions. In contrast, it is expected that the IMF mitochondria provide the ATP that enables the interaction between actin and myosin, thereby facilitating muscle contraction (56). Furthermore, SS and IMF mitochondria have also been shown to exhibit different functional, biochemical and compositional properties (3, 27, 163). These discrepancies may arise due to inherent differences in enzyme and lipid compositions or in their capacity for protein synthesis and import.

1.2.1 Mitophagy

As previously mentioned, mitochondria have long been considered as crucial organelles, primarily for their role in ATP synthesis. However, mitochondria have also established themselves as critical players in other cellular processes including calcium homeostasis (34), fuel utilization (88), intracellular signaling (29, 162) and apoptosis (131). Due to this wide spectrum of cellular functions, it is evident that mitochondria play a pivotal role in maintaining homeostasis within the cell. As a result, the requirement for a healthy mitochondrial pool is essential for cell survival.

As previously mentioned, autophagy is a highly conserved mechanism that involves the degradation of cellular components through the lysosomal machinery (102). Remarkably, this process can be highly specific, targeting only particular organelles, such as mitochondria. The selective removal of dysfunctional mitochondria by the autophagic machinery is known as mitophagy. This process is of particular importance in post-mitotic tissues like skeletal muscle fibres and neurons since it is the only established mechanism for eliminating dysfunctional and harmful organelles. Impairments in this system can be observed in several myopathies (49, 114), and is typically characterized by

the presence of abnormal mitochondria, oxidative stress, accumulation of polyubiquitinated proteins and structural defects to the sarcomere (97).

In order to serve as a quality control mechanism, the cell must be equipped with specialized proteins that can detect damaged mitochondria and mark them for degradation. Specifically, when mitochondria become dysfunctional, a loss of membrane potential results ($\Delta\Psi$). This loss in $\Delta\Psi$ results in the stabilization of the serine/threonine kinase phosphatase and tensin homolog (PTEN)- induced kinase 1 (PINK1) on the outer mitochondrial membrane (OMM) (98). Although PINK1 is constitutively degraded by mitochondrial specific enzymes, the loss in $\Delta\Psi$ prevents its import, allowing for the accumulation of PINK1 on the OMM (158). This stabilization of PINK1 facilitates the recruitment of the E3-ubiquitin ligase Parkin, which attaches ubiquitin moieties to various proteins, targeting them for degradation (98, 109). Among the most prominent targets of Parkin-mediated ubiquitination are the mitochondrial fusion proteins mitofusin 1 and mitofusin 2 (Mfn1 and Mfn2) (164). By promoting proteasomal degradation of Mfn1 and – 2, mitochondria become increasingly fragmented, which is necessary for the segregation of damaged mitochondrial fragments from the healthy mitochondrial network. Concurrently, the ubiquitination of OMM proteins results in the recruitment of p62, which functions as an adaptor protein. Since p62 has a ubiquitin binding domain and a microtubule-associated protein 1 light chain 3 (LC3) interacting region, it serves as an anchor between the tagged mitochondria and LC3-positive phagophores for subsequent clearance in the lysosome (63, 119).

Evidently, mitophagy serves as an adaptive response to cellular stress by eliminating damaged mitochondria in order to preserve mitochondrial and skeletal muscle

integrity. Defects in the autophagic machinery result in the accumulation of dysfunctional proteins and organelles that can promote myofibre degeneration, or aggravate muscle pathologies.

1.2.2 ROS

It is well known that mitochondria are the primary suppliers of ATP within the cell. However, through this energy-transducing process, electrons can escape the ETC and partially reduce oxygen giving rise to the formation of ROS. As a result, mitochondria are often cited as the predominant source of ROS within skeletal muscle fibres. Studies investigating mitochondria at the ultrastructural level have identified NADH dehydrogenase (complex I) and cytochrome bc1 (complex III) as the major sites of superoxide production (107, 134). Interestingly, work conducted by Brand and colleagues (133) revealed that the contribution of specific sites to the production of ROS was dependent on the substrate being oxidized, indicating that physiological or pathological changes in substrate utilization may be an important determinant for free radical generation.

In the context of exercise, the general consensus is that the increase in ROS production that occurs with contractile activity is directly related to the elevated oxygen consumption that occurs with increased mitochondrial activity. However, recent reports argue that mitochondria may not be the dominant source of ROS during exercise (142). Moreover, there is actually an inverse relationship between ROS production and oxygen consumption since mitochondria generate more ROS during basal (state 4) respiration compared to active (state 3) respiration (8). To lend further perspective, mitochondria are

predominantly in state 3 during aerobic contractile activity limiting the generation of ROS during contractions (130).

Historically, ROS have been viewed as toxic metabolic byproducts and causal agents of several pathologies. For instance, ROS have consistently been implicated in the development and pathogenesis of insulin resistance and type II diabetes. Cellular models of insulin resistance are consistently characterized by elevations in ROS (57) that are typically derived from mitochondria (7). Although these findings suggest that increases in ROS contribute to insulin resistance, there are data to suggest otherwise. For instance, there is evidence indicating that ROS is required for both glucose-induced insulin secretion by pancreatic β-cells (86), and enhanced insulin sensitivity (92).

It has also been suspected that increases in oxidant production contribute or exacerbate the aging process. However, the literature investigating the relationship between ROS and lifespan is mixed. In support of a causal role for oxidants, Schriner et al. (149) demonstrated that overexpression of catalase in murine mitochondria increased longevity and reduced the oxidative damage associated with aging. In contrast, some genetic models cast doubt on the idea that "less is better" when it comes to ROS. This has been demonstrated in SOD2 transgenic mice, since they do not have an increase in lifespan compared with their wild-type counterparts. Furthermore, in some cases these mice have displayed growth retardation and decreased fertility (135). Moreover, overexpressing a combination of major antioxidant proteins also failed to increase lifespan (122). To complicate matters further, mice heterozygous for either mitochondrial GPx4 or CLK1 display higher levels of oxidative stress, yet exhibit increases in longevity (89, 136).

Currently, a unified model regarding mitochondrially-derived ROS as being a beneficial or detrimental agent does not exist. However, there appears to be a small window or threshold where ROS can exert beneficial effects. The term hormesis is used to describe favourable adaptations in response to nonlethal stressors. Therefore, within the confines of this range, cellular stress can promote adaptations that contribute to organismal fitness. However, beyond this point, pathologies, senescence or cell death may ensue.

1.3.0 Nrf2-Keap1 Pathway

1.3.1 Nrf2 and Keap1 domain structure and interaction

Nuclear erythroid 2 p45-related factor 2 (Nrf2) belongs to the cap 'n' collar (CNC) family of transcription factors that share a highly conserved basic region leucine zipper (bZip) structure (104). The Nrf2 protein contains 605 amino acids that form seven conserved Nrf2-ECH homology (Neh) domains (Fig. 1A). Neh1 contains the CNC- bZip motif, which enables Nrf2 to bind to the antioxidant response element (ARE) sequence in the promoter of target genes. Furthermore, small Maf proteins heterodimerize with Nrf2 in this region to facilitate it's binding to the DNA and increase its transcriptional efficiency (64, 67, 72). The N-terminal Neh2 domain is regarded as the negative regulatory domain due to its interaction with Kelch-like ECH-associated protein 1 (Keap1) (66). Additionally, negative regulation of Nrf2 can occur in a Keap1-independent manner by targeting specific motifs located in the Neh6 domain (25, 99). While the Neh 3-5 domains appear to be critical for transactivation by binding to different components of the transcriptional apparatus (71, 113), repression of Nrf2 has recently been shown to occur through interactions with Neh 7 (176).

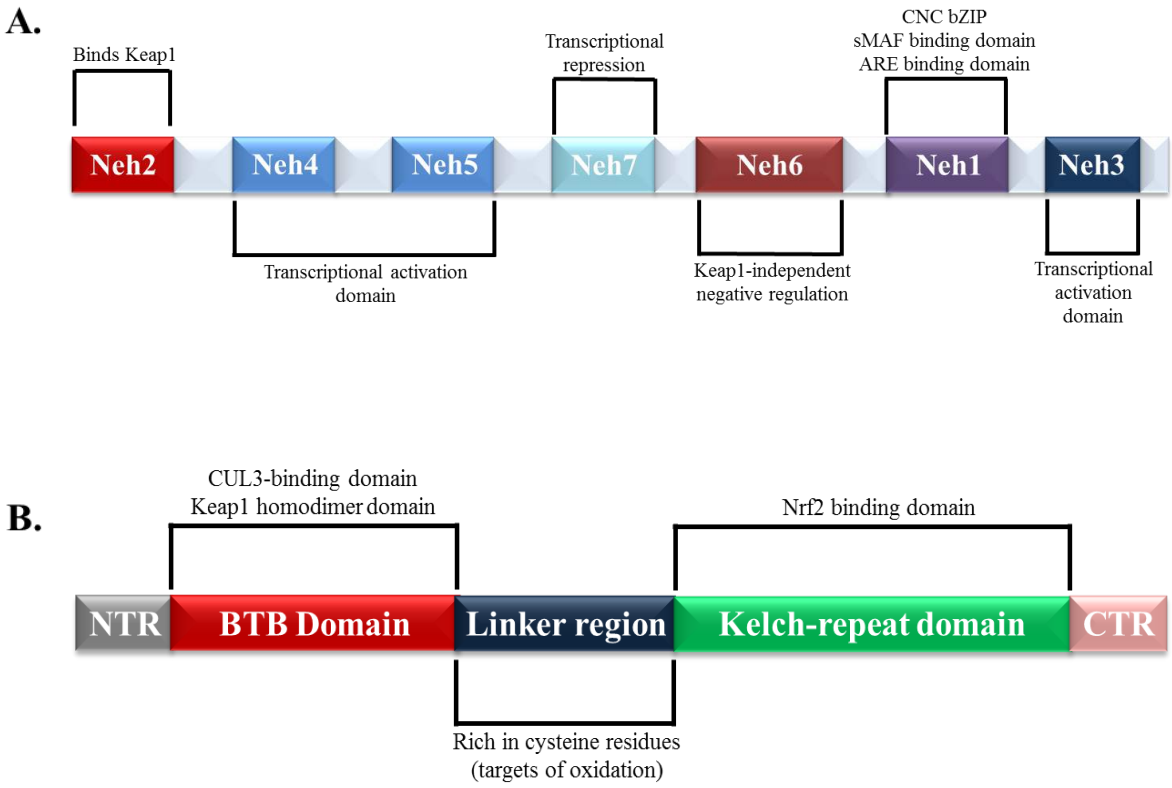

Figure 1. Domain structures of the transcription factor Nrf2 and its repressor Keap1. **(A)** The proposed positions of the Nrf2 ECH-homology 1-7 domains are indicated. The Neh1CNC-bZip domain is responsible for dimerization with the sMaf proteins and required for ARE-interaction. Neh2 domain interacts with Keap1. Neh3-5 are important for the recruitment of other factors necessary for transcription of target genes. Keap1 independent negative regulation of Nrf2 can occur through Neh6 and Neh7. **(B)** Domain structure of Keap1. BTB-domain of Keap1 is required to form a Keap1 homodimer. Linker region is rich in cysteine residues that can be modified by reactive oxygen species (ROS). The Kelch-repeat domain is critical for Nrf2 repression since it interacts with the Neh2 domain of Nrf2.

The activity of Nrf2 is tightly regulated by Keap1, which was identified through a yeast two-hybrid system using the Neh2 domain of Nrf2 as bait (66). Keap1 contains three major domains: an N-terminal BTB (broad complex, tramtrack, bric-a-brac) domain, a linker region, and a C-terminal Kelch domain (Fig. 1B). Findings from Zipper et al. demonstrated that the N-terminal BTB domain is required to form a Keap1 homodimer, which is also necessary for the sequestration of Nrf2 (186). Additionally, the Kelch domain is also important for the binding of Nrf2 since it interacts with the Neh2 domain of Nrf2 (87). Lastly, the cysteine-rich linker region has also been shown to be imperative for Keap1-mediated degradation of Nrf2 (182).

1.3.2 Redox balance of the cell – Nrf2 activation

Eukaryotic organisms are constantly challenged by an array of both endogenous and exogenous insults that can alter the redox balance of the cell. Therefore, in order to combat against these insults they have evolved an elaborate network of cytoprotective proteins that confer cellular protection by augmenting their expression in response to disturbances in oxidative stress. The transcription factor Nrf2 is regarded as the central regulator of the expression of antioxidant and phase II detoxification enzymes since it controls their inducible expression (Fig. 2). Abrogation of Nrf2 in mice blunts the expression of these enzymes consequently increasing their sensitivity to the toxic effects of various drugs (35) and chemical compounds (137). The inability of these mice to initiate a response that counteracts the adverse effects of exogenous insults illustrates the importance of Nrf2 in maintaining cellular redox homeostasis.

Although Nrf2 controls the inducible expression of its target genes, its activity is tightly regulated by Keap1 (111). Under basal conditions Keap1 binds Nrf2 and targets it for ubiquitination and proteasomal degradation via association with the Cul3-based E3

ubiquitin ligase complex (31, 76). Due to the negative regulatory system of Keap1, Nrf2 is rapidly turned over, with a half-life of less than 20 minutes (76). However, increases in oxidative stress promote the activation and stabilization of Nrf2. Nrf2 activation is thought to involve the modification of the sulfhydryl groups of specific cysteine residues found within the linker region of Keap1, which results in a conformational change that alters the binding capacity of Keap1 with Nrf2 (77, 182). This alteration in Keap1 structure is also thought to inhibit or mask the nuclear exporting signal (NES) within Keap1, which is thought to serve as another regulatory element in the sequestration of Nrf2 within the cytoplasm (171). This in turn, allows for Nrf2 to dissociate and have its nuclear localization signals (NLS) exposed, facilitating its entry into the nucleus. Nrf2 contains three different NLS (designated NLS1-3) that are essential for its entry and function within the nucleus (69, 166). Interestingly, NLS1 is contained within the Neh2 domain, the domain that is crucial for Nrf2-Keap1 interaction (65, 99). Therefore, under non-stressed conditions Keap1's interaction with Nrf2 at this domain likely conceals this sequence, helping to retain Nrf2 within the cytoplasm. Given the central importance of Nrf2 in maintaining health (22, 46, 106), the presence of several NLS may provide Nrf2 with an opportunity to respond to different signals. In any case, it is evident that oxidative conditions favour Nrf2 activation in order to mediate an intracellular response that will ultimately mitigate damage to the cell and help to bring it back to homeostasis.

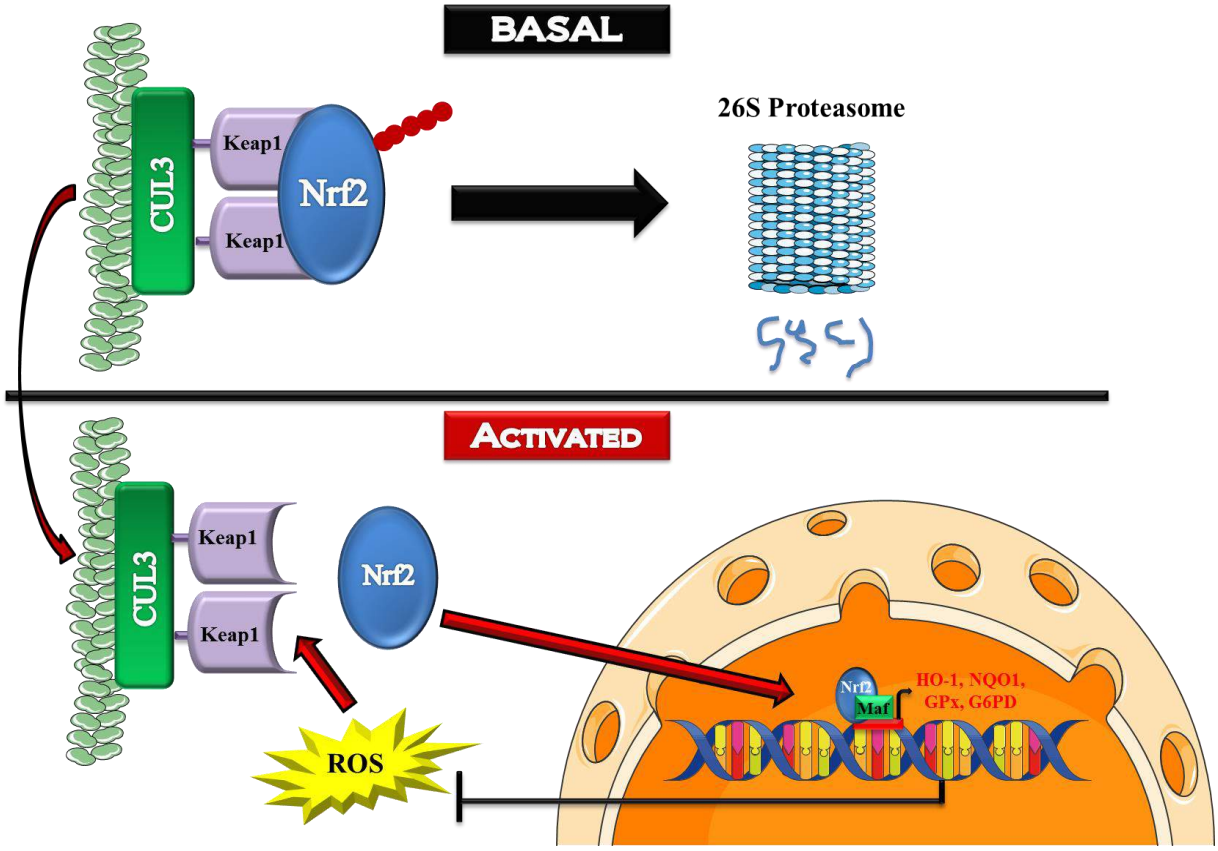

Figure 2. General scheme for the induction of gene expression through the Keap1-Nrf2 signaling pathway. Keap1 is a key regulator of Nrf2, serving as a molecular switch for the activation or repression of the Nrf2-mediated antioxidant response. A) Under basal conditions, the CUL3-Keap1 E3 ubiquitin ligase complex constantly targets Nrf2 for ubiquitination and degradation by the 26S proteasome. B) Upon activation, in response to increases in reactive oxygen species (ROS) or antioxidant response element inducers, distinct cysteine residues on Keap1 are modified, thereby disrupting the association between Keap1 and Nrf2. As such, Nrf2 is stabilized and accumulates in the nucleus where it heterodimerizes with small Maf proteins and binds to the antioxidant response element (ARE) within the promoter region of target genes. Increased expression of antioxidants and detoxification enzymes results in an adaptive response that enhances the resistance of cells to environmental stresses mediated by electrophiles and ROS.

1.3.3 Transcription of antioxidants – Nrf2/ARE regulation

The upstream regulatory regions of cytoprotective genes contain a consensus sequence known as the antioxidant response element (ARE). Through mutational analysis, Rushmore et al. were able to identify a core sequence (TGACnnnGC) required for phenolic antioxidant-induced gene regulation (139, 140). Since then studies have demonstrated that Nrf2 binds to the ARE in order to regulate the ARE-mediated antioxidant enzyme gene expression. Moreover, the Nrf2-ARE induction has been shown to respond to a number of different stimuli including xenobiotics, antioxidants, metals and UV irradiation (48, 51, 80). However, the absence of Nrf2 abolishes this response since Nrf2-null mice exhibit a marked reduction in several antioxidant and phase II detoxification enzyme genes that are required to protect the cell against increases in oxidative stress (64). These results indicate that Nrf2 is imperative for the activation of these genes.

Importantly, Nrf2 cannot bind to the ARE as a monomer or homodimer. ARE-mediated transcriptional activation requires Nrf2 to form a heterodimer with small Maf proteins. Evidence for this comes from small Maf mutant mice, who demonstrate an impaired ability to modulate ARE-dependent genes (72, 105). Additional regulatory mechanisms include the recruitment of coactivators that can modify the transcriptional activity of Nrf2 by interacting with the Neh4 or Neh5 domain, which are both important for Nrf2 transactivation. For instance, p300 or CBP was shown to cooperatively bind these sites, augmenting promoter-specific DNA binding of Nrf2 (71, 161). Although a number of *in vitro* and *in vivo* studies have demonstrated the importance of Nrf2 in

upregulating ARE-dependent gene expression, it is clear that the coordinated actions of other factors must also be in place.

Although Nrf2 activation in response to increases in oxidative stress is critical for mounting an appropriate defense response, constitutive activation of Nrf2 can be detrimental. For example, Keap1 knockout (KO) mice die postnatally due to hyperkeratosis of the esophagus and forestomach (173). While Keap1 certainly serves as the central regulatory node against Nrf2 activity, other factors are in place to aid in the tight regulation of Nrf2. Under non-stressed conditions BACH1 (BTB and CNC homology 1, basic leucine zipper transcription factor 1) forms a heterodimer with small Maf proteins on the ARE to repress gene expression (33, 59). However, in the presence of oxidative stress BACH1 is released from the ARE and replaced with Nrf2. In a similar fashion to Keap1, BACH1's role as a negative repressor of the ARE is likely to contribute to the homeostatic control of ARE-regulated gene expression

1.3.4 Role of antioxidants

1.3.4.1 NQO1

NADPH quinone oxidoreductase 1 (NQO1) is a cytosolic enzyme that is widely distributed in mammalian tissues, though the highest levels are typically observed in the heart and liver (185). The principal function of NQO1 is to catalyze the obligatory two-electron reduction of various quinone compounds and their derivatives by using NADPH or NADH as the hydride donor (36). This results in the detoxification of electrophilic compounds that could otherwise participate in further redox signaling, generating more reactive oxygen intermediates. Furthermore, NQO1 provides an additional layer of protection to the cell by scavenging superoxide (155) and ensuring that vitamin E and

coenzyme Q (CoQ) remain in their reduced and active forms in order to protect against the lipid peroxidation of cell membranes (154, 185).

Another critical biological function of NQO1 is the stabilization of the tumor suppressor protein p53. This protein-protein interaction between NQO1 and p53 works to stabilize p53 by preventing its degradation by the 20S proteasome (10). Although the exact nature of this interaction has not been fully elucidated, it appears that the catalytic activity of NQO1 is not required, suggesting that the oxidation of NADPH is not responsible for the stabilization of p53 (9). Similarly, NQO1 has been shown to exert the same regulatory actions to PGC-1α. Adamovich et al. (1) revealed that NQO1 binds and protects PGC-1α from 20S proteasomal degradation, which plays an important role in controlling PGC-1α protein level and activity under basal and physiologically induced conditions.

1.3.4.2 Heme Oxygenase-1

Heme Oxygenase-1 (HO-1) is an antioxidant protein that is rapidly upregulated in response to oxidative stress (75). The major enzymatic function of HO-1 is to degrade heme resulting in the generation of biliverdin, carbon monoxide (CO) and ferrous iron (100). Interestingly, the cytoprotective effects of HO-1 occur in a dual manner. First, HO-1 is essential for eliminating free heme and preventing it from participating in pro-oxidant reactions (75). Secondly, biliverdin is rapidly converted to bilirubin which has been shown to exhibit antioxidant properties of its own (41, 157). Furthermore, the generation of endogenous CO that occurs from the catabolism of free heme has even demonstrated protective effects through anti-apoptotic (175), anti-inflammatory (118) and mitochondrial quality control functions (81, 83).

HO-1 and CO also work in tandem to confer cytoprotection by promoting mitochondrial biogenesis. In cardiac cells, it was found that endogenous CO enhanced mitochondrial H_2O_2 production, resulting in the activation of Nrf2 and nuclear translocation of nuclear respiratory factor -1 (NRF-1), a well-known transcription factor for mitochondrial biogenesis (145, 172). Nuclear Nrf2 occupied the ARE sites in the promoter regions of HO-1, SOD2 and NRF-1, facilitating the transcription of these genes, while nuclear accumulation of NRF-1 promoted the activation of downstream genes that are required for mitochondrial biogenesis (126). This particular action of the HO-1/CO signaling axis appears to couple the pro-survival program of mitochondrial biogenesis with the upregulation of cellular antioxidant defenses.

1.3.4.3 GSH

The tripeptide glutathione (GSH) is considered to be the most abundant non-protein thiol in cells. The synthesis of GSH is ATP-dependent and occurs exclusively in the cytoplasm through the actions of γ-glutamylcysteine synthetase and GSH synthase. The key functional element of GSH is the reactive thiol-group that is present within its cysteine backbone. This allows GSH to participate in oxidation-reduction type reactions that facilitate the clearance of electrophiles and other redox species. Although GSH serves as a critical reducing agent and antioxidant within the cell, its functions extend beyond acting as a redox buffer.

In addition to controlling the redox environment within the cell, GSH can also modulate the formation of reactive oxygen species (ROS) within the mitochondrion. This is accomplished by a post-translational modification known as glutathionylation, which is the addition of GSH to the cysteine residue of target proteins. Mailloux et al. (94)

demonstrated that the mitochondrial uncoupling proteins 2 and 3 (UCP 2 and UCP3) contain reactive cysteines that can be conjugated to GSH, which ultimately controls its function. Glutathionylation prevented leaks through UCP2 and- 3 when ROS levels were low, however, increases in hydrogen peroxide (H_2O_2) resulted in the removal of the GSH moiety, thereby activating leaks and increasing state 4 respiration. Interestingly, complex 1 of the electron transport chain (ETC) also serves as a target for GSH conjugation. The work of Taylor et al. (165) revealed that mitochondrial complex 1 ROS production is linked to the oxidation of the mitochondrial GSH pool. Specific subunits that comprise complex 1 were shown to form mixed disulfides with GSH which elicited rapid increases in superoxide production. Although it seems counterintuitive that GSH would have a mechanism promoting increases in ROS, it may serve as a signaling mechanism that informs the cell of the redox environment within the mitochondria. This in turn could either signal for the clearance of mitochondria through the autophagic machinery (147), or initiate apoptosis (79).

1.3.5 Other transcription factors for regulating antioxidant capacity

In order to prevent against oxidative stress, the cell must respond to increases in ROS by upregulating the antioxidant defense system. Since antioxidants are necessary for reducing ROS levels, the redox regulation of transcription factors is an important component in determining the gene expression profile and cellular response to oxidative stress. Although Nrf2 is regarded as the master regulator of antioxidant gene expression, other factors including the forkhead box O (FOXO) family of transcription factors and PGC-1α have been shown to assists in the redox buffering of the cell by regulating antioxidant expression.

The FOXO transcription factors were first linked to stress resistance in *C.elegans* when mutant mice deficient for *daf-2,* which is orthologous to the mammalian insulin receptor, exhibited a phenotype characterized by extended lifespans and resistance to oxidative stress (53, 74). It was determined that this phenotype was mediated by the transcription factor DAF-16, a FOXO orthologue, since mutations in this gene abolished these traits (54). This work suggested that DAF-16, or its mammalian orthologue FOXO, may regulate transcriptional targets that protect against oxidative stress. Indeed, subsequent research in mammalian tissue found that FOXO regulates a number of antioxidants including MnSOD, CuZn-SOD, catalase, Prx3, Prx5, GPx-1 and Trx2 (24, 78, 96, 110, 117). The fact that FOXO regulates a battery of antioxidants ensures that ROS can be buffered in a number of different intracellular compartments. However, this assurance is reduced in cells that lack FOXO expression since they exhibit increased sensitivity to elevations in ROS, which can ultimately result in apoptosis (112, 115).

Although PGC-1α is a potent stimulator of mitochondrial biogenesis, it also appears to assist in the coordination of antioxidant expression. Interestingly, increases in mitochondrial ROS detoxifying enzymes have been shown to coincide with increases in PGC-1α and mitochondrial gene expression (160, 169). Since ROS are a by-product of mitochondrial metabolism it seems logical that PGC-1α would balance metabolic adaptations and requirements with cytotoxic protection to ensure mitochondrial and cellular integrity. In support of this, PGC-1α null mice display a blunted induction of the ROS defense system, predisposing these mice to oxidative injury and neuronal lesions (159). Furthermore, it has been demonstrated that PGC-1α is indispensable during

differentiation since its absence was characterized by increased ROS production, reduction in mitochondrial mass and function and muscle degeneration (12).

Despite the fact that ROS can serve as important signaling molecules, uncontrolled regulation is detrimental to the cell. Therefore, it is imperative that there are systems in place that can counteract and tightly regulate their abundance. As such, the functions of Nrf2, FOXO and PGC-1α serve to coordinate a line of defense against any outbursts in ROS. Evidently, impairments within any one of these systems renders the cell more susceptible to the deleterious effects of ROS.

1.4.0 Research Objectives

Therefore, based on the review of literature, the objectives of my thesis, using Nrf2 KO mice were:

1. To determine if Nrf2 is activated in skeletal muscle in response to exercise;
2. To investigate the tolerance and endurance capacity of Nrf2 KO mice by subjecting them to an exhaustive exercise test;
3. To examine the effect of Nrf2 on exercise-induced mitochondrial biogenesis;
4. To evaluate the effect of Nrf2 on mitochondrial respiration and ROS production;
5. To assess the role of Nrf2 in determining the contractile properties of skeletal muscle
6. To determine if age exacerbates the loss of Nrf2 on muscle performance or mitochondrial content

1.4.1 Hypothesis

We hypothesized that:

1. Nrf2 would be activated in skeletal muscle in response to exercise;
2. Nrf2 KO mice would have a lower endurance capacity relative to their WT counterparts;
3. The absence of Nrf2 would attenuate exercise-induced mitochondrial biogenesis;
4. Abrogation of Nrf2 would impair mitochondrial respiration and result in greater ROS production;
5. Force production and endurance would be impaired in the KO animals *in situ*;
6. Aging would exacerbate the loss of Nrf2.

Reference List

1. **Adamovich Y, Shlomai A, Tsvetkov P, Umansky KB, Reuven N, Estall JL, Spiegelman BM, Shaul Y**. The protein level of PGC-1α, a key metabolic regulator, is controlled by NADH-NQO1. *Mol Cell Biol* 33: 2603–2613, 2013.

2. **Adhihetty PJ, Leary MFNO, Chabi B, Wicks KL, Hood DA**. Effect of denervation on mitochondrially mediated apoptosis in skeletal muscle. 3: 1143–1151, 2007.

3. **Adhihetty PJ, Ljubicic V, Menzies KJ, Hood DA, Peter J**. Differential susceptibility of subsarcolemmal and intermyofibrillar mitochondria to apoptotic stimuli. *Am J Physiol Cell Physiol* 3: 994–1001, 2005.

4. **Adhihetty PJ, Uguccioni G, Leick L, Hidalgo J, Pilegaard H, Hood DA**. The role of PGC-1alpha on mitochondrial function and apoptotic susceptibility in muscle. *Am J Physiol Cell Physiol* 297: 217–225, 2009.

5. **Akimoto T, Pohnert SC, Li P, Zhang M, Gumbs C, Rosenberg PB, Williams RS, Yan Z**. Exercise stimulates Pgc-1alpha transcription in skeletal muscle through activation of the p38 MAPK pathway. *J Biol Chem* 280: 19587–93, 2005.

6. **Allen DL, Roy RR EV**. Myonuclear domains in muscle adaptation and disease. *Muscle Nerve* 22: 1350–1360, 1999.

7. **Anderson EJ, Lustig ME, Boyle KE, Woodlief TL, Kane DA, Lin C, Iii JWP, Kang L, Rabinovitch PS, Szeto HH, Houmard JA, Cortright RN, Wasserman DH, Neufer PD**. Mitochondrial H2O2 emission and cellular redox state link excess fat intake to insulin resistance in both rodents and humans. *J Clin Invest* 119: 573–581, 2009.

8. **Anderson EJ, Neufer PD, Ethan J, Ii T**. Type II skeletal myofibers possess unique properties that potentiate mitochondrial H 2 O 2 generation. *Am J Physiol Cell Physiol* 06519: 844–851, 2006.

9. **Anwar A, Dehn D, Siegel D, Kepa JK, Tang LJ, Pietenpol J a, Ross D**. Interaction of human NAD(P)H:quinone oxidoreductase 1 (NQO1) with the tumor suppressor protein p53 in cells and cell-free systems. *J Biol Chem* 278: 10368–73, 2003.

10. **Asher G, Lotem J, Cohen B, Sachs L, Shaul Y**. Regulation of p53 stability and p53-dependent apoptosis by NADH quinone oxidoreductase 1. *Proc Natl Acad Sci U S A* 98: 1188–1193, 2001.

11. **Baar K, Wende AR, Jones TE, Marison M, Nolte LA, Chen M, Kelly DP, Holloszy JO**. Adaptations of skeletal muscle to exercise: rapid increase in the transcriptional coactivator PGC-1. *FASEB* 16: 1879–86, 2002.

12. **Baldelli S, Aquilano K, Ciriolo MR**. PGC-1α buffers ROS-mediated removal of mitochondria during myogenesis. *Cell Death Dis* 5: e1515, 2014.

13. **Bergeron R, Ren JM, Cadman KS, Moore IK, Perret P, Pypaert M, Young LH, Semenkovich CF, Shulman GI**. Chronic activation of AMP kinase results in NRF-1 activation and mitochondrial biogenesis. *Am J Physiol Endocrinol Metab* 281: 1340–1346, 2001.

14. **Betik AC, Thomas MM, Wright KJ, Riel CD, Hepple RT**. Exercise training from late middle age until senescence does not attenuate the declines in skeletal muscle aerobic function. *Am J Physiol Regul Integr Comp Physiol* 297: 744–755, 2009.

15. **Bodine SC, Baehr LM**. Skeletal muscle atrophy and the E3 ubiquitin ligases MuRF1 and MAFbx/atrogin-1. *Am J Physiol Endocrinol Metab* 307: E469–84, 2014.

16. **Bodine SC, Latres E, Baumhueter S, Lai VK, Nunez L, Clarke B a, Poueymirou WT, Panaro FJ, Na E, Dharmarajan K, Pan ZQ, Valenzuela DM, DeChiara TM, Stitt TN, Yancopoulos GD, Glass DJ**. Identification of ubiquitin ligases required for skeletal muscle atrophy. *Science* 294: 1704–8, 2001.

17. **Brault JJ, Jespersen JG, Goldberg AL**. Peroxisome proliferator-activated receptor gamma coactivator 1alpha or 1beta overexpression inhibits muscle protein degradation, induction of ubiquitin ligases, and disuse atrophy. *J Biol Chem* 285: 19460–71, 2010.

18. **Cadenas E, Davies KJA**. Mitochondrial free radical generation, oxidative stress, and aging. *Free Radic Biol Med* 29: 222–230, 2000.

19. **Calvo JA, Daniels TG, Wang X, Paul A, Lin J, Spiegelman BM, Stevenson SC, Rangwala SM, Ja C, Tg D, Wang X, Paul A, Lin J, Bm S**. Muscle-specific expression of PPARgamma coactivator-1a improves exercise performance and increases peak oxygen uptake. *J Appl Physiol* 104: 1304–1312, 2008.

20. **Cartoni R, Léger B, Hock MB, Praz M, Crettenand A, Pich S, Ziltener J-L, Luthi F, Dériaz O, Zorzano A, Gobelet C, Kralli A, Russell AP**. Mitofusins 1/2 and ERRalpha expression are increased in human skeletal muscle after physical exercise. *J Physiol* 567: 349–58, 2005.

21. **Chabi B, Ljubicic V, Menzies KJ, Huang JH, Saleem A, Hood DA**. Mitochondrial function and apoptotic susceptibility in aging skeletal muscle. *Aging Cell* 7: 2–12, 2008.

22. **Chan K, Kan YW**. Nrf2 is essential for protection against acute pulmonary injury in mice. *Proc Natl Acad Sci U S A* 96: 12731–12736, 1999.

23. **Chen Z, Gibson TB, Robinson F, Silvestro L, Pearson G, Xu B, Wright A, Vanderbilt C, Cobb MH**. MAP Kinases. *Chem Rev* 101: 2449–76, 2001.

24. **Chiribau CB, Cheng L, Cucoranu IC, Yu Y-S, Clempus RE, Sorescu D**. FOXO3A regulates peroxiredoxin III expression in human cardiac fibroblasts. *J Biol Chem* 283: 8211–7, 2008.

25. **Chowdhry S, Zhang Y, McMahon M, Sutherland C, Cuadrado a, Hayes JD**. Nrf2 is controlled by two distinct β-TrCP recognition motifs in its Neh6 domain, one of which can be modulated by GSK-3 activity. *Oncogene* 32: 3765–81, 2013.

26. **Clarke B a, Drujan D, Willis MS, Murphy LO, Corpina R a, Burova E, Rakhilin S V, Stitt TN, Patterson C, Latres E, Glass DJ**. The E3 Ligase MuRF1 degrades myosin heavy chain protein in dexamethasone-treated skeletal muscle. *Cell Metab* 6: 376–85, 2007.

27. **Cogswell AM, Stevens RJ, Hood DA, York N, Mj O, Andria M**. Properties of skeletal muscle mitochondria from subsarcolemmal and intermyofibrillar isolated regions. .

28. **Cohen S, Brault JJ, Gygi SP, Glass DJ, Valenzuela DM, Gartner C, Latres E, Goldberg AL**. During muscle atrophy, thick, but not thin, filament components are degraded by MuRF1-dependent ubiquitylation. *J Cell Biol* 185: 1083–95, 2009.

29. **Collins Y, Chouchani ET, James a. M, Menger KE, Cocheme HM, Murphy MP**. Mitochondrial redox signalling at a glance. *J Cell Sci* 125: 1837–1837, 2012.

30. **Cruz-Jentoft AJ, Landi F, Topinková E, Michel J-P**. Understanding sarcopenia as a geriatric syndrome. *Curr Opin Clin Nutr Metab Care* 13: 1–7, 2010.

31. **Cullinan SB, Gordan JD, Jin J, Wade J, Diehl JA, Harper JW**. The Keap1-BTB Protein Is an Adaptor That Bridges Nrf2 to a Cul3-Based E3 Ligase : Oxidative Stress Sensing by a Cul3-Keap1 Ligase The Keap1-BTB Protein Is an Adaptor That Bridges Nrf2 to a Cul3-Based E3 Ligase : Oxidative Stress Sensing by a Cul3-Keap1 Li. (2004). doi: 10.1128/MCB.24.19.8477.

32. **Deval C, Mordier S, Obled C, Bechet D, Combaret L, Attaix D, Ferrara M**. Identification of cathepsin L as a differentially expressed message associated with skeletal muscle wasting. *Biochem J* 360: 143–150, 2001.

33. **Dhakshinamoorthy S, Jain AK, Bloom D a, Jaiswal AK**. Bach1 competes with Nrf2 leading to negative regulation of the antioxidant response element (ARE)-mediated NAD(P)H:quinone oxidoreductase 1 gene expression and induction in response to antioxidants. *J Biol Chem* 280: 16891–900, 2005.

34. **Duchen MR**. Mitochondria and calcium : from cell signalling to cell death. *J Physiol* 15: 57–68, 2000.

35. **Enomoto A, Itoh K, Nagayoshi E, Haruta J, Kimura T, Connor TO**. High Sensitivity of Nrf2 Knockout Mice to Acetaminophen Hepatotoxicity Associated with Decreased Expression of ARE- Regulated Drug Metabolizing Enzymes and Antioxidant Genes. *Toxicol Sci* 177: 169–177, 2001.

36. **Faig M, Bianchet MA, Talalay P, Chen S, Winski S, Ross D, Amzel LM**. Structures of recombinant human and mouse NAD(P)H : quinone oxidoreductases : Species comparison and structural changes with substrate binding and release. *Proc Natl Acad Sci U S A* 97: 3177–3182, 2000.

37. **Fulle S, Protasi F, Di Tano G, Pietrangelo T, Beltramin A, Boncompagni S, Vecchiet L, Fanò G**. The contribution of reactive oxygen species to sarcopenia and muscle ageing. *Exp Gerontol* 39: 17–24, 2004.

38. **Furuno K, Goodman MN GA**. Role of different proteolytic systems in the degradation of muscle proteins during denervation atrophy. *J Biol Chem* 265: 8550–8557, 1990.

39. **Garcia-Roves PM, Osler ME, Holmström MH, Zierath JR**. Gain-of-function R225Q mutation in AMP-activated protein kinase gamma3 subunit increases mitochondrial biogenesis in glycolytic skeletal muscle. *J Biol Chem* 283: 35724–34, 2008.

40. **Geng T, Li P, Okutsu M, Yin X, Kwek J, Zhang M, Yan Z**. PGC-1alpha plays a functional role in exercise-induced mitochondrial biogenesis and angiogenesis but not fiber-type transformation in mouse skeletal muscle. *Am J Physiol Cell Physiol* 298: 572–579, 2010.

41. **Gibbs PEM, Maines MD**. Biliverdin inhibits activation of NF-kappaB: reversal of inhibition by human biliverdin reductase. *Int J Cancer* 121: 2567–74, 2007.

42. **Gibson JN, Halliday D, Morrison WL, Stoward PJ, Hornsby GA, Watt PW, Murdoch G RM**. Decrease in human quadriceps muscle protein turnover consequent upon leg immobilization. *Clin Sci* 72: 503–509, 1987.

43. **Glover EI, Phillips SM, Oates BR, Tang JE, Tarnopolsky M a., Selby A, Smith K, Rennie MJ**. Immobilization induces anabolic resistance in human myofibrillar protein synthesis with low and high dose amino acid infusion. *J Physiol* 586: 6049–6061, 2008.

44. **Gomes MD, Lecker SH, Jagoe RT, Navon A, Goldberg AL**. Atrogin-1, a muscle-specific F-box protein highly expressed during muscle atrophy. *Proc Natl Acad Sci U S A* 98: 14440–5, 2001.

45. **Gordon JW, Rungi AA, Inagaki H HD**. Effects of contractile activity on mitochondrial transcription factor A expression in skeletal muscle. *J Appl Physiol* 90: 389–396, 2001.

46. **Gounder SS, Kannan S, Devadoss D, Miller CJ, Whitehead KS, Odelberg SJ, Firpo M a, Paine R, Hoidal JR, Abel ED, Rajasekaran NS**. Impaired transcriptional activity of Nrf2 in age-related myocardial oxidative stress is reversible by moderate exercise training. *PLoS One* 7: e45697, 2012.

47. **Gouspillou G, Bourdel-Marchasson I, Rouland R, Calmettes G, Biran M, Deschodt-Arsac V, Miraux S, Thiaudiere E, Pasdois P, Detaille D, Franconi J-M, Babot M, Trézéguet V, Arsac L, Diolez P**. Mitochondrial energetics is impaired in vivo in aged skeletal muscle. *Aging Cell* 13: 39–48, 2014.

48. **Gruber F, Mayer H, Lengauer B, Mlitz V, Sanders JM, Kadl A, Bilban M, de Martin R, Wagner O, Kensler TW, Yamamoto M, Leitinger N, Tschachler E**. NF-E2-related factor 2 regulates the stress response to UVA-1-oxidized phospholipids in skin cells. *FASEB J* 24: 39–48, 2010.

49. **Grumati P, Coletto L, Sabatelli P, Cescon M, Angelin A, Bertaggia E, Blaauw B, Urciuolo A, Tiepolo T, Merlini L, Maraldi NM, Bernardi P, Sandri M, Bonaldo P**. Autophagy is defective in collagen VI muscular dystrophies, and its reactivation rescues myofiber degeneration. *Nat Med* 16: 1313–20, 2010.

50. **Handschin C, Chin S, Li P, Liu F, Maratos-Flier E, Lebrasseur NK, Yan Z, Spiegelman BM**. Skeletal muscle fiber-type switching, exercise intolerance, and myopathy in PGC-1alpha muscle-specific knock-out animals. *J Biol Chem* 282: 30014–21, 2007.

51. **He X, Lin GX, Chen MG, Zhang JX, Ma Q**. Protection against chromium (VI)-induced oxidative stress and apoptosis by Nrf2. Recruiting Nrf2 into the nucleus and disrupting the nuclear Nrf2/Keap1 association. *Toxicol Sci* 98: 298–309, 2007.

52. **Holloszy JO**. Biochemical adaptations in muscle. Effects of exercise on mitochondrial oxygen uptake and respiratory enzyme activity in skeletal muscle. *J Biol Chem* 242: 2278–82, 1967.

53. **Honda Y HS**. The daf-2 gene network for longevity regulates oxidative stress resistance and Mn-superoxide dismutase gene expression in Caenorhabditis elegans. *FASEB* 13: 1385–1393, 1999.

54. **Honda Y HS**. Oxidative Stress and Life Span Determination in the Nematode Caenorhabditis elegans. *Ann N Y Acad Sci* 959: 466–474, 2002.

55. **Hood D a, Irrcher I, Ljubicic V, Joseph A-M**. Coordination of metabolic plasticity in skeletal muscle. *J Exp Biol* 209: 2265–75, 2006.

56. **Hood DA, Uguccioni G, Vainshtein A, D'souza D**. Mechanisms of exercise-induced mitochondrial biogenesis in skeletal muscle: implications for health and disease. *Compr Physiol* 1: 1119–1134, 2011.

57. **Houstis N, Rosen ED, Lander ES**. Reactive oxygen species have a causal role in multiple forms of insulin resistance. *Nature* 440: 944–8, 2006.

58. **Huang JH, Joseph A-M, Ljubicic V, Iqbal S, Hood D a**. Effect of age on the processing and import of matrix-destined mitochondrial proteins in skeletal muscle. *J Gerontol A Biol Sci Med Sci* 65: 138–46, 2010.

59. **Igarashi K, Hoshino H, Muto A, Suwabe N, Nishikawa S, Nakauchi H, Yamamoto M**. Multivalent DNA Binding Complex Generated by Small Maf and Bach1 as a Possible Biochemical Basis for -Globin Locus Control Region Complex *. *J Biol Chem* 273: 11783–11790, 1998.

60. **Iqbal S, Ostojic O, Singh K, Joseph A-M, Hood D a**. Expression of mitochondrial fission and fusion regulatory proteins in skeletal muscle during chronic use and disuse. *Muscle Nerve* 48: 963–70, 2013.

61. **Irrcher I, Adhihetty PJ, Sheehan T, Joseph A, Hood DA**. PPARgamma coactivator-1a expression during thyroid hormone- and contractile activity-induced mitochondrial adaptations. *Am J Physiol Cell Physiol* 284: 1669–1677, 2003.

62. **Irrcher I, Ljubicic V, Kirwan AF, Hood DA**. AMP-activated protein kinase-regulated activation of the PGC-1alpha promoter in skeletal muscle cells. *PLoS One* 3: e3614, 2008.

63. **Isogai S, Morimoto D, Arita K, Unzai S, Tenno T, Hasegawa J, Sou Y, Komatsu M, Tanaka K, Shirakawa M, Tochio H**. Crystal structure of the ubiquitin-associated (UBA) domain of p62 and its interaction with ubiquitin. *J Biol Chem* 286: 31864–74, 2011.

64. **Itoh K, Chiba T, Takahashi S, Ishii T, Igarashi K, Katoh Y, Oyake T, Hayashi N, Satoh K, Hatayama ØI**. An Nrf2 / Small Maf Heterodimer Mediates the Induction of Phase II Detoxifying Enzyme Genes through Antioxidant Response Elements. *Biochem Biophys Res Commun* 322: 313–322, 1997.

65. **Itoh K, Wakabayashi N, Katoh Y, Ishii T, Connor TO, Yamamoto M**. Keap1 regulates both cytoplasmic-nuclear shuttling and degradation of Nrf2 in response to electrophiles. *Genes Cells* 1: 379–391, 2003.

66. **Itoh K, Wakabayashi N, Katoh Y, Ishii T, Igarashi K, Engel JD, Yamamoto M**. Keap1 represses nuclear activation of antioxidant responsive elements by Nrf2 through binding to the amino-terminal Neh2 domain. (1999). doi: 10.1101/gad.13.1.76.

67. **Itoh KEN, Igarashi K, Hayashi N, Nishizawa M**. Cloning and Characterization of a Novel Erythroid Cell-Derived CNC Family Transcription Factor Heterodimerizing with the Small Maf Family Proteins. *Mol Cell Biol* 15: 4184–4193, 1995.

68. **Jäger S, Handschin C, St-Pierre J SB**. AMP-activated protein kinase (AMPK) action in skeletal muscle via direct phosphorylation of PGC-1alpha. *Proc Natl Acad Sci U S A* 104: 12017–12022, 2007.

69. **Jain AK, Bloom D a, Jaiswal AK**. Nuclear import and export signals in control of Nrf2. *J Biol Chem* 280: 29158–68, 2005.

70. **Joseph A-M, Adhihetty PJ, Wawrzyniak NR, Wohlgemuth SE, Picca A, Kujoth GC, Prolla T a, Leeuwenburgh C**. Dysregulation of mitochondrial quality control processes contribute to sarcopenia in a mouse model of premature aging. *PLoS One* 8: e69327, 2013.

71. **Katoh Y, Itoh K, Yoshida E, Miyagishi M, Yamamoto M**. Two domains of Nrf2 cooperatively bind CBP , a CREB binding protein , and synergistically activate transcription. *Genes Cells* 6: 857–868, 2001.

72. **Katsuoka F, Motohashi H, Ishii T, Aburatani H, Engel JD, Yamamoto M**. Genetic Evidence that Small Maf Proteins Are Essential for the Activation of Antioxidant Response Element-Dependent Genes. *Mol Cell Biol* 25: 8044–8051, 2005.

73. **Kedar V, Mcdonough H, Arya R, Li H, Rockman HA, Patterson C**. Muscle-specific RING finger 1 is a bona fide ubiquitin ligase that degrades cardiac troponin I. *Proc Natl Acad Sci U S A* 101: 18135–18140, 2004.

74. **Kenyon C**. The first long-lived mutants: discovery of the insulin/IGF-1 pathway for ageing. *Philos Trans R Soc Lond B Biol Sci* 366: 9–16, 2011.

75. **Keyse SM, Tyrrell REXM**. Heme oxygenase is the major 32-kDa stress protein induced in human skin fibroblasts by UVA radiation , hydrogen peroxide , and sodium arsenite. *Proc Natl Acad Sci U S A* 86: 99–103, 1989.

76. **Kobayashi A, Kang M, Okawa H, Zenke Y, Chiba T, Igarashi K, Ohtsuji M**. Oxidative Stress Sensor Keap1 Functions as an Adaptor for Cul3-Based E3 Ligase To Regulate Proteasomal Degradation of Nrf2 Oxidative Stress Sensor Keap1 Functions as an Adaptor for Cul3-Based E3 Ligase To Regulate Proteasomal Degradation of Nrf2. *Mol Cell Biol* 24: 7130–7139, 2004.

77. **Kobayashi M, Yamamoto M**. Nrf2-Keap1 regulation of cellular defense mechanisms against electrophiles and reactive oxygen species. *Adv Enzyme Regul* 46: 113–40, 2006.

78. **Kops GJPL, Dansen TB, Polderman PE, Bos JL**. Forkhead transcription factor FOXO3a protects quiescent cells from oxidative stress. *Nature* 419: 316–321, 2002.

79. **Kroemer G RJ**. Mitochondrial control of cell death. *Nat Med* 6: 513–519, 2000.

80. **Kwak M, Wakabayashi N, Jennifer L, Yamamoto M, Kensler TW, Greenlaw JL**. Antioxidants Enhance Mammalian Proteasome Expression through the Keap1-Nrf2 Signaling Pathway Antioxidants Enhance Mammalian Proteasome Expression through the Keap1-Nrf2 Signaling Pathway. (2003). doi: 10.1128/MCB.23.23.8786.

81. **Lancel S, Montaigne D, Marechal X, Marciniak C, Hassoun SM, Decoster B, Ballot C, Blazejewski C, Corseaux D, Lescure B, Motterlini R, Neviere R**. Carbon Monoxide Improves Cardiac Function and Mitochondrial Population Quality in a Mouse Model of Metabolic Syndrome. *PLoS One* 7: 1–11, 2012.

82. **Leary MFO, Vainshtein A, Iqbal S, Ostojic O, Hood DA**. Adaptive plasticity of autophagic proteins to denervation in aging skeletal muscle Adaptive plasticity of autophagic proteins to denervation in aging skeletal muscle. , 2013.

83. **Lee S-J, Ryter SW, Xu J-F, Nakahira K, Kim HP, Choi AMK, Kim YS**. Carbon monoxide activates autophagy via mitochondrial reactive oxygen species formation. *Am J Respir Cell Mol Biol* 45: 867–73, 2011.

84. **Lehman JJ, Barger PM, Kovacs A, Saffitz JE, Medeiros DM, Kelly DP**. Peroxisome proliferator – activated receptor γ coactivator-1 promotes cardiac mitochondrial biogenesis. *J Clin Invest* 106: 847–856, 2000.

85. **Leick L, Wojtaszewski JFP, Johansen ST, Kiilerich K, Comes G, Hellsten Y, Hidalgo J, Pilegaard H**. PGC-1alpha is not mandatory for exercise- and training-induced adaptive gene responses in mouse skeletal muscle. *Am J Physiol Endocrinol Metab* 294: 463–474, 2008.

86. **Leloup C, Magnan C, Karaca M, Castel J, Carneiro L, Colombani A, Ktorza A, Casteilla L, Pe L**. Mitochondrial Reactive Oxygen Species Are Obligatory Signals for Glucose-Induced Insulin Secretion. *Diabetes* 58: 673–681, 2009.

87. **Li X, Zhang D, Hannink M, Beamer LJ**. Crystal structure of the Kelch domain of human Keap1. *J Biol Chem* 279: 54750–8, 2004.

88. **Liesa M, Shirihai OS**. Mitochondrial dynamics in the regulation of nutrient utilization and energy expenditure. *Cell Metab* 17: 491–506, 2013.

89. **Liu X, Jiang N, Hughes B, Bigras E, Shoubridge E, Hekimi S**. Evolutionary conservation of the clk-1 -dependent mechanism of longevity : loss of mclk1 increases cellular fitness and lifespan in mice. *Genes Dev* 19: 2424–2434, 2005.

90. **Ljubicic V, Hood D a**. Diminished contraction-induced intracellular signaling towards mitochondrial biogenesis in aged skeletal muscle. *Aging Cell* 8: 394–404, 2009.

91. **Ljubicic V, Joseph AM, Adhihetty PJ, Huang JH, Saleem A, Uguccioni G, Hood DA**. Molecular basis for an attenuated mitochondrial adaptive plasticity in aged skeletal muscle. *Aging (Albany NY)* 1: 818–30, 2009.

92. **Loh K, Deng H, Fukushima A, Cai X, Boivin B, Galic S, Bruce C, Shields BJ, Skiba B, Ooms LM, Stepto N, Wu B, Mitchell C a, Tonks NK, Watt MJ, Febbraio M a, Crack PJ, Andrikopoulos S, Tiganis T**. Reactive oxygen species enhance insulin sensitivity. *Cell Metab* 10: 260–72, 2009.

93. **Macaluso F, Myburgh KH**. Current evidence that exercise can increase the number of adult stem cells. *J Muscle Res Cell Motil* 33: 187–98, 2012.

94. **Mailloux RJ, Seifert EL, Bouillaud F, Aguer C, Collins S, Harper M-E**. Glutathionylation acts as a control switch for uncoupling proteins UCP2 and UCP3. *J Biol Chem* 286: 21865–75, 2011.

95. **Mammucari C, Milan G, Romanello V, Masiero E, Rudolf R, Del Piccolo P, Burden SJ, Di Lisi R, Sandri C, Zhao J, Goldberg AL, Schiaffino S, Sandri M**. FoxO3 controls autophagy in skeletal muscle in vivo. *Cell Metab* 6: 458–71, 2007.

96. **Marinkovic D, Zhang X, Yalcin S, Luciano JP, Brugnara C, Huber T, Ghaffari S**. Foxo3 is required for the regulation of oxidative stress in erythropoiesis. *J Clin Invest* 117: 2133–2144, 2007.

97. **Masiero E, Agatea L, Mammucari C, Blaauw B, Loro E, Komatsu M, Metzger D, Reggiani C, Schiaffino S, Sandri M**. Autophagy Is Required to Maintain Muscle Mass. *Cell Metab* 10: 507–515, 2009.

98. **Matsuda N, Sato S, Shiba K, Okatsu K, Saisho K, Gautier C a., Sou Y -s., Saiki S, Kawajiri S, Sato F, Kimura M, Komatsu M, Hattori N, Tanaka K**. PINK1 stabilized by mitochondrial depolarization recruits Parkin to damaged mitochondria and activates latent Parkin for mitophagy. *J Cell Biol* 189: 211–221, 2010.

99. **McMahon M, Thomas N, Itoh K, Yamamoto M, Hayes JD**. Redox-regulated turnover of Nrf2 is determined by at least two separate protein domains, the redox-sensitive Neh2 degron and the redox-insensitive Neh6 degron. *J Biol Chem* 279: 31556–67, 2004.

100. **Medical SF, Francisco X**. Microsomal Heme Oxygenase. Characterization of the enzyme. *J Biol Chem* 244: 6388–6394, 1969.

101. **Miller CJ, Gounder SS, Kannan S, Goutam K, Muthusamy VR, Firpo M a, Symons JD, Paine R, Hoidal JR, Rajasekaran NS**. Disruption of Nrf2/ARE signaling impairs antioxidant mechanisms and promotes cell degradation pathways in aged skeletal muscle. *Biochim Biophys Acta* 1822: 1038–50, 2012.

102. **Mizushima N, Levine B, Cuervo AM, Klionsky DJ**. Autophagy fights disease through cellular self-digestion. *Nature* 451: 1069–1075, 2008.

103. **Mizushima N, Yamamoto A, Matsui M, Yoshimori T, Ohsumi Y**. In Vivo Analysis of Autophagy in Response to Nutrient Starvation Using Transgenic Mice Expressing a Fluorescent Autophagosome Marker. *Mol Biol Cell* 15: 1101–1111, 2004.

104. **Motohashi H, Connor TO, Katsuoka F, Douglas J, Yamamoto M**. Integration and diversity of the regulatory network composed of Maf and CNC families of transcription factors. *Gene* 294: 1–12, 2002.

105. **Motohashi H, Katsuoka F, Engel JD, Yamamoto M**. Small Maf proteins serve as transcriptional cofactors for keratinocyte differentiation in the Keap1 – Nrf2 regulatory pathway. *Proc Natl Acad Sci U S A* 101: 6379–6384, 2004.

106. **Motohashi H, Yamamoto M**. Nrf2-Keap1 defines a physiologically important stress response mechanism. *Trends Mol Med* 10: 549–57, 2004.

107. **Muller FL, Liu Y, Van Remmen H**. Complex III releases superoxide to both sides of the inner mitochondrial membrane. *J Biol Chem* 279: 49064–73, 2004.

108. **Munoz KA, Satarug S TM**. Time course of the response of myofibrillar and sarcoplasmic protein metabolism to unweighting of the soleus muscle. *Metabolism* 42: 1006–1012, 1993.

109. **Narendra D, Tanaka A, Suen D-F, Youle RJ**. Parkin is recruited selectively to impaired mitochondria and promotes their autophagy. *J Cell Biol* 183: 795–803, 2008.

110. **Nemoto S, Finkel T**. Redox Regulation of Forkhead Proteins Through a p66shc - Dependent Signaling Pathway. *Science (80-)* 295: 2450–2451, 2002.

111. **Nguyen T, Sherratt PJ, Nioi P, Yang CS, Pickett CB**. Nrf2 controls constitutive and inducible expression of ARE-driven genes through a dynamic pathway involving nucleocytoplasmic shuttling by Keap1. *J Biol Chem* 280: 32485–92, 2005.

112. **Ning Y, Li Z, Qiu Z**. FOXO1 silence aggravates oxidative stress-promoted apoptosis in cardiomyocytes by reducing autophagy. *J Toxicol Sci* 40: 637–645, 2015.

113. **Nioi P, Nguyen T, Sherratt PJ, Pickett CB**. The Carboxy-Terminal Neh3 Domain of Nrf2 Is Required for Transcriptional Activation. *Mol Cell Biol* 25: 10895–10906, 2005.

114. **Nogalska A, D'Agostino C, Terracciano C, Engel WK, Askanas V**. Impaired autophagy in sporadic inclusion-body myositis and in endoplasmic reticulum stress-provoked cultured human muscle fibers. *Am J Pathol* 177: 1377–87, 2010.

115. **Nogueira V, Park Y, Chen C-C, Xu P-Z, Chen M-L, Tonic I, Unterman T, Hay N**. Akt determines replicative senescence and oxidative or oncogenic premature senescence and sensitizes cells to oxidative apoptosis. *Cancer Cell* 14: 458–70, 2008.

116. **O'Neill HM, Maarbjerg SJ, Crane JD, Jeppesen J, Jørgensen SB, Schertzer JD, Shyroka O, Kiens B, van Denderen BJ, Tarnopolsky MA, Kemp BE, Richter EA SG**. AMP-activated protein kinase (AMPK) beta1beta2 muscle null mice reveal an essential role for AMPK in maintaining mitochondrial content and glucose uptake during exercise. *Proc Natl Acad Sci U S A* 108: 16092–16097, 2011.

117. **Olmos Y, Sánchez-Gómez FJ, Wild B, García-Quintans N, Cabezudo S, Lamas S, Monsalve M**. SirT1 regulation of antioxidant genes is dependent on the formation of a FoxO3a/PGC-1α complex. *Antioxid Redox Signal* 19: 1507–21, 2013.

118. **Otterbein LE, Bach FH, Alam J, Soares M, Tao Lu H, Wysk M, Davis RJ, Flavell RA CA**. Carbon monoxide has anti-inflammatory effects involving the mitogen-activated protein kinase pathway. *Nat Med* 6: 422–428, 2000.

119. **Pankiv S, Clausen TH, Lamark T, Brech A, Bruun J-A, Outzen H, Øvervatn A, Bjørkøy G, Johansen T**. p62/SQSTM1 binds directly to Atg8/LC3 to facilitate degradation of ubiquitinated protein aggregates by autophagy. *J Biol Chem* 282: 24131–45, 2007.

120. **Paul PK, Bhatnagar S, Mishra V, Srivastava S, Darnay BG, Choi Y, Kumar A**. The E3 ubiquitin ligase TRAF6 intercedes in starvation-induced skeletal muscle atrophy through multiple mechanisms. *Mol Cell Biol* 32: 1248–59, 2012.

121. **Paul PK, Gupta SK, Bhatnagar S, Panguluri SK, Darnay BG, Choi Y, Kumar A**. Targeted ablation of TRAF6 inhibits skeletal muscle wasting in mice. *J Cell Biol* 191: 1395–411, 2010.

122. **Pérez VI, Van Remmen H, Bokov A, Epstein CJ, Vijg J, Richardson A**. The overexpression of major antioxidant enzymes does not extend the lifespan of mice. *Aging Cell* 8: 73–5, 2009.

123. **Pette D SR**. Myosin isoform , muscle fiber types and transition. *Microsc Res Tech* 50: 500–509, 2000.

124. **Phillips SM, Glover EI, Rennie MJ**. Alterations of protein turnover underlying disuse atrophy in human skeletal muscle. *J Appl Physiol* 107: 645–54, 2009.

125. **Phillips SM**. A Brief Review of Critical Processes in Exercise-Induced Muscular Hypertrophy. *Sport Med* 44: 71–77, 2014.

126. **Piantadosi C a, Carraway MS, Babiker A, Suliman HB**. Heme oxygenase-1 regulates cardiac mitochondrial biogenesis via Nrf2-mediated transcriptional control of nuclear respiratory factor-1. *Circ Res* 103: 1232–40, 2008.

127. **Picard M, Gentil BJ, McManus MJ, White K, St Louis K, Gartside SE, Wallace DC, Turnbull DM**. Acute exercise remodels mitochondrial membrane interactions in mouse skeletal muscle. *J Appl Physiol* 115: 1562–71, 2013.

128. **Picard M, Ritchie D, Thomas MM, Wright KJ, Hepple RT**. Alterations in intrinsic mitochondrial function with aging are fiber type-specific and do not explain differential atrophy between muscles. *Aging Cell* 10: 1047–55, 2011.

129. **Polge C, Heng A-E, Jarzaguet M, Ventadour S, Claustre A, Combaret L, Béchet D, Matondo M, Uttenweiler-Joseph S, Monsarrat B, Attaix D, Taillandier D**. Muscle actin is polyubiquitinylated in vitro and in vivo and targeted for breakdown by the E3 ligase MuRF1. *FASEB J* 25: 3790–802, 2011.

130. **Powers SK, Ji LL, Kavazis AN, Jackson MJ**. Reactive oxygen species: impact on skeletal muscle. *Compr Physiol* 1: 941–69, 2011.

131. **Pradelli L a, Bénéteau M, Ricci J-E**. Mitochondrial control of caspase-dependent and -independent cell death. *Cell Mol life Sci* 67: 1589–97, 2010.

132. **Puigserver P, Rhee J, Lin J, Wu Z, Yoon JC, Zhang C, Krauss S, Mootha VK, Lowell BB, Spiegelman BM**. Cytokine Stimulation of Energy Expenditure through p38 MAP Kinase Activation of PPARgamma Coactivator-1. *Mol Cell* 8: 971–982, 2001.

133. **Quinlan CL, Perevoshchikova I V, Hey-Mogensen M, Orr AL, Brand MD**. Sites of reactive oxygen species generation by mitochondria oxidizing different substrates. *Redox Biol* 1: 304–12, 2013.

134. **Quinlan CL, Treberg JR, Perevoshchikova I V, Orr AL, Brand MD**. Native rates of superoxide production from multiple sites in isolated mitochondria measured using endogenous reporters. *Free Radic Biol Med* 53: 1807–17, 2012.

135. **Raineri I, Carlson EJ, Gacayan R, Carra S, Oberley TD, Huang TT EC**. Strain-dependent high-level expression of a transgene for manganese superoxide dismutase is associated with growth retardation and decreased fertility. *Free Radic Biol Med* 31: 1018–1030, 2001.

136. **Ran Q, Liang H, Ikeno Y, Qi W, Prolla TA, Ii LJR, Wolf N, Vanremmen H, Richardson A**. Reduction in Glutathione Peroxidase 4 Increases Life Span Through Increased Sensitivity to Apoptosis. *journals Gerontol Ser A, Biol Sci Med Sci Gerontol* 62: 932–942, 2007.

137. **Rangasamy T, Cho CY, Thimmulappa RK, Zhen L, Srisuma SS, Kensler TW, Yamamoto M, Petrache I, Tuder RM, Biswal S**. Genetic ablation of Nrf2 enhances susceptibility to cigarette smoke – induced emphysema in mice. *J Clin Invest* 114: 1248–1259, 2004.

138. **Roy RR, Monke SR, Allen DL, Edgerton VR**. Modulation of myonuclear number in functionally overloaded and exercised rat plantaris fibers. *J Appl Physiol* 87: 634–642, 1999.

139. **Rushmore TH, Morton MR, Pickett CB**. The Antioxidant Responsive Element ACTIVATION BY OXIDATIVE STRESS AND IDENTIFICATION OF REQUIRED FOR FUNCTIONAL ACTIVITY. *J Biol Chem* 266: 11632–11639, 1991.

140. **Rushmore, TH, Pickett C**. Transcriptional Subunit Gene Regulation of the Rat Glutathione. *J Biol Chem* 265: 14648–14653, 1990.

141. **Safdar A, deBeer J, Tarnopolsky M a**. Dysfunctional Nrf2-Keap1 redox signaling in skeletal muscle of the sedentary old. *Free Radic Biol Med* 49: 1487–93, 2010.

142. **Sakellariou GK, Jackson MJ, Vasilaki A**. Redefining the major contributors to superoxide production in contracting skeletal muscle . The role of NADPH oxidases. *Free Radic Res* 48: 12–29, 2014.

143. **Saleem A, Adhihetty PJ, Hood DA**. Role of p53 in mitochondrial biogenesis and apoptosis in skeletal muscle. *Physiol Genomics* 37: 58–66, 2009.

144. **Sandri M**. Protein breakdown in muscle wasting: role of autophagy-lysosome and ubiquitin-proteasome. *Int J Biochem Cell Biol* 45: 2121–9, 2013.

145. **Scarpulla RC**. Nuclear activators and coactivators in mammalian mitochondrial biogenesis. [Online]. *Biochim Biophys Acta* 1576: 1–14, 2002. http://www.ncbi.nlm.nih.gov/pubmed/12031478.

146. **Scarpulla RC**. Transcriptional Paradigms in Mammalian Mitochondrial Biogenesis and Function. *Physiol Rev* 88: 611–638, 2008.

147. **Scherz-Shouval R, Shvets E, Fass E, Shorer H, Gil L, Elazar Z**. Reactive oxygen species are essential for autophagy and specifically regulate the activity of Atg4. *EMBO J* 26: 1749–60, 2007.

148. **Schiaffino S, Hanzlíková V**. Studies on the Effect of Denervation in Developing Muscle II . The Lysosomal System. *J Ultrastruct Res* 39: 1–14, 1972.

149. **Schriner SE, Linford NJ, Martin GM, Treuting P, Ogburn CE, Emond M, Coskun PE, Ladiges W, Wolf N, Remmen H Van, Wallace DC, Rabinovitch PS**. Extension of Murine Life Span by Overexpression of Catalase Targeted to Mitochondria. *Science (80-)* 308: 1909–1912, 2005.

150. **Scorrano L**. Keeping mitochondria in shape: a matter of life and death. *Eur J Clin Invest* 43: 886–93, 2013.

151. **Seale P, Polesskaya A RM**. Adult Stem Cell Specification by Wnt Signaling in Muscle Regeneration. *Cell cycle* 2: 418–419, 2003.

152. **Shanely RA, Van Gammeren D, Deruisseau KC, Zergeroglu a M, McKenzie MJ, Yarasheski KE, Powers SK**. Mechanical ventilation depresses protein synthesis in the rat diaphragm. *Am J Respir Crit Care Med* 170: 994–999, 2004.

153. **Sherwin CM**. Voluntary wheel running : a review and novel interpretation. *Anim Behav* 56: 11–27, 1998.

154. **Siegel D, Bolton EM, Burr JA, Liebler DC, Ross D**. The Reduction of a-Tocopherolquinone by Human NAD(P)H : Quinone Oxidoreductase : The Role of a-Tocopherolhydroquinone as a Cellular Antioxidant. *Mol Pharmacol* 305: 300–305, 1997.

155. **Siegel D, Gustafson DL, Dehn DL, Han JY, Boonchoong P, Berliner LJ, Ross D**. NAD(P)H : Quinone Oxidoreductase 1 : Role as a Superoxide Scavenger. *Mol Pharmacol* 65: 1238–1247, 2004.

156. **Singh K, Hood DA**. Effect of denervation-induced muscle disuse on mitochondrial protein import. 3: 138–145, 2011.

157. **Stocker R, Yamamoto Y, Mcdonagh AF, Glazer AN, Ames BN**. Bilirubin is an Antioxidant of Possible Physiological Importance Author(s): Roland Stocker, Yorihiro Yamamoto, Antony F. McDonagh, Alexander N. Glazer and Bruce N. Ames Source: *Science (80-)* 235: 1043–1046, 1987.

158. **Stotland A, Gottlieb RA**. Mitochondrial quality control : Easy come , easy go. *Biochim Biophys Acta* 1853: 2802–2811, 2015.

159. **St-Pierre J, Drori S, Uldry M, Silvaggi JM, Rhee J, Jäger S, Handschin C, Zheng K, Lin J, Yang W, Simon DK, Bachoo R, Spiegelman BM**. Suppression of reactive oxygen species and neurodegeneration by the PGC-1 transcriptional coactivators. *Cell* 127: 397–408, 2006.

160. **St-Pierre J, Lin J, Krauss S, Tarr PT, Yang R, Newgard CB, Spiegelman BM**. Bioenergetic analysis of peroxisome proliferator-activated receptor gamma coactivators 1alpha and 1beta (PGC-1alpha and PGC-1beta) in muscle cells. *J Biol Chem* 278: 26597–603, 2003.

161. **Sun Z, Chin YE, Zhang DD**. Acetylation of Nrf2 by p300/CBP augments promoter-specific DNA binding of Nrf2 during the antioxidant response. *Mol Cell Biol* 29: 2658–72, 2009.

162. **Tait SWG, Green DR**. Mitochondria and cell signalling. *J Cell Sci* 125: 807–15, 2012.

163. **Takahashi M, Hood DA**. Protein Import into Subsarcolemmal and Intermyofibrillar Skeletal. *J Biol Chem* 271: 27285–27291, 1996.

164. **Tanaka A, Cleland MM, Xu S, Narendra DP, Suen D-F, Karbowski M, Youle RJ**. Proteasome and p97 mediate mitophagy and degradation of mitofusins induced by Parkin. *J Cell Biol* 191: 1367–80, 2010.

165. **Taylor ER, Hurrell F, Shannon RJ, Lin T-K, Hirst J, Murphy MP**. Reversible glutathionylation of complex I increases mitochondrial superoxide formation. *J Biol Chem* 278: 19603–10, 2003.

166. **Theodore M, Kawai Y, Yang J, Kleshchenko Y, Reddy SP, Villalta F, Arinze IJ**. Multiple nuclear localization signals function in the nuclear import of the transcription factor Nrf2. *J Biol Chem* 283: 8984–94, 2008.

167. **Tintignac L a, Lagirand J, Batonnet S, Sirri V, Leibovitch MP, Leibovitch S a**. Degradation of MyoD mediated by the SCF (MAFbx) ubiquitin ligase. *J Biol Chem* 280: 2847–56, 2005.

168. **Vainshtein A, Desjardins EM, Armani A, Sandri M, Hood D a**. PGC-1α modulates denervation-induced mitophagy in skeletal muscle. *Skelet Muscle* 5, 2015.

169. **Valle I, Alvarez-Barrientos A, Arza E, Lamas S, Monsalve M**. PGC-1alpha regulates the mitochondrial antioxidant defense system in vascular endothelial cells. *Cardiovasc Res* 66: 562–73, 2005.

170. **Vega RB, Huss JM KD**. The Coactivator PGC-1 Cooperates with Peroxisome Proliferator-Activated Receptor a in Transcriptional Control of Nuclear Genes Encoding Mitochondrial Fatty Acid Oxidation Enzymes. *Mol Cell Biol* 20: 1868–1876, 2000.

171. **Velichkova M, Hasson T**. Keap1 Regulates the Oxidation-Sensitive Shuttling of Nrf2 into and out of the Nucleus via a Crm1-Dependent Nuclear Export Mechanism Keap1 Regulates the Oxidation-Sensitive Shuttling of Nrf2 into and out of the Nucleus via a Crm1-Dependent Nuclear Export M. *Mol Cell Biol* 25: 4501–4513, 2005.

172. **Virbasius J V, Scarpulla RC**. Activation of the human mitochondrial transcription factor A gene by nuclear respiratory factors : A potential regulatory link between nuclear and mitochondrial gene expression in organelle biogenesis. *Proc Natl Acad Sci U S A* 91: 1309–1313, 1994.

173. **Wakabayashi N, Itoh K, Wakabayashi J, Motohashi H, Noda S, Takahashi S, Imakado S, Kotsuji T, Otsuka F, Roop DR, Harada T, Engel JD, Yamamoto M**. Keap1-null mutation leads to postnatal lethality due to constitutive Nrf2 activation. *Nat Genet* 35: 238–45, 2003.

174. **Wallberg AE, Yamamura S, Malik S, Spiegelman BM, Roeder RG**. Coordination of p300-Mediated Chromatin Remodeling and TRAP / Mediator Function through Coactivator PGC-1a. *Mol Cell* 12: 1137–1149, 2003.

175. **Wang G, Hamid T, Keith RJ, Zhou G, Partridge CR, Xiang X, Kingery JR, Lewis RK, Li Q, Rokosh DG, Ford R, Spinale FG, Riggs DW, Srivastava S, Bhatnagar A, Bolli R, Prabhu SD**. Cardioprotective and antiapoptotic effects of heme oxygenase-1 in the failing heart. *Circulation* 121: 1912–25, 2010.

176. **Wang H, Liu K, Geng M, Gao P, Wu X, Hai Y, Li Y, Li Y, Luo L, Hayes JD, Wang XJ, Tang X**. RXRα inhibits the NRF2-ARE signaling pathway through a direct interaction with the Neh7 domain of NRF2. *Cancer Res* 73: 3097–108, 2013.

177. **Wang X, Blagden C, Fan J, Nowak SJ, Taniuchi I, Littman DR, Burden SJ**. Runx1 prevents wasting , myofibrillar disorganization , and autophagy of skeletal muscle. *Genes Dev* 19: 1715–1722, 2005.

178. **Wenz T, Rossi SG, Rotundo RL, Spiegelman BM, Moraes CT**. Increased muscle PGC-1alpha expression protects from sarcopenia and metabolic disease during aging. *Proc Natl Acad Sci U S A* 106: 20405–20410, 2009.

179. **Winder WW, Holmes BF, Rubink DS, Jensen EB, Chen M, Holloszy JO**. Activation of AMP-activated protein kinase increases mitochondrial enzymes in skeletal muscle. *J Appl Physiol* 88: 2219–2226, 2000.

180. **Wu Z, Puigserver P, Andersson U, Zhang C, Adelmant G, Mootha V, Troy a, Cinti S, Lowell B, Scarpulla RC, Spiegelman BM**. Mechanisms controlling mitochondrial biogenesis and respiration through the thermogenic coactivator PGC-1. *Cell* 98: 115–24, 1999.

181. **Yan Z, Lira VA GN**. Exercise training-induced regulation of mitochondrial quality. *Exerc Sport Sci Rev* 40: 159–164, 2012.

182. **Zhang DD, Hannink M**. Distinct Cysteine Residues in Keap1 Are Required for Keap1-Dependent Ubiquitination of Nrf2 and for Stabilization of Nrf2 by Chemopreventive Agents and Oxidative Stress Distinct Cysteine Residues in Keap1 Are Required for Keap1-Dependent Ubiquitination of. *Mol Cell Biol* 23: 8137–8151, 2003.

183. **Zhang Y, Uguccioni G, Ljubicic V, Irrcher I, Iqbal S, Singh K, Ding S, Hood DA**. Multiple signaling pathways regulate contractile activity-mediated PGC-1α gene expression and activity in skeletal muscle cells. *Physiol Rep* 2: 1–12, 2014.

184. **Zhao J, Brault JJ, Schild A, Cao P, Sandri M, Schiaffino S, Lecker SH, Goldberg AL**. FoxO3 coordinately activates protein degradation by the autophagic/lysosomal and proteasomal pathways in atrophying muscle cells. *Cell Metab* 6: 472–83, 2007.

185. **Zhu H, Li Y**. NAD(P)H: quinone oxidoreductase 1 and its potential protective role in cardiovascular diseases and related conditions. *Cardiovasc Toxicol* 12: 39–45, 2012.

186. **Zipper LM, Mulcahy RT**. The Keap1 BTB/POZ dimerization function is required to sequester Nrf2 in cytoplasm. *J Biol Chem* 277: 36544–52, 2002.

Chapter 2: Manuscript

(Submitted to Journal of Applied Physiology for publication)

The role of Nrf2 in skeletal muscle phenotype and mitochondrial function

Matthew J. Crilly, Liam D. Tryon and David A. Hood

School of Kinesiology and Health Science, York University
Toronto, Ontario, M3J 1P3, Canada

Muscle Health Research Centre, York University
Toronto, Ontario, M3J 1P3, Canada

Running Title: Nrf2 function in muscle

Key Words: Mitochondrial biogenesis, exercise, endurance training, contractile properties, endurance performance

To whom correspondence should be addressed: David A. Hood
School of Kinesiology
York University, Toronto, ON
M3J 1P3, Canada

Abstract

Nuclear factor erythroid 2–related factor 2 (Nrf2) is a transcription factor that confers cellular protection by upregulating antioxidant enzymes in response to oxidative stress. However, Nrf2 function within skeletal muscle remains to be elucidated. Thus, we examined the role of Nrf2 in mediating changes in skeletal muscle phenotype using Nrf2 wild-type (WT) and knockout (KO) mice at 3 and 12 months of age. Basally, Nrf2 did not impact muscle mitochondrial content in young and older animals. In IMF mitochondria, lack of Nrf2 resulted in a 40% reduction in state 4 respiration, which coincided with a 68% increase in ROS production. Nrf2 abrogation impaired *in situ* muscle performance, characterized by a 48% greater rate of fatigue, and a 35% decrease in force production within the first 5 minutes of stimulation. Acute treadmill exercise resulted in a 1.5-fold increase in Nrf2 activation, via enhanced DNA binding in WT animals. In response to training COX activity increased by 20% in the WT animals, however this response was attenuated in the KO mice. Despite this, exercise training was capable of normalizing respiration, ROS production and muscle endurance performance to that found in WT levels. Interestingly, antioxidant enzyme expression did not differ between genotypes regardless of training status or age, indicating alternative regulatory mechanisms. Our results suggest that Nrf2-mediated transcriptional activity is increased by acute exercise and that Nrf2 is required for normal exercise-induced adaptations in mitochondrial content, but that improvements in mitochondrial function resulting from exercise appear to be Nrf2-independent.

Introduction

Eukaryotic organisms are constantly challenged by an array of both endogenous and exogenous insults that can alter the redox balance of the cell. Therefore, in order to combat these insults, cells have evolved an elaborate network of proteins that confer cellular protection by augmenting their expression in response to disturbances in oxidative stress. Nuclear factor erythroid 2–related factor 2 (Nrf2) is a transcription factor that has a pivotal role in mediating this intracellular antioxidant response since it upregulates the expression of numerous antioxidant and phase II detoxification enzymes, in response to increases in oxidative stress (30). Mice deficient for Nrf2 exhibit a marked reduction in the expression of these enzymes, consequently increasing their sensitivity to the toxic effects of various drugs (12) and chemical compounds (32). The inability of these mice to initiate a response that counteracts the adverse effects of oxidative stress illustrates the importance of Nrf2 in maintaining cellular redox homeostasis.

Under quiescent conditions, the Nrf2 signaling pathway is negatively regulated by Kelch-like ECH associating protein 1 (Keap1). Keap1 constitutively targets Nrf2 for ubiquitin conjugation and subsequent proteasome degradation in the cytoplasm by acting as a substrate adaptor for the Cul3-based E3 ubiquitin ligase complex (10, 19). Due to the negative regulatory system of Keap1, Nrf2 is rapidly turned over, with a half-life of less than 20 minutes (19). However, increases in oxidative stress promote the activation and stabilization of Nrf2. Nrf2 activation is thought to involve the modification of the sulfhydryl groups of specific cysteine residues found within the linker region of Keap1, which results in a conformational change that alters the binding capacity of Keap1 with Nrf2 (20, 43). In turn, this promotes the translocation of Nrf2 to the nucleus where it can

interact and form heterodimers with small Maf proteins (16, 17), recruit transcriptional coactivators (38, 40) to help remodel chromatin structure, and bind to the antioxidant response element (ARE) found within the promoter region of target genes (30). The fact that Keap1 contains distinct cysteine residues (43) that can be targeted and modified by electrophiles, reactive oxygen species (ROS) or antioxidant response element-inducers, suggests that the Keap1-Nrf2 interaction functions as a sensor of the redox state of the cell.

While it is well-established that Nrf2 is important for antioxidant expression, emerging evidence also suggests that Nrf2 signaling protects the structure and function of skeletal muscle, in part, through the preservation of redox homeostasis. For instance, Safdar et al. (34) reported a significant decrease in nuclear Nrf2 expression in elderly humans leading a sedentary lifestyle, while recreationally active individuals exhibited improved Nrf2 function. Disruption of Nrf2 has also been shown to induce oxidative stress resulting in greater ubiquitination, lipid peroxidation and pro-apoptotic signals in skeletal muscle of aged Nrf2 KO mice (25). Further, aged Nrf2 KO mice also demonstrate impaired muscle regeneration following acute endurance exercise stress due to a decrease in Pax7 and MyoD expression (29). Interestingly, Nrf2 has also been implicated in regulating mitochondrial content (31) and function (15, 18) in some cell types. The work conducted by Piantadosi et al. (31) revealed that nuclear respiratory factor 1 (NRF-1) contains multiple ARE's within its promoter that become occupied by Nrf2 upon induction by ROS. Exhaustive exercise has also been shown to be a particular stressor capable of inducing Nrf2 activation, nuclear accumulation and ARE-binding within cardiomyocytes (28). However, the role of Nrf2 in mediating changes in

mitochondrial content and function in skeletal muscle remains to be elucidated. Therefore, the purpose of our study was to examine the role of Nrf2 within skeletal muscle, its impact on mitochondrial content, and its relationship to exercise performance in young and middle-aged mice. Furthermore, we also subjected both Nrf2 wild-type (WT) and knockout (KO) animals to a six-week training protocol to determine if Nrf2 was required for mitochondrial biogenesis in skeletal muscle.

Methods

Animals. Nrf2 KO and heterozygous mice (maintained on a C57BL/6J background) were obtained from the Jackson Laboratory (Bar Harbor, Maine, USA). Animals were bred in accordance with the guidelines of the York University Animal Care Committee. Progeny were genotyped by obtaining ear clippings, which were subsequently used for crude DNA extraction. DNA extracts were incubated with Jumpstart RED-Taq DNA polymerase (Sigma; St. Louis, Missouri, USA), as well as forward and reverse primers specific to the wildtype or mutant nucleotide sequences, and amplified using polymerase chain reaction (PCR). The reaction products were separated on a 1.0% agarose gel, and visualized with the use of ethidium bromide. Nrf2 WT and KO animals were used at 3 and 12 months of age.

Voluntary wheel running. At 3 months of age, Nrf2 WT and KO mice were aged matched and assigned to a control or running group. The mice were housed individually, allowed access to food and water ad libitum, and kept on a 12:12-h light-dark cycle. Runners had access to a freely rotating wheel, while the revolutions were recorded by a magnetic counter. The number of revolutions was recorded every 24 hours and converted into distance (kilometres) per day. The duration of the training protocol was ~6-8 weeks.

Following the training protocol mice were subjected to an endurance exercise capacity test and *in situ* stimulation for further performance analysis.

***Acute In situ muscle stimulation*.** The stimulation protocol was performed as described previously (36). Briefly, the sciatic nerve of the gastrocnemius muscle from one leg was stimulated at 0.25 tetanic contractions per second (TPS), 0.5 TPS and 1 TPS for 3 minutes each.

These intensities were sufficient to induce moderate and more severe muscle fatigue, respectively. Following the *in situ* stimulation protocol, the stimulated muscle was excised, quickly frozen and weighed.

***COX activity*.** COX enzyme activity was measured as previously described (41) by determining the maximal rate of oxidation of fully reduced cytochrome c, evaluated as a change in absorbance at 550 nm using a microplate reader (Bio-Tek synergy HT, BioTek Instruments, Inc., Winooski, VT, USA).

Immunoblotting. Whole muscle protein extracts from the gastrocnemius muscle were separated using SDS-PAGE and subsequently transferred onto a nitrocellulose membrane. Following the transfer, the membranes were blocked for 1 hour with a solution of 5% skim milk in 1X TBST (Tris-buffered saline-Tween 20: 25 mM Tris·HCl, pH 7.5, 1 mM NaCl, and 0.1% Tween 20). Membranes were then incubated overnight at 4°C with antibody directed against HO-1 **(**Abcam, ab13248), NQO1 (Abcam, ab34173), G6PD (Cell Signaling, 8866) and GPx1 (Abcam, ab22604). After three 5 minute washes with TBST, blots were incubated at room temperature for 1 hour with the appropriate secondary antibody coupled with horseradish peroxidase. Antibody-bound protein was revealed using the enhanced chemiluminescence method. Quantification was performed

with Image J Software (NIH, Bethesda, MD, USA), and values were normalized to the appropriate loading controls.

Mitochondrial isolation. The tibialis anterior, gastrocnemius, quadriceps and triceps muscles from both sides of the animal were minced, homogenized and subjected to differential centrifugation to isolate SS and IMF mitochondrial fractions, as described previously (8). Mitochondria were suspended in resuspension buffer (100 mM KCl, 10 mM MOPS, and 0.2% BSA). Following the isolation procedure, SS and IMF were used to assess mitochondrial respiration and reactive oxygen species (ROS) production.

Mitochondrial Respiration. Fifty microliters of isolated mitochondrial samples were incubated with 250 μl of VO_2 buffer (in mM: 250 sucrose, 50 KCl, 25 Tris, and 10 K2HPO4, pH 7.4) in a Clark oxygen electrode respiratory chamber (Strathkelvin Instruments, North Lanarkshire, Scotland) with continuous stirring at 30°C. Mitochondrial oxygen consumption was measured in the presence of exogenously added 10 mM glutamate to assess state 4 respiration followed by 0.44 mM ADP to elicit state 3 respiration. Finally, NADH was added during state 3 measurements to evaluate the integrity of the inner mitochondrial membrane.

Mitochondrial ROS production. SS and IMF mitochondria (75μg) were incubated with 50 μM dichlorodihydrofluorescein diacetate (H2DCF-DA) and VO_2 buffer at 37°C for 30 min in a white polystyrene 96-well plate. The fluorescence emission (between 485 and 528 nm) is directly proportional to ROS production and was measured with a Synergy HT microplate reader. ROS production was assessed under both state 4 and state 3 respiration.

Nrf2 activation assay. Nrf2 activation and antioxidant response element binding efficacy under both basal and acute exercise stress conditions were evaluated in WT and KO mice using nuclear extracts obtained from the TA muscle, using a Trans AM Nrf2 kit (50296, Active Motif, Carlsbad, CA). A 10μg aliquot of nuclear protein was incubated with immobilized oligonucleotides containing the ARE consensus binding site (5′GTCACAGTACTCAGCAGAATCTG-3’**)**. Active Nrf2 that bound to the oligo was detected with the Nrf2 primary antibody and subsequent HRP-conjugated secondary antibody. Specific activity of Nrf2 in the nuclear extracts was determined using a plate reader at 450 nm, and absorbance was expressed as the direct activity of Nrf2.

Endurance exercise capacity test. Nrf2 WT and KO mice were acclimated to the treadmill for two days prior to the test. On the exercise testing day, the mice ran on the treadmill with a fixed slope of 10%. Mice ran for 5m/min for 5 minutes followed by 10m/min for 10 minutes, 15m/min for 15 minutes and 20m/min for 20 minutes. The speed was then increased by 2m/min every 2 minutes until exhaustion was achieved. Exhaustion was defined as the inability of the animal to run on the treadmill for 10 seconds despite prodding.

Nuclear and cytosolic fractionation. Immediately following the endurance exercise capacity test, the TA muscle was immediately removed and placed into ice-cold phosphate buffered saline with protease inhibitors. Nuclear and cytosolic fractionation was conducted using the NE-PER Nuclear and Cytoplasmic Extraction Reagents kit (Thermo Fisher Scientific) according to the manufacturer’s protocol.

Statistical Analysis. Data were analyzed using Graphpad 6.0 software. Values are reported as means ± SEM. A Student’s T-Test was used to analyze the Nrf2 activation

assay and comparisons between slopes during the initial two-minutes of *in situ* stimulation. State 4 and state 3 respiration and ROS were analyzed using an ANOVA. All other data were analyzed with a 2-Way ANOVA unless otherwise indicated. Significance levels were set at $P<0.05$ using a Bonferonni post-hoc test.

Results

Response of Nrf2KO mice to voluntary exercise. To evaluate the effect of Nrf2 on exercise-induced adaptations, both WT and KO mice were subjected to six-weeks of voluntary running wheel exercise training. Throughout the six week period, the WT and KO mice exhibited no differences in running performance, as both genotypes averaged ~11 km/day (Fig. 1A). Body mass and gastrocnemius weight were evaluated in the WT and KO mice at 3 and 12 months of age, respectively, to determine the effect of training, or age. There was no effect of training or genotype on body mass (Fig. 1B) or gastrocnemius mass (Fig. 1C). Although the WT and KO mice at 12 months of age did not differ from each other in body mass, the older animals had a ~38% greater body mass relative to their younger counterparts, and they displayed a ~19% reduction in gastrocnemius mass. These results indicate that the Nrf2 KO mice do not differ from their WT counterparts in their voluntary running performance or phenotypic traits at 3 and 12 months of age.

Endurance performance of Nrf2 KO mice following 6 weeks of wheel running. Following the six-weeks of voluntary wheel running we assessed the exercise tolerance of WT and KO mice by subjecting them to an endurance exercise capacity test. Untrained Nrf2 KO mice exhibited a similar running distance and time to exhaustion to their WT counterparts (Figs. 2A, 2B). In addition, both genotypes adapted equally well to training, with 109% and 134% increases in running distance in the KO and WT mice, respectively.

As expected, the WT and KO older animals displayed attenuated endurance capacities, characterized by 28% and 17% lower distances and times to exhaustion, relative to the young untrained mice. Lactate levels were elevated from approximately 2 mM at rest, to 7-11 mM following exercise. There were no effects of age, training status or genotype on lactate levels (Fig. 2C).

In situ stimulation and force production. To further evaluate the role of Nrf2 in force generation and fatigability in isolated muscle, we stimulated the gastrocnemius-plantaris-soleus muscle group *in situ* in anesthetized mice at 0.25, 0.50 and 1 TPS (Fig. 3A). Maximum tetanic force, time to peak tension and half relaxation were similar in all groups (Table 1). However, within the first two minutes of stimulation, the KO untrained animals demonstrated a 48% greater rate of fatigue ($p<0.05$) relative to the WT untrained animals (Fig. 3B). Indeed, the untrained KO mice demonstrated significantly increased rates of fatigue as determined by lower force generation at both the 5 and 9 minute time points (Figs. 3C, 3D). Endurance training abolished this defect and normalized the fatigue in the KO animals to that found in WT untrained animals. Collectively, these results suggest that Nrf2 is important for the maintenance of fatigue resistance in skeletal muscle.

Adaptability of Nrf2 KO mice following 6 weeks of wheel running. To investigate whether differences in muscle fatigability could be attributed to changes in mitochondrial content, and to evaluate whether Nrf2 was required for mitochondrial adaptations to exercise, we measured COX activity, a well-established biochemical indicator of mitochondrial volume. There was no observed difference in COX activity between the WT and KO animals at either 3 or 12 months of age (Fig. 4A). While training enhanced

COX activity by 20% in the WT animals, this increase was only 10% in the KO mice, suggesting that Nrf2 could be required for exercise-induced mitochondrial adaptations. To verify this further, we used immunoblotting to measure alternative mitochondrial markers (Fig. 4B). Thus, we also probed for COXI (Figs. 4B, 4C) and COXIV (Figs. 4B, 4D) in whole muscle samples as an ancillary measure of mitochondrial content, however, no effect of genotype or training was observed. However, a significant increase in TFAM expression in the trained animals relative to their untrained counterparts was noted in both WT and KO animals (Fig. 4E). Surprisingly, TFAM expression was significantly higher overall in KO animals. Thus, Nrf2 is involved in exercise-induced mitochondrial biogenesis in a protein-specific manner. This involvement would imply that Nrf2 could be activated during exercise. To verify this in response to an exhaustive bout of exercise, we utilized nuclear extracts from WT tibialis anterior muscle at 3 months of age in an ARE-oligonucleotide-based transactivation assay. Following the exhaustive bout of exercise, skeletal muscle Nrf2 activity was significantly increased (1.5-fold) compared to the sedentary WT mice (Fig. 4F). These results suggest that exercise is capable of increasing Nrf2-DNA binding and transcriptional activity in skeletal muscle.

Respiration and ROS production. To determine if the absence of Nrf2 has an effect on respiration or ROS production, we isolated both the subsarcolemmal (SS) and intermyofibrillar (IMF) mitochondria. Lack of Nrf2 did not affect either state 4 or state 3 respiration rates in SS mitochondria (Fig. 5A). However, state 4 respiration in IMF mitochondria was reduced by 40% in the untrained KO animals relative to WT controls (Fig. 5B). Six weeks of voluntary wheel running completely rescued this effect, and augmented state 3 respiration rates by 33% ($p<0.05$). In addition, although no differences

were observed in the SS mitochondria (Fig. 5C), ROS production in IMF mitochondria was particularly affected by the loss of Nrf2. Under state 4 conditions we observed a 68% ($p<0.05$) increase in ROS in the KO untrained animals compared to the WT animals (Fig. 5D). Training was sufficient to rescue this response in the KO animals. Taken together, these results indicate that the SS and IMF mitochondria respond differently to the loss of Nrf2. In particular, IMF mitochondria exhibit a greater dependence on Nrf2-driven gene expression for the maintenance of basal respiration rates.

Compositional differences in isolated IMF mitochondria following training. To determine if compositional differences account for some of the functional discrepancies between the WT and KO IMF mitochondria we measured different electron transport chain (ETC) subunits as well as TFAM. Interestingly, we did not observe any difference in either COXI or COXIV protein expression (Fig. 6A). However, we did observe a main effect of training regarding UQCRC2 (Fig. 6B) and TFAM expression (Fig. 6C).

Antioxidant enzyme expression. To assess whether Nrf2-deficiency influenced the levels of key antioxidant enzymes, we examined NQO1, HO-1, G6PD and GPx1 protein levels in muscle since these are well-established downstream targets of Nrf2 identified in other tissues. Abrogation of Nrf2 resulted in significant reductions in NQO1 protein expression (Fig. 7A). Training could not rescue this effect in the KO animals, indicating that NQO1 expression is heavily reliant on the presence of Nrf2 under both basal and stressful conditions. Curiously, despite the reductions observed in NQO1, we did not find any differences in the level of other Nrf2 targets in muscle between WT and KO animals (Figs 7B, 7C, 7D).

Differences in antioxidant enzyme expression with age. To investigate whether the lack of effect of Nrf2 KO on antioxidant enzyme expression was influenced by age, we compared young and older animals. Interestingly, we observed a 45% increase ($p<0.05$) in NQO1 expression in the older WT animals compared to the young (Fig. 8A). However, significant reductions in NQO1 continued to be observed in the older KO animals. Conversely, HO-1 expression was increased 62% ($p<0.05$) in the older KO animals relative to the WT young mice (Fig. 8B). Age and genotype did not influence the expression of either G6PD or GPx1 (Figs 8C, 8D).

Discussion

Exercise is a potent stimulus and metabolic stressor that is capable of provoking adaptations in skeletal muscle which allow it to meet repeated increases in metabolic demand. One of the most dramatic phenotypic adaptations that occurs in response to exercise training is the increase in mitochondrial content and ultrastructure, a process commonly referred to as mitochondrial biogenesis. Although mitochondrial regulation depends on the interplay between transcription factors such as NRF-1/2, PPARα, ERRα and Sp1, in addition to members of the PGC-1 family of regulated coactivators (PGC-1α and PGC-1β) (37), the role of Nrf2 in regulating mitochondrial content and function within skeletal muscle has not been established. Through a wealth of experimental evidence, the prevailing view of Nrf2 is that it sits at the crux of cellular defense mechanisms that are important for adaptive and survival responses under conditions of stress (7, 11, 30, 42). However, it is becoming apparent that Nrf2 has a much broader function since it has emerging roles in metabolism, bioenergetics, skeletal muscle integrity as well as mitochondrial content and function (15, 18, 25, 26, 29, 31, 34, 39,

42). For instance, genetic deletion of Nrf2 in mouse liver leads to a reduction in mitochondrial content (44) . In embryonic fibroblast, loss of Nrf2 was shown to impair mitochondrial respiration, resulting in a greater reliance on glycolysis for ATP generation (15). It has also been demonstrated in cultured cells that Nrf2 knockout affects the efficiency of mitochondrial fatty acid oxidation (24) and increases the susceptibility of mitochondria to the permeability transition (39). Our data also suggest that Nrf2 is required for basal mitochondrial function since the ablation of Nrf2 impaired state 4 respiration rates of IMF mitochondria in muscle from KO animals by 40%, and ROS emission in the IMF mitochondria was significantly elevated in the null animals during state 4 conditions. These results are in accordance with those obtained in MEFs (15) and cortical neurons (21). However, abrogation of Nrf2 did not result in an increase in ROS production within the myocardium (28) suggesting that there may be tissue-specific differences in the dependence of mitochondrial function of Nrf2. Although we did not observe any compositional differences in the IMF mitochondria of WT and KO animals using a limited number of organelle markers, it is possible that changes in mitochondrial respiration and ROS production could be due to differences in uncoupling protein 3 (UCP3) expression. Anedda et al. (5) identified an ARE within the UCP3 promoter that bound Nrf2 after exposure to H_2O_2. Furthermore, siRNA against Nrf2 prevented the H_2O_2 – induced UCP3 expression, which culminated in an increase in oxidative stress and cell death. Indeed, we have previously shown that UCP3 content is 1.3-fold greater in IMF compared with SS mitochondria, which may partially explain the dissimilar effects of Nrf2 abrogation on mitochondrial function between the two subfractions (22).

Given the impact of Nrf2 on mitochondrial function, we sought to investigate the exercise tolerance of the KO animals by subjecting them to an exhaustive run at both 3 and 12 months of age. Interestingly, the untrained KO mice displayed comparable distances and times to exhaustion, as well as similar lactate production relative to their WT counterparts. While, the reductions in endurance capacity evident in the 12 month old animals are consistent with the notion that older animals typically display lower endurance and greater rates of fatigue (23), the absence of Nrf2 did not hinder running performance even at an older age. The lack of any difference in endurance capacity between the young untrained WT and KO animals is likely because active (state 3) respiration was comparable between the two genotypes. Given that mitochondrial respiration during aerobic contractile activity likely reflects rates similar to state 3 respiration *in vitro*, this suggests that the KO mice would not have experienced a functional deficit in ATP provision sufficient enough to inhibit their running capacity. Interestingly, this did not translate into identical muscle performance when we investigated the contractile properties of skeletal muscle of Nrf2 WT and KO mice *in situ*. Our findings demonstrated that while there was no difference in the maximal strength of the muscle, the endurance capacity of Nrf2 KO skeletal muscle was reduced. This difference between whole body and isolated muscle performance characteristics may be due to behavioural differences between WT and KO mice. Muramatsu et al. (27) have argued that dopaminergic and serotonergic neurotransmission is enhanced in the KO animals, which increases their ability to resist stress. Therefore, the use of the *in situ* muscle preparation was advantageous in eliminating whole body exercise effects, ultimately allowing us to delineate any inherent differences in muscle contractile activity.

The greater rate of fatigue observed in the untrained KO animals may be partially attributed to high levels of ROS exposure. Indeed, we did observe a profound increase in mitochondrially-derived ROS in the KO animals. Additionally, Kovac et al. (21) found that NADPH oxidase 2 (NOX2) is dramatically upregulated under conditions of Nrf2-deficiency. Recently, it has been argued that the NOX enzymes are the major ROS generating source in contracting skeletal muscle (35). We speculate that an increase in ROS generation, partly as a result of mitochondrial dysfunction, may have promoted alterations in myofilament structure and function (6, 9, 14), diminished myofilament calcium sensitivity (3, 4), or influenced cross-bridge kinetics (4), leading to a greater rate of fatigue.

While evidence pertaining to the importance of Nrf2 for mitochondrial function is beginning to accumulate, no research has been devoted to understanding the relationship between Nrf2 in muscle during stressful conditions. Research conducted by Piantadosi et al. (31) revealed that in response to increases in ROS, Nrf2 translocates to the nucleus and occupies several ARE's within the NRF-1 promoter. These findings, along with our observation that exercise can activate Nrf2 in skeletal muscle, suggest that Nrf2 may participate in the signaling events that culminate in the expansion of the mitochondrial reticulum with exercise training. The exercise-induced activation of Nrf2 is likely mediated by an increase in ROS production, since previous reports have shown that ROS can be a primary trigger promoting the dissociation of Nrf2 from Keap1, resulting in an increase in nuclear translocation and transcription of putative targets (19, 20, 33, 43).

To explicitly explore the relationship between Nrf2 and mitochondrial content we subjected WT and KO animals to six weeks of voluntary wheel running. Basally, we did

not observe any difference in COX activity between the two genotypes at either 3 or 12 months of age. However, significant training-induced increases in COX activity were only observed in the WT animals, suggesting that Nrf2 is required for exercise-induced increases in the activity of this terminal enzyme of the electron transport chain. However, Nrf2 did not appear to be required for the training-induced increases in TFAM or UQCRC2. Thus, Nrf2 appears to be required for the exercise-induced increases in only a subset of mitochondrial proteins. Interestingly, despite the blunted change in COX activity, training augmented the respiratory deficit which was evident in the absence of Nrf2, ultimately restoring it to WT levels. This suggests that Nrf2 is required for the normal, stoichiometric protein adaptations in response to training, but is not required for the associated improvements in organelle function. Similar results have been reported by our laboratory using PGC-1α KO animals, whereby training elicited improvements in respiration back to normal levels despite, the absence of PGC-1α (2). Therefore, chronic exercise training likely stimulates alternative regulatory proteins that are capable of augmenting respiration to compensate for the blunted increase in mitochondrial content observed with the absence of Nrf2.

One of our most striking findings was the marked reduction in NQO1 expression in the Nrf2 null animals, a result suggesting that the primary regulation of NQO1 is Nrf2-dependent. NQO1 is an oxidoreductase which is typically located within the cytoplasm. These drastic reductions in NQO1 could predispose the KO animals to metabolic abnormalities, since NQO1-deficient mice exhibit higher levels of hepatic triglycerides and are insulin resistant (13). In addition, low NQO1 expression can have ramifications for the stability of PGC-1α, since NQO1 appears to be critical for the protection and

stabilization of both basal and physiologically-induced PGC-1α protein (1). Interestingly, its low expression in Nrf2 KO animals was not rescued by endurance training, suggesting that improvements in metabolic conditions associated with NQO1 deficiency would likely benefit more from pharmacological interventions.

In summary, our results suggest that Nrf2-mediated transcriptional activity is increased by acute exercise, and that Nrf2 is required for normal, exercise-induced adaptations in mitochondrial proteins. Chronic exercise rescued the deficits in respiration in an Nrf2-independent manner. We speculate that this effect of exercise may be due to a compensatory upregulation of alternative regulatory proteins which impact the expression of functional mitochondrial components in the absence of Nrf2, highlighting the ability of exercise training to activate a broad array of signaling pathways leading to physiological adaptations.

Grants

This work was supported by funding from the Natural Sciences and Engineering Research Council of Canada (NSERC) to D.A. Hood. D.A Hood holds a Canada Research Chair in Cell Physiology.

Disclosures

No conflicts of interest, financial or otherwise, are declared by the authors.

Author contributions

M.J.C and L.D.T performed the experiments; M.J.C analyzed the data; M.J.C and D.A.H interpreted the results of the experiments; M.J.C prepared the figures; M.J.C and D.A.H drafted, edited and revised the manuscript; M.J.C, L.D.T and D.A.H approved the final version of the manuscript; D.A.H developed the concept and research design.

References

1. **Adamovich Y, Shlomai A, Tsvetkov P, Umansky KB, Reuven N, Estall JL, Spiegelman BM, Shaul Y**. The protein level of PGC-1α, a key metabolic regulator, is controlled by NADH-NQO1. *Mol Cell Biol* 33: 2603–2613, 2013.

2. **Adhihetty PJ, Uguccioni G, Leick L, Hidalgo J, Pilegaard H, Hood DA**. The role of PGC-1alpha on mitochondrial function and apoptotic susceptibility in muscle. *Am J Physiol Cell Physiol* 297: 217–225, 2009.

3. **Andrade FH, Reid MB, Allen DG, Westerblad H**. Effect of hydrogen peroxide and dithiothreitol on contractile function of single skeletal muscle fibres from the mouse. *J Physiol* 509: 565–575, 1998.

4. **Andrade FH, Reid MB, Westerblad H**. Contractile response of skeletal muscle to low peroxide concentrations: myofibrillar calcium sensitivity as a likely target for redox-modulation. *FASEB* 15: 309–11, 2001.

5. **Anedda A, López-Bernardo E, Acosta-Iborra B, Saadeh Suleiman M, Landázuri MO, Cadenas S**. The transcription factor Nrf2 promotes survival by enhancing the expression of uncoupling protein 3 under conditions of oxidative stress. *Free Radic Biol Med* 61: 395–407, 2013.

6. **Callahan LA, Nethery D, Stofan D, Dimarco A, Supinski G**. Free Radical – Induced Contractile Protein Dysfunction in Endotoxin-Induced Sepsis. *Am J Respir Cell Mol Biol* 24: 210–7, 2001.

7. **Chan K, Kan YW**. Nrf2 is essential for protection against acute pulmonary injury in mice. *Proc Natl Acad Sci U S A* 96: 12731–12736, 1999.

8. **Cogswell AM, Stevens RJ, Hood DA**. Properties of skeletal muscle mitochondria from subsarcolemmal and intermyofibrillar isolated regions. *Am J Physiol* 264: C383–389, 1993.

9. **Crowder M, Cooke R**. The effect of myosin sulphydryl modification on the mechanics of fibre contraction. *J Muscle Res Cell Motil* 5: 131–146, 1984.

10. **Cullinan S, Gordan J, Jin J, Harper J, Diehl J**. The Keap1-BTB Protein Is an Adaptor That Bridges Nrf2 to a Cul3-Based E3 Ligase : Oxidative Stress Sensing by a Cul3-Keap1 Ligase The Keap1-BTB Protein Is an Adaptor That Bridges Nrf2 to a Cul3-Based E3 Ligase : Oxidative Stress Sensing by a Cul3-Keap1 Li. *Mol Cell Biol* 24: 8477–8486, 2004.

11. **Cullinan SB, Zhang D, Hannink M, Arvisais E, Kaufman RJ, Diehl JA**. Nrf2 Is a Direct PERK Substrate and Effector of PERK-Dependent Cell Survival. *Mol Cell Biol* 23: 7198–7209, 2003.

12. **Enomoto A, Itoh K, Nagayoshi E, Haruta J, Kimura T, Connor TO**. High Sensitivity of Nrf2 Knockout Mice to Acetaminophen Hepatotoxicity Associated with Decreased Expression of ARE- Regulated Drug Metabolizing Enzymes and Antioxidant Genes. *Toxicol Sci* 177: 169–177, 2001.

13. **Gaikwad A, Long D, Stringer J, Jaiswal A**. In vivo role of NAD(P)H:quinone oxidoreductase 1 (NQO1) in the regulation of intracellular redox state and accumulation of abdominal adipose tissue. *J Biol Chem* 276: 22559–64, 2001.

14. **Heusch P, Canton M, Aker S, van de Sand A, Konietzka I, Rassaf T, Menazza S, Brodde O, Di Lisa F, Heusch G, Schulz R**. The contribution of reactive oxygen species and p38 mitogen-activated protein kinase to myofilament oxidation and progression of heart failure in rabbits. *Br J Pharmacol* 160: 1408–16, 2010.

15. **Holmström KM, Baird L, Zhang Y, Hargreaves I, Chalasani A, Land JM, Stanyer L, Yamamoto M, Dinkova-Kostova AT, Abramov AY**. Nrf2 impacts cellular bioenergetics by controlling substrate availability for mitochondrial respiration. *Biol Open* 2: 761–70, 2013.

16. **Itoh K, Chiba T, Takahashi S, Ishii T, Igarashi K, Katoh Y, Oyake T, Hayashi N, Satoh K, Hatayama ØI**. An Nrf2 / Small Maf Heterodimer Mediates the Induction of Phase II Detoxifying Enzyme Genes through Antioxidant Response Elements. *Biochem Biophys Res Commun* 322: 313–322, 1997.

17. **Katsuoka F, Motohashi H, Ishii T, Aburatani H, Engel JD, Yamamoto M**. Genetic Evidence that Small Maf Proteins Are Essential for the Activation of Antioxidant Response Element-Dependent Genes. *Mol Cell Biol* 25: 8044–8051, 2005.

18. **Kim T-H, Hur E, Kang S-J, Kim J-A, Thapa D, Lee YM, Ku SK, Jung Y, Kwak M-K**. NRF2 blockade suppresses colon tumor angiogenesis by inhibiting hypoxia-induced activation of HIF-1α. *Cancer Res* 71: 2260–75, 2011.

19. **Kobayashi A, Kang M, Okawa H, Zenke Y, Chiba T, Igarashi K, Ohtsuji M**. Oxidative Stress Sensor Keap1 Functions as an Adaptor for Cul3-Based E3 Ligase To Regulate Proteasomal Degradation of Nrf2 Oxidative Stress Sensor Keap1 Functions as an Adaptor for Cul3-Based E3 Ligase To Regulate Proteasomal Degradation of Nrf2. *Mol Cell Biol* 24: 7130–7139, 2004.

20. **Kobayashi M, Yamamoto M**. Nrf2-Keap1 regulation of cellular defense mechanisms against electrophiles and reactive oxygen species. *Adv Enzyme Regul* 46: 113–40, 2006.

21. **Kovac S, Angelova PR, Holmström KM, Zhang Y, Dinkova-Kostova AT, Abramov AY**. Nrf2 regulates ROS production by mitochondria and NADPH oxidase. *Biochim Biophys Acta* 1850: 794–801, 2015.

22. **Ljubicic V, Adhihetty PJ, Hood DA**. Role of UCP3 in state 4 respiration during contractile activity-induced mitochondrial biogenesis. *J Appl Physiol* 97: 976–83, 2004.

23. **Ljubicic V, Joseph AM, Adhihetty PJ, Huang JH, Saleem A, Uguccioni G, Hood DA**. Molecular basis for an attenuated mitochondrial adaptive plasticity in aged skeletal muscle. *Aging (Albany NY)* 1: 818–30, 2009.

24. **Ludtmann MHR, Angelova PR, Zhang Y, Abramov AY, Dinkova-Kostova AT**. Nrf2 affects the efficiency of mitochondrial fatty acid oxidation. *Biochem J* 457: 415–24, 2014.

25. **Miller CJ, Gounder SS, Kannan S, Goutam K, Muthusamy VR, Firpo MA, Symons JD, Paine R, Hoidal JR, Rajasekaran NS**. Disruption of Nrf2/ARE signaling impairs antioxidant mechanisms and promotes cell degradation pathways in aged skeletal muscle. *Biochim Biophys Acta* 1822: 1038–50, 2012.

26. **Mitsuishi Y, Taguchi K, Kawatani Y, Shibata T, Nukiwa T, Aburatani H, Yamamoto M, Motohashi H**. Nrf2 redirects glucose and glutamine into anabolic pathways in metabolic reprogramming. *Cancer Cell* 22: 66–79, 2012.

27. **Muramatsu H, Katsuoka F, Toide K, Shimizu Y, Furusako S, Yamamoto M**. Nrf2 deficiency leads to behavioral, neurochemical and transcriptional changes in mice. *Genes Cells* 18: 899–908, 2013.

28. **Muthusamy VR, Kannan S, Sadhaasivam K, Gounder SS, Davidson CJ, Boeheme C, Hoidal JR, Wang L, Rajasekaran NS**. Acute exercise stress activates Nrf2/ARE signaling and promotes antioxidant mechanisms in the myocardium. *Free Radic Biol Med* 52: 366–76, 2012.

29. **Narasimhan M, Hong J, Atieno N, Muthusamy VR, Davidson CJ, Abu-Rmaileh N, Richardson RS, Gomes A V, Hoidal JR, Rajasekaran NS**. Nrf2 deficiency promotes apoptosis and impairs PAX7/MyoD expression in aging skeletal muscle cells. *Free Radic Biol Med* 71: 402–14, 2014.

30. **Nguyen T, Sherratt PJ, Nioi P, Yang CS, Pickett CB**. Nrf2 controls constitutive and inducible expression of ARE-driven genes through a dynamic pathway involving nucleocytoplasmic shuttling by Keap1. *J Biol Chem* 280: 32485–92, 2005.

31. **Piantadosi CA, Carraway MS, Babiker A, Suliman HB**. Heme oxygenase-1 regulates cardiac mitochondrial biogenesis via Nrf2-mediated transcriptional control of nuclear respiratory factor-1. *Circ Res* 103: 1232–40, 2008.

32. **Rangasamy T, Cho CY, Thimmulappa RK, Zhen L, Srisuma SS, Kensler TW, Yamamoto M, Petrache I, Tuder RM, Biswal S**. Genetic ablation of Nrf2 enhances susceptibility to cigarette smoke – induced emphysema in mice. *J Clin Invest* 114: 1248–1259, 2004.

33. **Rushmore TH, Morton MR, Pickett CB**. The antioxidant responsive element. Activation by oxidative stress and identification of the DNA consensus sequence required for functional activity. *J Biol Chem* 266: 11632–11639, 1991.

34. **Safdar A, DeBeer J, Tarnopolsky MA**. Dysfunctional Nrf2-Keap1 redox signaling in skeletal muscle of the sedentary old. *Free Radic Biol Med* 49: 1487–93, 2010.

35. **Sakellariou G, Jackson MJ, Vasilaki A**. Redefining the major contributors to superoxide production in contracting skeletal muscle. The role of NAD(P)H oxidases. *Free Radic Res* 48: 12–29, 2014.

36. **Saleem A, Adhihetty PJ, Hood DA**. Role of p53 in mitochondrial biogenesis and apoptosis in skeletal muscle. *Physiol Genomics* 37: 58–66, 2009.

37. **Scarpulla RC**. Transcriptional Paradigms in Mammalian Mitochondrial Biogenesis and Function. *Physiol Rev* 88: 611–638, 2008.

38. **Shen G, Hebbar V, Nair S, Xu C, Li W, Lin W, Keum YS, Han J, Gallo MA, Kong AN**. Regulation of Nrf2 transactivation domain activity. The differential effects of mitogen-activated protein kinase cascades and synergistic stimulatory effect of Raf and CREB-binding protein. *J Biol Chem* 279: 23052–60, 2004.

39. **Strom J, Xu B, Tian X, Chen QM**. Nrf2 protects mitochondrial decay by oxidative stress. *FASEB J* 30: 66–80, 2016.

40. **Sun Z, Chin YE, Zhang DD**. Acetylation of Nrf2 by p300/CBP augments promoter-specific DNA binding of Nrf2 during the antioxidant response. *Mol Cell Biol* 29: 2658–72, 2009.

41. **Vainshtein A, Kazak L, Hood DA**. Effects of endurance training on apoptotic susceptibility in striated muscle. *J Appl Physiol* 110: 1638–1645, 2011.

42. **Wu KC, Cui JY, Klaassen CD**. Beneficial role of Nrf2 in regulating NADPH generation and consumption. *Toxicol Sci* 123: 590–600, 2011.

43. **Zhang DD, Hannink M**. Distinct Cysteine Residues in Keap1 Are Required for Keap1-Dependent Ubiquitination of Nrf2 and for Stabilization of Nrf2 by Chemopreventive Agents and Oxidative Stress Distinct Cysteine Residues in Keap1 Are Required for Keap1-Dependent Ubiquitination of. *Mol Cell Biol* 23: 8137–8151, 2003.

44. **Zhang Y-KJ, Wu KC, Klaassen CD**. Genetic activation of Nrf2 protects against fasting-induced oxidative stress in livers of mice. *PLoS One* 8: e59122, 2013.

Figure Legends

Table 1. Contractile properties of Nrf2 WT and KO skeletal muscle.

Figure 1: Voluntary wheel running and body and gastrocnemius weight in Nrf2 WT and KO mice. (A) Weekly average wheel running distance accumulated by 3 month old Nrf2 wild-type (WT) and knockout (KO) mice over a period of 6 weeks (n=9-10); UT=untrained, T=trained. **(B)** Body and **(C)** gastrocnemius weight of Nrf2 WT and KO mice following the 6 week training period (n=6-10). Data are means ± SEM. **P*<0.05; 2-way ANOVA produced a main effect of age.

Figure 2: Endurance exercise capacity test. Following the six weeks of voluntary wheel running, the running performance of untrained, trained and aged mice were compared by subjecting them to an exhaustive bout of exercise. Running performance was measured by recording both the **(A)** distance (n=6-9) and **(B)** time (n=6-9) to exhaustion. **P*<0.05 T vs. UT; ¶<0.05 main effect of age, 2-way ANOVA. **(C)** Lactate production was also measured before and after exercise. **P*<0.05, 2-way ANOVA produced a main effect of exercise.

Figure 3: Muscle performance in response to acute *in situ* stimulation. (A) The gastrocnemius muscle of WT UT, WT T, KO UT and KO T mice was stimulated at 0.25, 0.50 and 1 tetanic contraction per second (TPS) with force production being used as an index of muscle fatigue (n=8-10). **(B)** Graphical representation depicting the linear regression of the WT UT and KO UT fatigue rate within the first two minutes of stimulation. **P*<0.05 WT UT vs. KO UT, Student's t-test. **(C)** Force production at 5 minutes of stimulation. **P*<0.05 WT UT vs. KO UT; ¶<0.05 KO UT vs. KO T, ANOVA.

(D) Force production at end of stimulation. ¶<0.05 KO UT vs. KO T, ANOVA. Data are means ± SEM.

Figure 4: Adaptations to training in the Nrf2 WT and KO animals. (**A)** COX activity (n=6-7) of the gastrocnemius muscle in response to voluntary wheel running or age. ***P*<0.01 T vs. UT, 2-way ANOVA. **(B)** Western blots of COX1, COXIV and TFAM from whole muscle samples in Nrf2 WT and KO mice following six weeks of voluntary wheel running. Graphical representation of **(C)** COXI (n=3) **(D)** COXIV (n=7-9) and **(E)** TFAM (n=7-9). **P*<0.05 vs. UT, ¶<0.05 main effect of genotype, 2-way ANOVA. Data are means ± SEM. **(F)** ARE-based transactivation assay (n=7) to determine if exercise can induce Nrf2 activation; bars represent fold-change in acute exercise group relative to sedentary mice. **P*<0.05, Student's t-test. Data are means ± SEM.

Figure 5: Respiration and ROS production in isolated mitochondria from Nrf2 WT and KO animals. Oxygen consumption in isolated **(A)** SS (n=6-8) and **(B)** IMF mitochondria (n=10) during state 4 and state 3 respiration. **P*<0.05 KO UT vs. WT UT; ¶<0.05 T vs. UT, ANOVA. Reactive oxygen species (ROS) production in the **(C)** SS and **(D)** IMF mitochondria during state 4 and state 3 respiration. **P*<0.05 KO UT vs. WT UT; ¶ *P*<0.05 KO T vs. KO UT. Data are means ± SEM.

Figure 6: Compositional differences in isolated IMF mitochondria from trained and untrained mice. Western blots depicting COXI (n=6), COXIV (n=6), TFAM (n=6), UQCRC2 (n=6) protein expression in isolated IMF mitochondria. Graphical representation of **(A)** UQCRC2 and **(B)** TFAM. **P*<0.05 main effect of training, 2-way ANOVA. Data are means ± SEM.

Figure 7: Antioxidant enzyme expression in skeletal muscle of trained and untrained mice. Western blots depicting **(A)** NQO1 (n=6), **(B)** HO-1 (n=7), **(C)** G6PD (n=9) and **(D)** GPx1 (n=9) protein expression in WT and KO mice in both untrained and trained conditions. **P*<0.05; 2-way ANOVA produced a main effect of genotype. Data are means ± SEM.

Figure 8: Antioxidant enzyme expression in young and middle-aged WT and KO mice. Western blots depicting **(A)** NQO1 (n=7) **(B)** HO-1 (n=5-7) **(C)** G6PD (n=5-7) and **(D)** GPx1 (6-7) protein expression in young and middle-aged WT and KO mice. **P*<0.05 versus WT Y, ANOVA; ¶ *P*<0.05 KO A vs. WT Y/A, ANOVA. Data are means ± SEM.

Table 1

Condition	GW (mg)	GW(mg)/BW(g)	TW/GW (mN/mg)	TET/GW (mN/mg)	TPT (msec)	½ RT (msec)
WT UT	173.5 ± 5.45	5.87±0.17	1.83 ± 0.35	6.72 ± 0.54	21.36 ± 1.16	35.36 ± 1.76
WT T	162.4 ± 8.53	5.69±0.16	2.39 ± 0.27	6.56 ± 0.59	22.17 ± 2.01	34 ± 4.12
KO UT	169.40 ± 5.92	5.71 ± 0.14	2.01 ± 0.14	5.43 ± 0.57	18.67 ± 1.91	32.4 ± 2.29
KO T	176.89 ± 10.93	5.62 ± 22	2.25 ± 0.21	6.91 ± 0.67	21.0 ± 1.77	30.36 ± 0.36

Data are represented as means ± SEM; n=9-10. GW, Gastrocnemius weight; BW, Body weight; TW, maximum twitch force; TET, maximum tetanic force; TPT, time to peak twitch tension; ½ RT, half relaxation time.

Figure 1

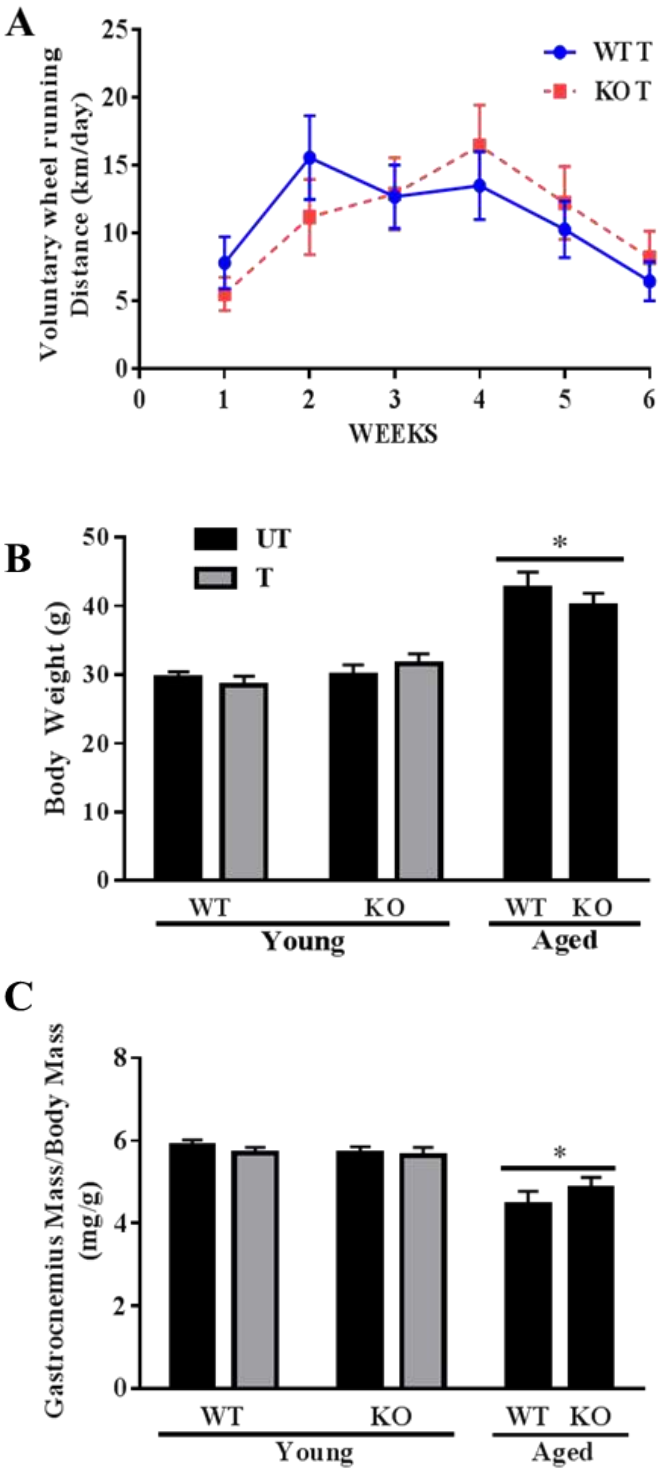
A
Voluntary wheel running
Distance (km/day)
25
20
15
10
5
0
0
1
2
3
4
5
6
WEEKS
WT T
KO T
B
Body Weight (g)
50
40
30
20
10
0
UT
T
*
WT
KO
WT
KO
Young
Aged
C
Gastrocnemius Mass/Body Mass
(mg/g)
8
6
4
2
0
*
WT
KO
WT
KO
Young
Aged

Figure 2

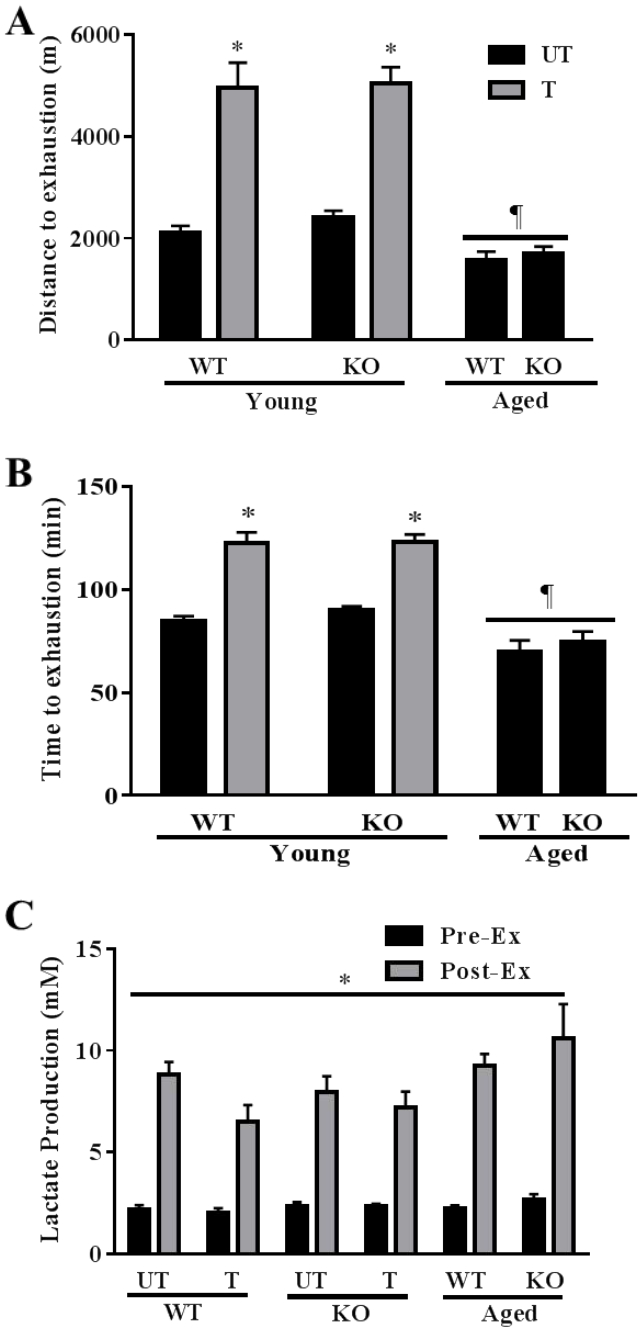
A
Distance to exhaustion (m)
6000
4000
2000
0
*
*
¶
UT
T
WT
KO
WT KO
Young
Aged
B
Time to exhaustion (min)
150
100
50
0
*
*
¶
WT
KO
WT KO
Young
Aged
C
Lactate Production (mM)
15
10
5
0
Pre-Ex
Post-Ex
*
UT
T
UT
T
WT
KO
WT
KO
Aged

Figure 3

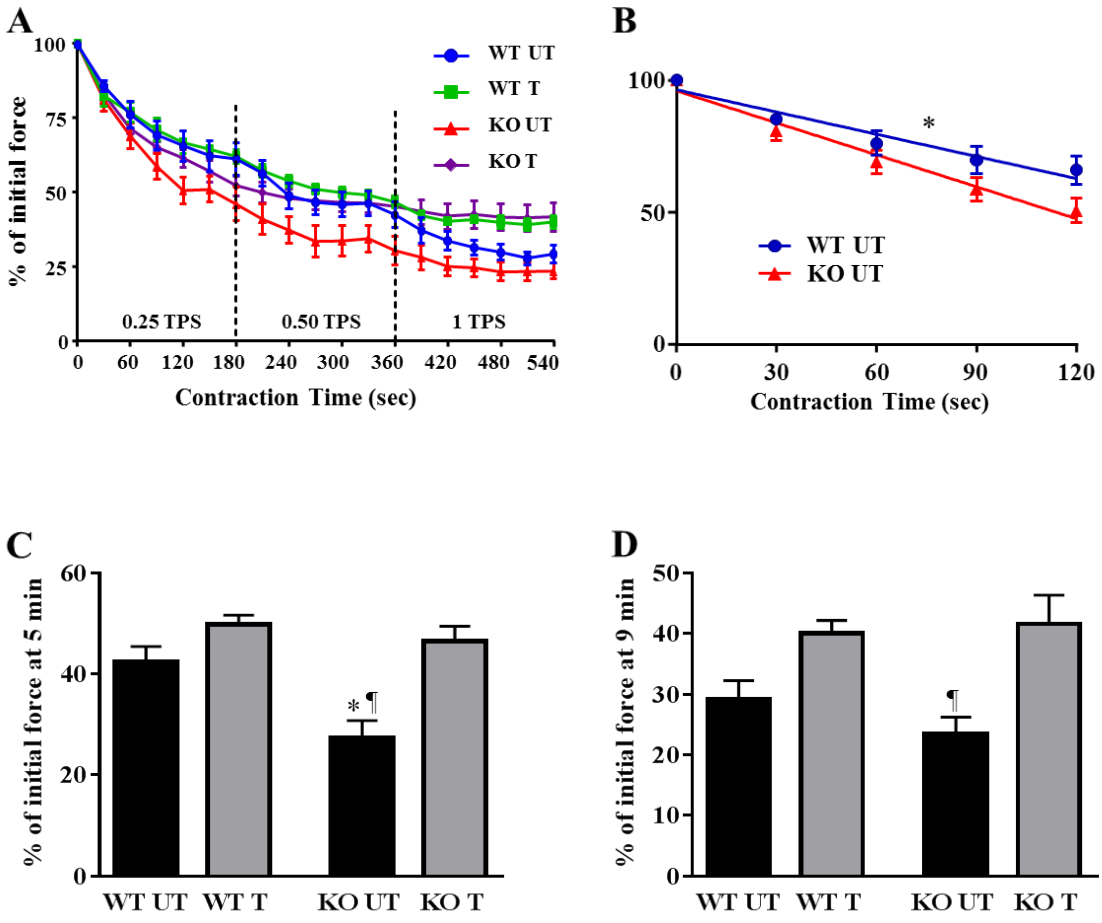
A
100
75
50
25
0
% of initial force
WT UT
WT T
KO UT
KO T
0.25 TPS
0.50 TPS
1 TPS
0 60 120 180 240 300 360 420 480 540
Contraction Time (sec)
B
100
50
0
*
WT UT
KO UT
0 30 60 90 120
Contraction Time (sec)
C
60
40
20
0
% of initial force at 5 min
*¶
WT UT WT T KO UT KO T
D
50
40
30
20
10
0
% of initial force at 9 min
¶
WT UT WT T KO UT KO T

Figure 4

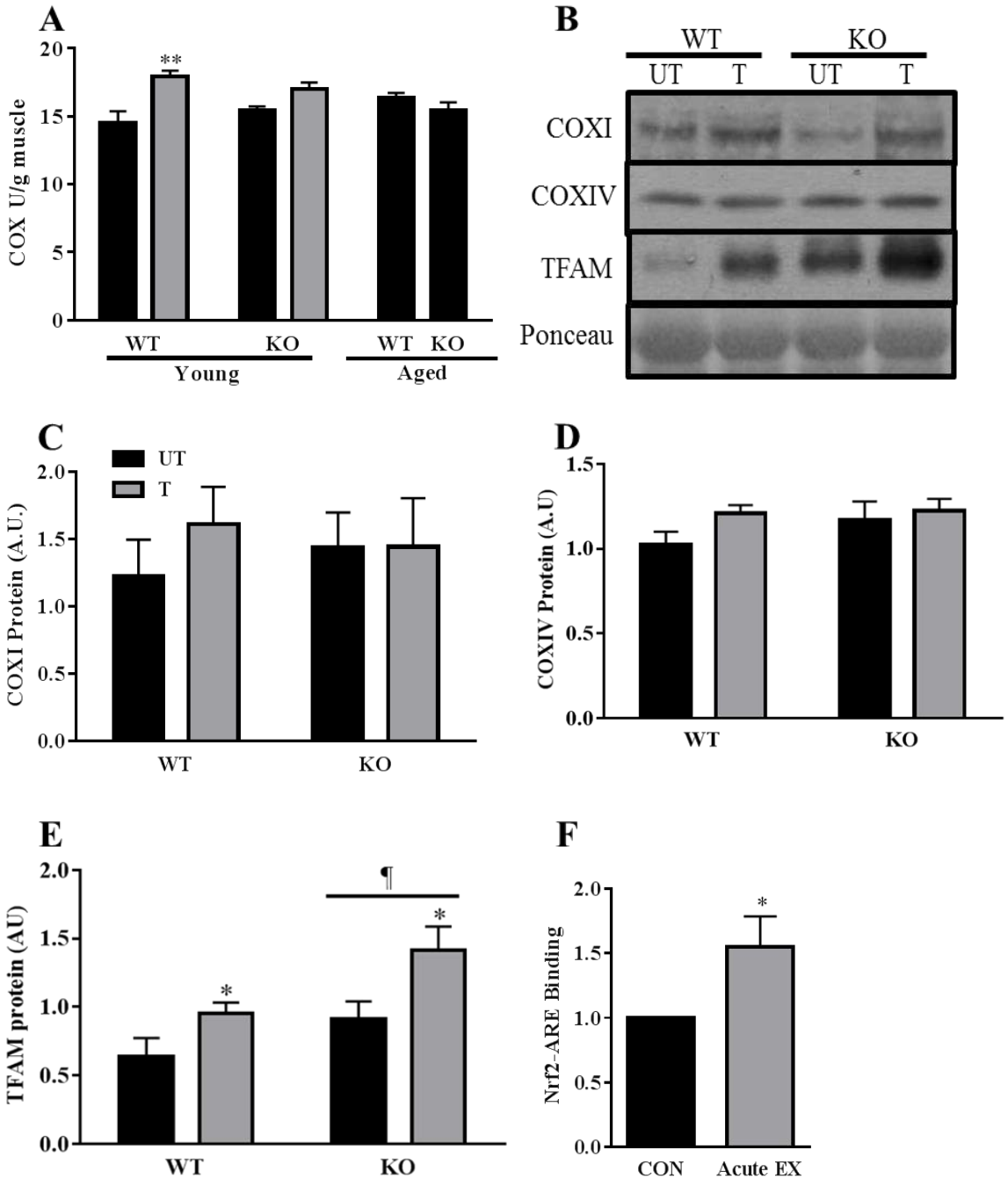
A
COX U/g muscle
20
15
10
5
0
**
WT
KO
WT
KO
Young
Aged
B
WT
KO
UT
T
UT
T
COXI
COXIV
TFAM
Ponceau
C
UT
T
COXI Protein (A.U.)
2.0
1.5
1.0
0.5
0.0
WT
KO
D
COXIV Protein (A.U)
1.5
1.0
0.5
0.0
WT
KO
E
TFAM protein (AU)
2.0
1.5
1.0
0.5
0.0
*
¶
*
WT
KO
F
Nrf2-ARE Binding
2.0
1.5
1.0
0.5
0.0
*
CON
Acute EX

Figure 5

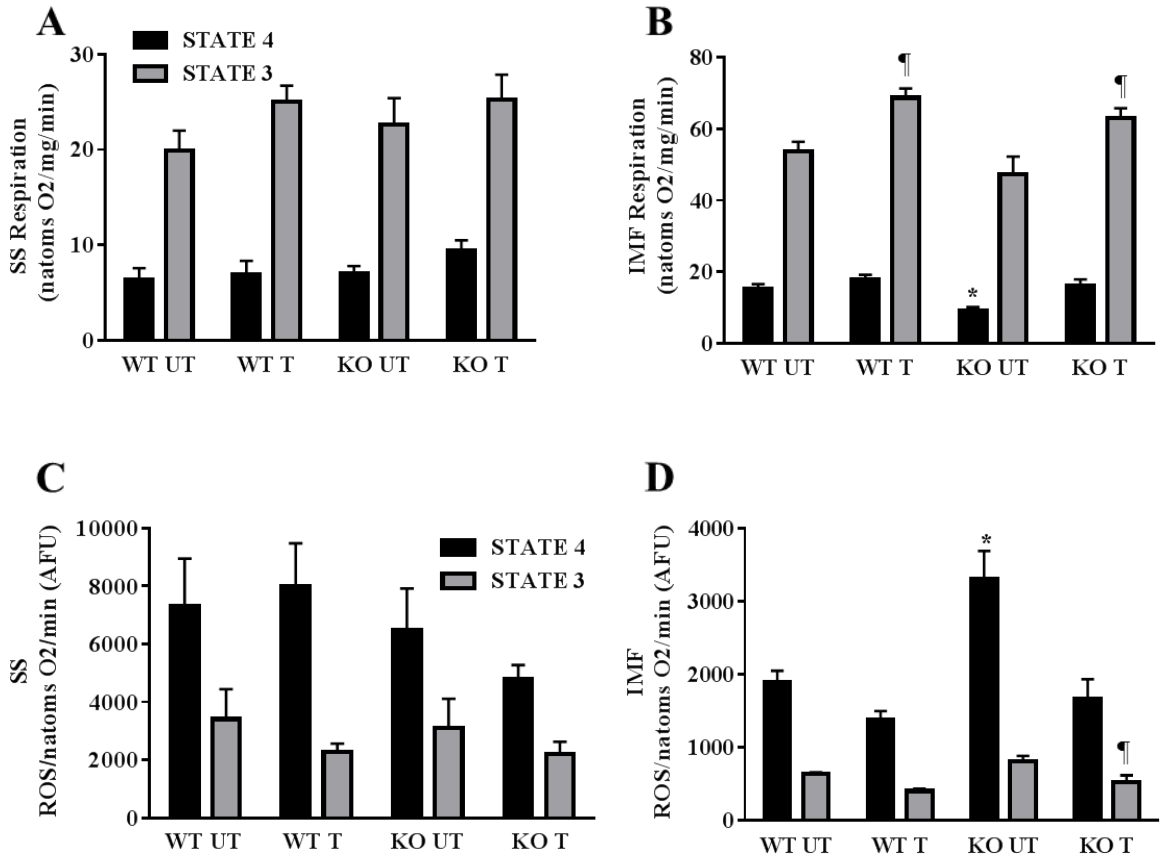
A
STATE 4
STATE 3
SS Respiration (natoms O2/mg/min)
30
20
10
0
WT UT
WT T
KO UT
KO T
B
IMF Respiration (natoms O2/mg/min)
80
60
40
20
0
¶
*
¶
WT UT
WT T
KO UT
KO T
C
SS ROS/natoms O2/min (AFU)
10000
8000
6000
4000
2000
0
STATE 4
STATE 3
WT UT
WT T
KO UT
KO T
D
IMF ROS/natoms O2/min (AFU)
4000
3000
2000
1000
0
*
¶
WT UT
WT T
KO UT
KO T

Figure 6

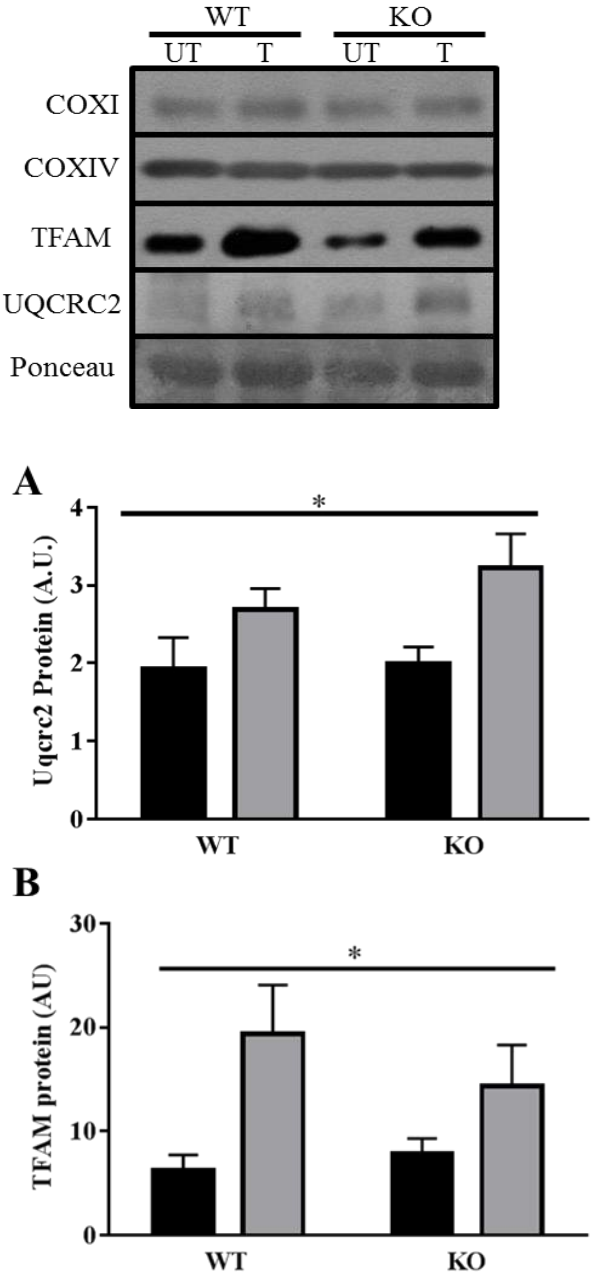
WT
KO
UT
T
UT
T
COXI
COXIV
TFAM
UQCRC2
Ponceau
A
*
Uqcrc2 Protein (A.U.)
4
3
2
1
0
WT
KO
B
*
TFAM protein (AU)
30
20
10
0
WT
KO

Figure 7

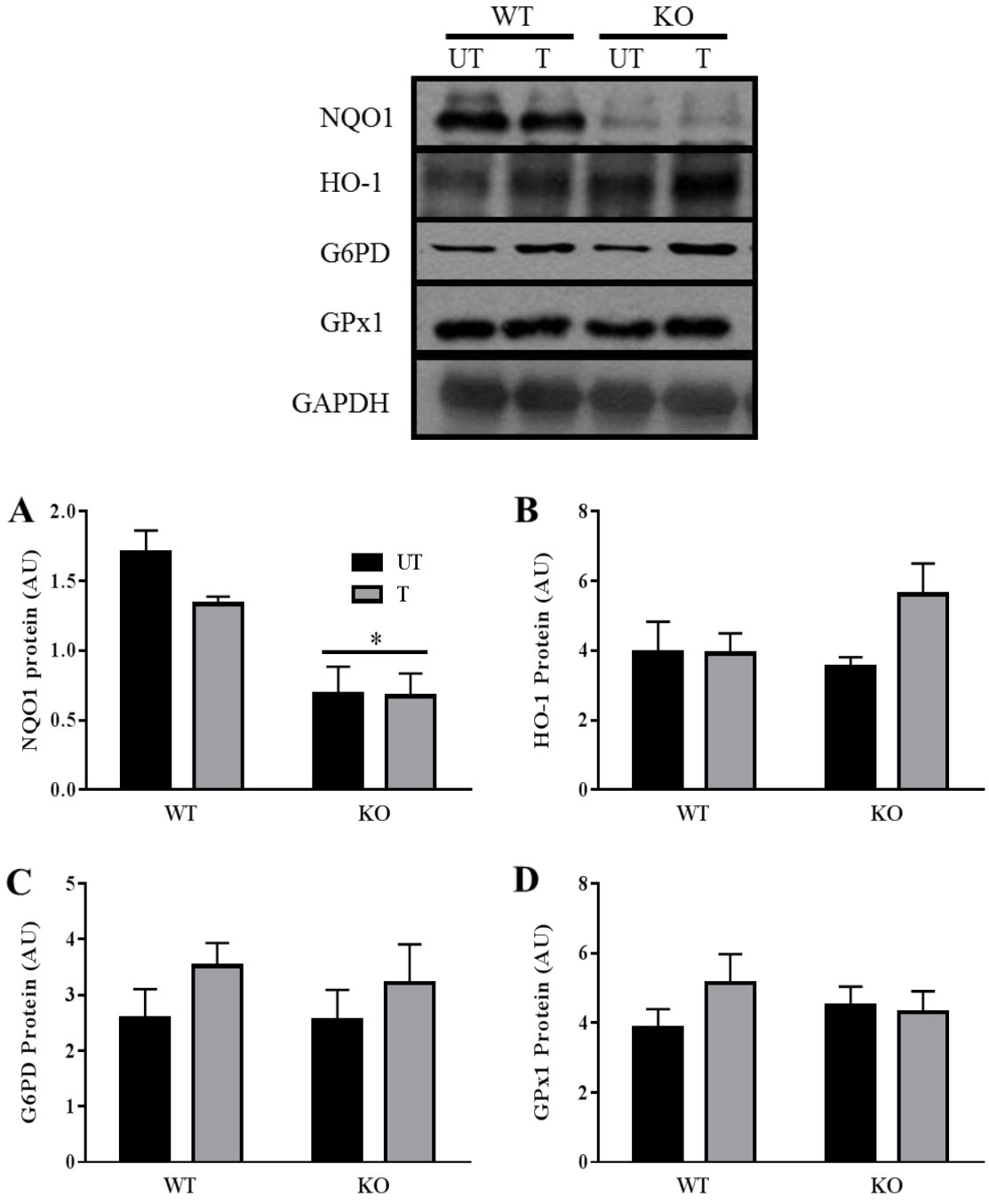
WT
KO
UT
T
UT
T
NQO1
HO-1
G6PD
GPx1
GAPDH
A
NQO1 protein (AU)
2.0
1.5
1.0
0.5
0.0
UT
T
*
WT
KO
B
HO-1 Protein (AU)
8
6
4
2
0
WT
KO
C
G6PD Protein (AU)
5
4
3
2
1
0
WT
KO
D
GPx1 Protein (AU)
8
6
4
2
0
WT
KO

Figure 8

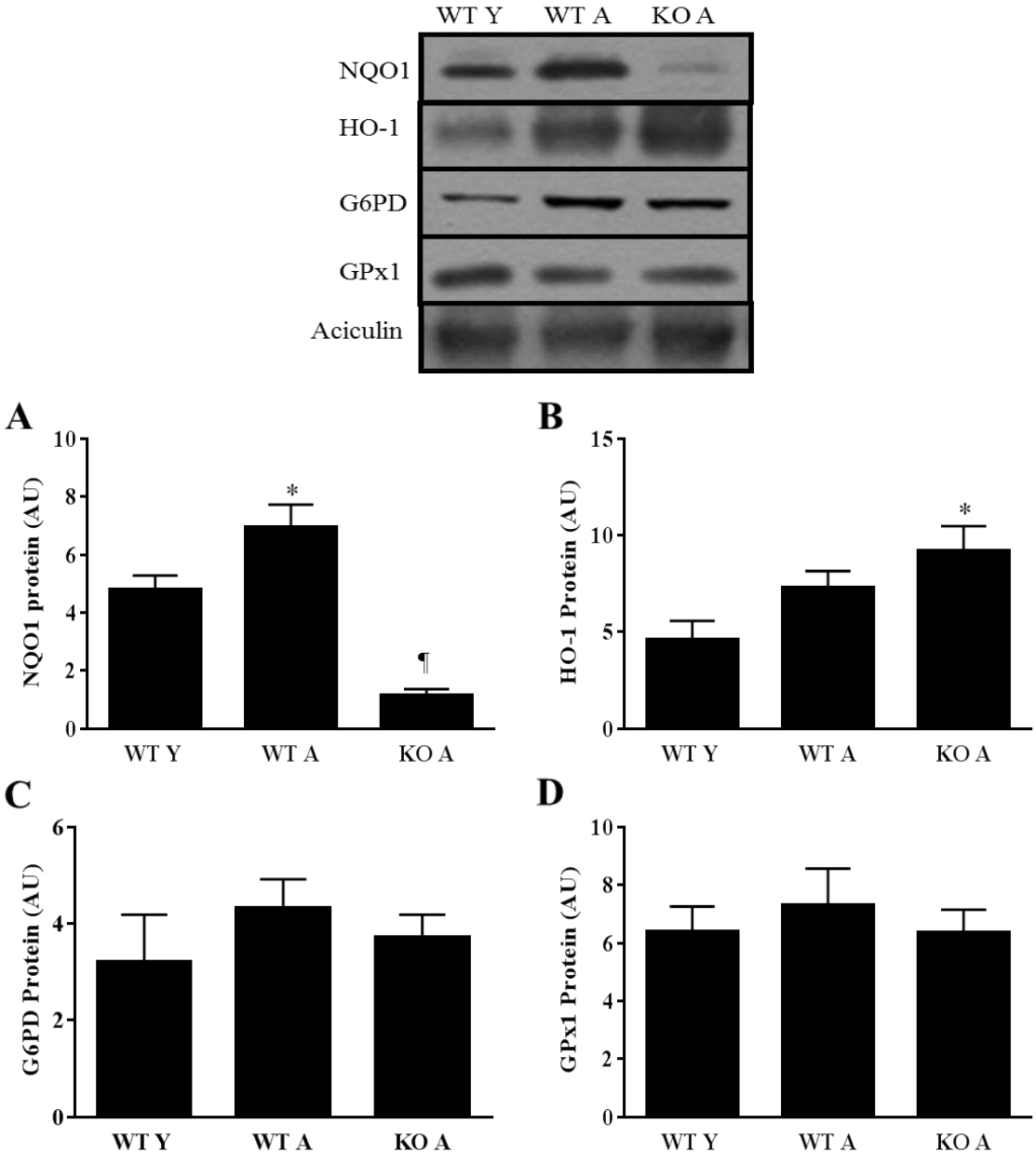
WT Y
WT A
KO A
NQO1
HO-1
G6PD
GPx1
Aciculin
A
NQO1 protein (AU)
10
8
6
4
2
0
*
¶
WT Y
WT A
KO A
B
HO-1 Protein (AU)
15
10
5
0
*
WT Y
WT A
KO A
C
G6PD Protein (AU)
6
4
2
0
WT Y
WT A
KO A
D
GPx1 Protein (AU)
10
8
6
4
2
0
WT Y
WT A
KO A

Summary and Future Work

The results obtained from this thesis are important for understanding the role of Nrf2 in skeletal muscle and its impact on exercise-induced mitochondrial adaptations. This is a novel avenue of research since most studies investigating Nrf2 have either employed a cell culture approach to discern the intricate mechanisms of the Keap1-Nrf2 interaction, or utilized tissues other than skeletal muscle to elucidate the importance of Nrf2 in various pathologies. However, no research has been devoted to understanding the impact of Nrf2 on skeletal muscle mitochondria and the ability of exercise to restore functional deficits.

Therefore, this thesis sought to investigate the following objectives: 1) To determine if Nrf2 is activated in skeletal muscle in response to exercise; 2) to examine whether Nrf2 is required for exercise-induced mitochondrial adaptations; 3) to evaluate the impact of Nrf2 on mitochondrial respiration and ROS production, and 4) to determine if age exacerbates the effect of the loss of Nrf2. Our results illustrate that the effect of Nrf2 is required to maintain normal mitochondrial respiration in control muscle. Further, we have shown that exercise results in the activation of Nrf2, and that it is required for mitochondrial content adaptations in response to training. However, we also established that exercise was capable of restoring the functional deficits in mitochondrial function and fatigue resistance in the Nrf2 KO mice, suggesting that Nrf2 is not required for exercise-induced adaptations in organelle function.

Given the present findings, future research should focus on the following:

1. Exploring the ramifications of Nrf2 abrogation on mitochondrial physiology in skeletal muscle, specifically, indices such as protein import or permeability transition in the SS and IMF fractions.
2. Elucidating the role of Nrf2 in mitochondrial clearance (i.e. mitophagy). Through the use of colchicine treatment and flow cytometry, potential disparities in mitophagy flux and membrane potential can be determined.
3. Establishing the role of Nrf2 in the context of muscle disuse. Based on our supplementary findings we have shown that Nrf2 is reduced in response to denervation, which may partially be attributed to the marked increase observed in Keap1 protein expression. Moreover, studies can utilize the Nrf2 activator sulforaphane in an attempt to attenuate the atrophy response that ensues with denervation.
4. Investigating the relationship of Nrf2 with other mitochondrial regulators such as PGC-1α, AMPK and SIRT1.

APPENDIX A – Data Tables and Statistical Analyses

Table 1A: Voluntary wheel running

WT T - wheel running distance (km/day)												
week	**n=1**	**n=2**	**n=3**	**n=4**	**n=5**	**n=6**	**n=7**	**n=8**	**n=9**	**n=10**	**AVG**	**SEM**
1	6.19	2.53	13.83		7.01	3.3	18.23	12.65	1.92	4.6	**8.21**	**1.92**
2	23.26	1.11	19.75	0.17	7.81	23.97	27.13	21.59	11.03	19.69	**15.09**	**3.09**
3	19.04	0.74	11.03	0.53	15.02	21.52	18.2	18.61	11.74	10.29	**12.94**	**2.33**
4	15.72	2	15.96	1.94	28.53	11.61	16.29	15.83	8.89	18.05	**12.97**	**2.50**
5	16.81	1.89	14.17	6.7	21.29	10.2	2.77	10.2	3.26	15.34	**9.70**	**2.09**
6	9.16	1.22	8.27	3.92	6.94	0.67	8.87	10.22	1.06	14.08	**5.59**	**1.44**

KO T - wheel running distance (km/day)												
week	**n=1**	**n=2**	**n=3**	**n=4**	**n=5**	**n=6**	**n=7**	**n=8**	**n=9**	**n=10**	**AVG**	**SEM**
1	6.04	5.14	3.07	2.05	1.34		9.81	12.44	6.7	3.03	**5.51**	**1.23**
2	26.2	9.22	8.01	6.05	3.76	0.24	24.8	17.94	8.46	7.04	**11.17**	**2.78**
3	10.61	8.98	8.84	7.81	8.14	0.36	24.64	27.9	18.82	12.76	**12.89**	**2.67**
4	4.84	16.43	22.83	19.75	25.4	0.37	27.02	24.67	17.07	5.95	**16.43**	**3.01**
5	10.19	5.44	28.22	21.52	9.91	0.49	15.02	17.31	10.94	3.06	**12.21**	**2.70**
6	7.06	5.67	14.93	16.04	2.99	0.12		15.34	8.12	3.41	**8.19**	**1.97**

2-WAY ANOVA			
Source of Variation	**P value**	**P value summary**	**Significant?**
Interaction	0.4977	ns	No
Genotype	0.9888	ns	No
Training	0.0388	*	Yes

Bonferroni Post-Hoc - WT vs KO at each time point				
weeks	**difference**	**t**	**P value**	**Summary**
1	-0.765	1.048	P>0.05	ns
2	0.366	0.5013	P>0.05	ns
3	-1.116	1.488	P>0.05	ns
4	1.131	1.549	P>0.05	ns
5	-0.3512	0.4682	P>0.05	ns
6	-1.482	1.976	P>0.05	ns

Table 1B: Body weight of WT and KO animals (UT vs. T; Young vs. Older mice).

Body Weight (g)						
N	**WT UT**	**WT T**	**KO UT**	**KO T**	**WT A**	**KO A**
1	26.20	31.30	24.60	33.20	46.1	39.3
2	30.40	27.30	30.40	32.60	48.8	41.3
3	31.60	30.00	35.70	30.50	44.1	40.6
4	29.30	31	34.7	29.6	47.9	38.5
5	32.30	29.3	33.5	26.3	35	33.2
6	24.40	27.6	33.9	25.5	43.2	47.3
7	29.70	21.7	24	34.3	33.1	
8	31.00	24	23.2	32.7		
9	32.80	27.2	32.3	39.9		
10	28.30	35.9	26.9			
AVG	**29.60**	**28.53**	**29.92**	**31.62**	**42.60**	**40.03**
SEM	**0.85**	**1.26**	**1.52**	**1.45**	**2.34**	**1.86**

2-WAY ANOVA			
Source of Variation	**P value**	**P value summary**	**Significant?**
Interaction	0.2151	ns	No
Genotype	0.8229	ns	No
Training/Age	< 0.0001	****	Yes

POST-HOC TEST				
Bonferroni	**Mean Diff.**	**t-value**	**P-value**	**Summary**
WT:UT vs. WT:T	1.07	0.5408	P>0.05	ns
WT:UT vs. WT:**Aged**	-13	5.963	P<0.05	****
WT:UT vs. KO:UT	-0.32	0.1617	P>0.05	ns
WT:UT vs. KO:T	-2.022	0.9949	P>0.05	ns
WT:UT vs. KO:**Aged**	-10.43	4.567	P<0.05	***
WT:T vs. WT:**Aged**	-14.07	6.454	P<0.05	****
WT:T vs. KO:UT	-1.39	0.7026	P>0.05	ns
WT:T vs. KO:T	-3.092	1.521	P>0.05	ns
WT:T vs. KO:**Aged**	-11.5	5.035	P<0.05	***
WT:**Aged** vs. KO:UT	12.68	5.816	P<0.05	****
WT:**Aged** vs. KO:T	10.98	4.924	P<0.05	***
WT:**Aged** vs. KO:**Aged**	2.567	1.043	P>0.05	ns
KO:UT vs. KO:T	-1.702	0.8374	P>0.05	ns
KO:UT vs. KO:**Aged**	-10.11	4.427	P<0.05	***
KO:T vs. KO:**Aged**	-8.411	3.607	P<0.05	*

Table 1C: Gastroc weight of WT and KO animals (UT vs. T; Young vs. Older mice).

Gastrocnemius weight/Body weight (mg/g)						
N	**WT UT**	**WT T**	**KO UT**	**KO T**	**WT A**	**KO A**
1	6.45	5.88	6.38	6.72	4.49	5.11
2	5.49	5.64	5.72	6.26	4.04	5.21
3	5.51	5.57	5.41	5.77	5.33	5.69
4	6.62	5.87	5.07	5.78	3.59	3.84
5	5.42	5.94	5.34	5.89	5.49	4.70
6	5.66	5.18	5.40	5.37	3.68	4.57
7	5.62	6.27	6.25	4.96		
8	5.55	4.83	5.65	5.14		
9	6.13	6.25	5.73	4.71		
10	6.29	5.52	6.17			
AVG	**5.87**	**5.69**	**5.71**	**5.62**	**4.44**	**4.85**
SEM	**0.14**	**0.14**	**0.14**	**0.21**	**0.33**	**0.26**

2-WAY ANOVA			
Source of Variation	**P value**	**P value summary**	**Significant?**
Interaction	0.3464	ns	No
Genotype	0.7075	ns	No
Training/Age	< 0.0001	****	Yes

POST-HOC TEST				
Bonferroni	**Mean Diff.**	**t-value**	**P-value**	**Summary**
WT:UT vs. WT:T	0.179	0.7171	P>0.05	ns
WT:UT vs. WT:**Aged**	1.437	4.986	P<0.05	***
WT:UT vs. KO:UT	0.162	0.649	P>0.05	ns
WT:UT vs. KO:T	0.2518	0.9817	P>0.05	ns
WT:UT vs. KO:**Aged**	1.021	3.541	P<0.05	*
WT:T vs. WT:**Aged**	1.258	4.365	P<0.05	**
WT:T vs. KO:UT	-0.017	0.0681	P>0.05	ns
WT:T vs. KO:T	0.07278	0.2838	P>0.05	ns
WT:T vs. KO:**Aged**	0.8417	2.92	P>0.05	ns
WT:**Aged** vs. KO:UT	-1.275	4.424	P<0.05	***
WT:**Aged** vs. KO:T	-1.186	4.03	P<0.05	**
WT:**Aged** vs. KO:**Aged**	-0.4167	1.293	P>0.05	ns
KO:UT vs. KO:T	0.08978	0.35	P>0.05	ns
KO:UT vs. KO:**Aged**	0.8587	2.979	P>0.05	ns
KO:T vs. KO:**Aged**	0.7689	2.614	P>0.05	ns

Table 2A: Endurance exercise capacity test – Distance to exhaustion

Distance to exhaustion (m)						
N	**WT UT**	**WT T**	**KO UT**	**KO T**	**WT A**	**KO A**
1	1730	6254	2642	5234	1632	2042
2	2514	2514	2042	4490	1370	1587
3	2841	5937	2042	5731	1987	1107
4	2097	4057	1987	5731	1107	1779
5	2211	5331	2707	3891	2329	1681
6	2211	6147	2329	3417	1411	1987
7	1681	6147	2211	4761	1107	
8	1681	5529	2514	6042		
9	2042	2592	3194	6042		
10						
AVG	**2112.00**	**4945.33**	**2407.56**	**5037.67**	**1563.29**	**1697.17**
SEM	**130.98**	**504.32**	**132.47**	**319.18**	**172.34**	**137.88**

2-WAY ANOVA			
Source of Variation	**P value**	**P value summary**	**Significant?**
Interaction	0.9299	ns	No
Genotype	0.4755	ns	No
Training/Age	< 0.0001	****	Yes

POST-HOC TEST				
Bonferroni	**Mean Diff.**	**t-value**	**P-value**	**Summary**
WT:UT vs. WT:T	-2833	7.2	P<0.05	****
WT:UT vs. WT:**Aged**	548.7	1.304	P>0.05	ns
WT:UT vs. KO:UT	-295.6	0.7511	P>0.05	ns
WT:UT vs. KO:T	-2926	7.435	P<0.05	****
WT:UT vs. KO:**Aged**	414.8	0.9429	P>0.05	ns
WT:T vs. WT:**Aged**	3382	8.039	P<0.05	****
WT:T vs. KO:UT	2538	6.449	P<0.05	****
WT:T vs. KO:T	-92.33	0.2346	P>0.05	ns
WT:T vs. KO:**Aged**	3248	7.383	P<0.05	****
WT:**Aged** vs. KO:UT	-844.3	2.007	P>0.05	ns
WT:**Aged** vs. KO:T	-3474	8.259	P<0.05	****
WT:**Aged** vs. KO:**Aged**	-133.9	0.2883	P>0.05	ns
KO:UT vs. KO:T	-2630	6.684	P<0.05	****
KO:UT vs. KO:**Aged**	710.4	1.615	P>0.05	ns
KO:T vs. KO:**Aged**	3341	7.593	P<0.05	****

Table 2B: Endurance exercise capacity test—Time to exhaustion

Time to exhaustion (min)						
N	**WT UT**	**WT T**	**KO UT**	**KO T**	**WT A**	**KO A**
1	78	136	94	126	75	84
2	92	92	84	118	70	75
3	97	133	84	131	83	50
4	85	113	83	131	50	79
5	87	127	95	111	89	77
6	87	135	89	105	71	83
7	77	135	87	121	50	
8	77	129	92	134		
9	84	104	102	134		
10						
AVG	**84.89**	**122.67**	**90.00**	**123.44**	**69.71**	**74.67**
SEM	**2.29**	**5.31**	**2.11**	**3.48**	**5.68**	**5.13**

2-WAY ANOVA			
Source of Variation	**P value**	**P value summary**	**Significant?**
Interaction	0.8245	ns	No
Genotype	0.2862	ns	No
Training/Age	< 0.0001	****	Yes

POST-HOC TEST				
Bonferroni	**Mean Diff.**	**t-value**	**P-value**	**Summary**
WT:UT vs. WT:T	-37.78	6.931	P<0.05	****
WT:UT vs. WT:**Aged**	15.17	2.604	P>0.05	ns
WT:UT vs. KO:UT	-5.111	0.9378	P>0.05	ns
WT:UT vs. KO:T	-38.56	7.074	P<0.05	****
WT:UT vs. KO:**Aged**	10.22	1.678	P>0.05	ns
WT:T vs. WT:**Aged**	52.95	9.088	P<0.05	****
WT:T vs. KO:UT	32.67	5.994	P<0.05	****
WT:T vs. KO:T	-0.7778	0.1427	P>0.05	ns
WT:T vs. KO:**Aged**	48	7.877	P<0.05	****
WT:**Aged** vs. KO:UT	-20.29	3.482	P<0.05	*
WT:**Aged** vs. KO:T	-53.73	9.222	P<0.05	****
WT:**Aged** vs. KO:**Aged**	-4.952	0.7699	P>0.05	ns
KO:UT vs. KO:T	-33.44	6.136	P<0.05	****
KO:UT vs. KO:**Aged**	15.33	2.516	P>0.05	ns
KO:T vs. KO:**Aged**	48.78	8.005	P<0.05	****

Table 2C: Endurance exercise capacity test – lactate production

	Lactate production (mM)											
	WT UT		WT T		KO UT		KO T		WT A		KO A	
N	Pre-	Post-	Pre-	Post-	Pre-	Post-	Pre-	Post-	Pre-	Post-	Pre-	Post-
1	2.4	9.5	1.3	5.2	2.7	8.7	2.4	5.9	2.1	8.1	3.6	11.5
2	1.9	10.6	1.3	11.5	1.5	12.7	3.2	10.3	1.8	9.3	2.1	5.8
3	2	7.8	2.7	8.2	2.9	5.8	1.6	4.7	2.4	9.2	2.7	15
4	1.1	9	1.5	8.1	1.7	6.4	2.2	7.8	3	11.8	2.8	7.9
5	1.3	8.1	1.7	3.5	1.5	8.7	2.3	9.8	1.9	7.8	3.6	12.9
6	2.2	6	2.6	6.4	2.2	6.4	2.3	9.1	2.5	9.3	2.1	
7	2.5	8.4	2	4	2.5	5.4	2.3	4	1.8		1.5	14.5
8	3.5	12.3	2.3	6.2	2.4	9.3	2.3	5.4				
9	2.5	7.8	2.9	5.4	3.4	8.3	2.3	7.9				
AVG	2.16	8.83	2.03	6.50	2.31	7.97	2.32	7.21	2.21	9.25	2.63	11.27
SEM	0.24	0.61	0.21	0.82	0.22	0.76	0.14	0.77	0.17	0.58	0.30	1.51

2-WAY ANOVA			
Source of Variation	P value	P value summary	Significant?
Interaction	0.0458	*	Yes
Genotype	0.0079	**	Yes
Training/Age	< 0.0001	****	Yes

POST-HOC TEST				
Bonferroni	Mean Diff.	t-value	P-value	Summary
UT:Pre- vs. UT:Post-	-6.678	8.404	P<0.05	****
UT:Pre- vs. T:Pre-	0.1222	0.1538	P>0.05	ns
UT:Pre- vs. T:Post-	-4.344	5.467	P<0.05	****
UT:Pre- vs. UT:Pre-	-0.1556	0.1958	P>0.05	ns
UT:Pre- vs. UT:Post-	-5.811	7.313	P<0.05	****
UT:Pre- vs. T:Pre-	-0.1667	0.2097	P>0.05	ns
UT:Pre- vs. T:Post-	-5.056	6.362	P<0.05	****
UT:Pre- vs. WT :Pre-	-0.05873	0.06914	P>0.05	ns
UT:Pre- vs. WT :Post-	-7.094	7.985	P<0.05	****
UT:Pre- vs. KO :Pre-	-0.473	0.5568	P>0.05	ns
UT:Pre- vs. KO :Post-	-8.464	9.003	P<0.05	****
UT:Post- vs. T:Pre-	6.8	8.557	P<0.05	****
UT:Post- vs. T:Post-	2.333	2.936	P>0.05	ns
UT:Post- vs. UT:Pre-	6.522	8.208	P<0.05	****
UT:Post- vs. UT:Post-	0.8667	1.091	P>0.05	ns
UT:Post- vs. T:Pre-	6.511	8.194	P<0.05	****
UT:Post- vs. T:Post-	1.622	2.041	P>0.05	ns
UT:Post- vs. WT :Pre-	6.619	7.792	P<0.05	****
UT:Post- vs. WT :Post-	-0.4167	0.469	P>0.05	ns

Table 2D: COX Activity in WT and KO mice (UT vs. T; Young vs. Older mice)

COX Activity U/g muscle						
N	**WT UT**	**WT T**	**KO UT**	**KO T**	**WT A**	**KO A**
1	10.74	18.63	16.04	17.59	15.81	15.65
2	16.92		16.01	18.34	15.78	16.08
3	14.53	18.40	14.86	18.36	17.28	14.67
4	16.04	18.44	15.26	16.98	14.83	16.37
5	11.92	16.04	14.08	14.94	16.81	13.06
6	15.46	17.80	15.83	15.92	16.54	16.92
7	15.87	18.41	15.98	16.97	17.49	
8						
9						
10						
AVG	**14.50**	**17.95**	**15.44**	**17.01**	**16.36**	**15.46**
SEM	**0.87**	**0.40**	**0.28**	**0.47**	**0.36**	**0.57**

2-WAY ANOVA			
Source of Variation	**P value**	**P value summary**	**Significant?**
Interaction	0.1411	ns	No
Genotype	0.4949	ns	No
Training/Age	0.0002	***	Yes

POST-HOC TEST				
Bonferroni	**Mean Diff.**	**t-value**	**P-value**	**Summary**
WT:UT vs. WT:T	-3.456	4.512	P<0.05	**
WT:UT vs. WT:**Aged**	-1.866	2.535	P>0.05	ns
WT:UT vs. KO:UT	-0.94	1.277	P>0.05	ns
WT:UT vs. KO:T	-2.517	3.42	P<0.05	*
WT:UT vs. KO:**Aged**	-0.9612	1.255	P>0.05	ns
WT:T vs. WT:**Aged**	1.59	2.076	P>0.05	ns
WT:T vs. KO:UT	2.516	3.285	P<0.05	*
WT:T vs. KO:T	0.939	1.226	P>0.05	ns
WT:T vs. KO:**Aged**	2.495	3.139	P>0.05	ns
WT:**Aged** vs. KO:UT	0.9257	1.258	P>0.05	ns
WT:**Aged** vs. KO:T	-0.6514	0.8851	P>0.05	ns
WT:**Aged** vs. KO:**Aged**	0.9045	1.181	P>0.05	ns
KO:UT vs. KO:T	-1.577	2.143	P>0.05	ns
KO:UT vs. KO:**Aged**	-0.02119	0.02766	P>0.05	ns
KO:T vs. KO:**Aged**	1.556	2.031	P>0.05	ns

Table 2E: Nrf2 Activation in response to exhaustive exercise

Fold-Change (Exercise vs. Control)		
N	**CON**	**Acute EX**
1	1	2.62
2	1	1.23
3	1	0.94
4	1	1.66
5	1	0.99
6	1	2.14
7	1	1.25
AVG		**1.55**
SEM		**0.24**

Unpaired t test	P value	P value summary	Significantly different? (P < 0.05)	One- or two-tailed P value?	t, df
	0.0397	*	Yes	Two-tailed	t=2.307 df=12

Table 3A: Muscle fatigability (acute in situ stimulation)

Contraction Time (Sec)	WT UT									
0	100	100	100	100	100	100		97.28	100	
30	95	86	81	85.91	80.91	85.97		89.67	81	
60	93	76	73	68.58	71.84	82.91		90.69	52.9	
90	92	67	68	58.85	60.62	75		83.11	49.37	
120	92	66	56	52.82	59.1	73.47		77.24	47.95	
150	93	61	52	59.94	52.77	61.19		70.52	47.5	
180	96	60	55	50.07	53.27	61.51		66.27	46.82	
210	83	54	54	40.91	52.77	62.83		54.87	48.06	
240	75	48	47	35.27	44.27	53.19		48.92	38.73	
270	71	44	43	30.11	47.37	51.44		45.06	39.87	
300	69	39	43	30.26	50.46	52.96		44.53	37.26	
330	67	42	42	33.35	51.77	58.55		40.71	34.75	
360	64	41	39	27.37	45.49	55.05		33.69	33.51	
390	54	32	33	21.29	38.82	55.92		30.88	30.88	
420	45	33	34	17.38	37.94	43.64		30.79	26.51	
450	39	32	32	19.41	35.56	38.49		30.79	23.44	
480	36	29	29	14.9	34.99	38.37		30.03	25.82	
510	33	26	29	14.04	33.69	29.28		30.07	27.53	
540	30	30	28	11.71	41.75	37.17		29.27	25.25	

Contraction Time (Sec)	WT T									
0	100	100	100	100	100	100	100		100	100
30	78.83	93	86.53	81.83	83.9	86.99	57.49		89.77	83.68
60	78.5	92	78.65	75.12	74.78	78.92	54.75		83.09	76.63
90	74.19	90	69.99	73.2	64.71	68.5	46.68		79.58	71.96
120	69.11	86	70.06	66	60.35	62.13	43.74		73.6	69.34
150	66.37	77	69.95	64.53	55.69	63.5	47.93		68.81	66.68
180	66.56	73	61.39	64.03	55.64	58.15	48.63		65.8	64.87
210	61.19	69	54.91	61.77	50.28	56.28	45.58		58.64	57.58
240	59.15	62	53	60.05	45.07	49.36	46.88		55.31	53.47
270	55.75	58	47.95	58.04	44.86	48.57	45.18		53.08	48.07
300	53.29	60	48.26	52.64	40.82	44.07	48.31		50.98	50
330	50.52	50	49.59	59.8	40.76	44.36	47.72		50.39	48.34
360	46.66	45	45.77	60.34	40.48	39.92	48.24		47.02	47.46
390	42.3	40	41.89	50.71	39.15	34.49	45.63		44.83	40.57
420	34.98	41	39.84	51	39.38	37.78	39.26		38.88	40.17
450	39.93	44	40.49	49.71	38	39.57	38.67		37.62	40.13
480	37.89	32	45.53	51.8	33.3	37.92	44.47		37.12	38.76
510	36.3	31	45.16	52.97	35.06	36.42	37.7		36.07	41.05
540	36.49	36	44.1	54.94	33.68	37.21	41.86		35.75	40.29

Contraction Time (Sec)	KO UT									
0	100	100	100	100	100	100	100	100	100	100
30	78	96	76	81.15	100.44	56.26	77.38	84.98	77.56	83.48
60	75	80	55	68.85	92.85	46.85	76.41	68.39	54.23	72.33
90	78	73	38	61.75	75.67	40.14	49.51	56.32	55.39	59.16
120	78	69	34	52.36	56.96	32.34	40.59	46.69	46.79	49.21
150	77	68	40	50.63	54.29	29.33	52.73	45.91	44.8	46.6
180	76	77	37	50.29	34.41	23.22	36.1	44.32	44.38	37.1
210	71	66	35	46.87	32.22	20.62	41.29	32.4	30.06	33.65
240	63	61	30	43.83	29.68	19.43	34.69	35.92	27.83	27.38
270	64	56	31	44.13	19.96	10.72	21.06	33.76	28.72	25.35
300	63	55	29	44.68	19.42	13.41	22.33	36.35	28.34	24.91
330	60	57	30	41.8	23.92	19.92	25.07	30.31	29.56	26.03
360	59	50	30	35.21	18.57	10.91	14.19	30.39	32.99	22.59
390	52	50	24	32.17	18.13	10.11	21.77	25.93	23.84	22.44
420	34	46	20	35.34	16.11	15.02	17.41	19.04	26.25	21.54
450	31	44	21	32.58	16.74	14.22	19.03	18.54	27.98	20.57
480	33	43	20	26.92	14.34	9.2	16.01	23.78	26.44	19.83
510	35	44	19	24.85	15.05	12.91	14.95	18.24	29.32	20.12
540	35	40	23	22.15	15.76	13.01	15.94	20.87	27.37	22.14

Contraction Time (Sec)	KO T									
0	100	100	100	100		100	100	100	100	
30	93	86	73.12	78.43		81.97	84.13	83	84	
60	73	74	61.19	77.27		70.04	73.07	69	74	
90	72	66	55.06	69.95		65.95	61.62	64	66	
120	72	65	48.22	70.99		64.65	54.47	56	60	
150	70	58	43.04	70.72		60.56	43.59	55	55	
180	55	56	41.14	68.26		59.26	39.6	47	51	
210	57	51	41.22	67.04		56.25	37.77	43	45	
240	47	55	41.34	64.63		55.17	37.58	41	41	
270	50	50	40.81	63.28		53.45	38.87	40	40	
300	52	51	40.52	60.75		52.08	39.25	37	39	
330	54	48	40.81	62.11		52.16	38.11	37	38	
360	47	46	38.53	65.54		51.07	39.22	37	37	
390	51	40	37.7	67.03		49.07	32.52	35	35	
420	51	47	35.62	65.16		42.39	30.77	32	31	
450	51	52	34.8	65.67		47.34	31.68	27	30	
480	48	48	32.43	65.03		46.62	31.04	31	30	
510	49	50	31.46	64.63		45.47	28.79	31	30	
540	46	53	31.98	66.32		44.9	29.93	32	29	

Table 3B: Linear regression (fatigue rates between WT UT vs. KO UT)

Linear Regression		
	WT UT	**KO UT**
Best-fit values		
Slope	-0.2787 ± 0.04176	-0.4038 ± 0.04026
Y-intercept when X=0.0	96.23 ± 3.069	96.09 ± 2.959
X-intercept when Y=0.0	345.3	238
1/slope	-3.588	-2.477
95% Confidence Intervals		
Slope	-0.3632 to -0.1941	-0.4848 to -0.3227
Y-intercept when X=0.0	90.01 to 102.4	90.13 to 102.0
X-intercept when Y=0.0	277.9 to 470.6	207.2 to 283.7
Goodness of Fit		
R square	0.5396	0.6769
Sy.x	11.21	12.08
Is slope significantly non-zero?		
F	44.53	100.6
DFn, DFd	1.000, 38.00	1.000, 48.00
P value	< 0.0001	< 0.0001
Deviation from zero?	Significant	Significant
Data		
Number of X values	5	5
Maximum number of Y replicates	8	10
Total number of values	40	50
Number of missing values	10	0
Equation	Y = -0.2787*X + 96.23	Y = -0.4038*X + 96.09

Table 3C: Force production (% of initial at 5 minutes of stimulation)

Force production at 5 minutes				
N	**WT UT**	**WT T**	**KO UT**	**KO T**
1	39	53.29	29	52
2	43	60	44.68	51
3	30.26	48.26	19.42	40.52
4	50.46	52.64	13.41	60.75
5	52.96	40.82	22.33	52.08
6	44.53	44.07	36.35	39.25
7	37.26	48.31	28.34	37
8		50.98	24.91	39
9		50		
10				
AVG	**42.50**	**49.82**	**27.31**	**46.45**
SEM	**2.95**	**1.84**	**3.47**	**3.05**

ANOVA				
ANOVA TABLE	**SS**	**df**	**MS**	**P-value**
Between	2436	3	811.9	< 0.0001
Within	1803	28	64.4	
Total	4239	31		

POST-HOC TEST				
Bonferroni	**Mean Diff.**	**t-value**	**P-value**	**Summary**
WT UT vs. **WT T**	-7.323	1.811	P>0.05	ns
WT UT vs. **KO UT**	15.19	3.657	P<0.05	**
WT UT vs. **KO T**	-3.954	0.952	P>0.05	ns
WT T vs. **KO UT**	22.51	5.773	P<0.05	****
WT T vs. **KO T**	3.369	0.8639	P>0.05	ns
KO UT vs. **KO T**	-19.15	4.771	P<0.05	***

Table 3D: Force production (% of initial at 9 minutes of stimulation)

Force production at 9 minutes				
N	**WT UT**	**WT T**	**KO UT**	**KO T**
1	30	36.49	35	46
2	30	36	40	53
3	28	44.1	23	31.98
4	11.71	54.94	22.15	66.32
5	41.75	33.68	15.76	44.9
6	37.17	37.21	13.01	29.93
7	29.27	41.86	15.94	32
8	25.25	35.75	20.87	29
9		40.29	27.37	
10			22.14	
AVG	**29.14**	**40.04**	**23.22**	**41.64**
SEM	**3.12**	**2.17**	**3.38**	**4.73**

ANOVA				
ANOVA TABLE	**SS**	**df**	**MS**	**P-value**
Between	2058	3	686.1	0.0006
Within	2791	31	90.04	
Total	4850	34		

POST-HOC TEST				
Bonferroni	**Mean Diff.**	**t-value**	**P-value**	**Summary**
WT UT vs. **WT T**	-10.89	2.362	P>0.05	ns
WT UT vs. **KO UT**	5.62	1.249	P>0.05	ns
WT UT vs. **KO T**	-12.5	2.634	P>0.05	ns
WT T vs. **KO UT**	16.51	3.787	P<0.05	**
WT T vs. **KO T**	-1.606	0.3482	P>0.05	ns
KO UT vs. **KO T**	-18.12	4.025	P<0.05	**

Table 4A: SS mitochondrial State 4 Respiration (n atoms O2/mg protein/ min)

SS Respiration State 4				
N	**WT UT**	**WT T**	**KO UT**	**KO T**
1	9.44	4.95	4.07	12.55
2	10.05	7.59	9.84	8.72
3	3.64	5.42	7.83	8.95
4	8.02	7.11	6.96	6.57
5	3.01	3.19	8.99	13.33
6	2.78	14.64	5.98	5.85
7	7.63	5.65	5.46	10.11
8				
9				
10				
AVG	**6.37**	**6.94**	**7.02**	**9.44**
SEM	**1.18**	**1.40**	**0.77**	**1.06**

ANOVA				
ANOVA TABLE	**SS**	**df**	**MS**	**P-value**
Between	16.5	3	5.499	0.6879
Within	276.8	25	11.07	
Total	293.3	28		

POST-HOC TEST				
Bonferroni	**Mean Diff.**	**t-value**	**P-value**	**Summary**
WT UT vs. **WT T**	-0.5686	0.3197	P>0.05	ns
WT UT vs. **KO UT**	-0.6514	0.3663	P>0.05	ns
WT UT vs. **KO T**	-2.002	1.162	P>0.05	ns
WT T vs. **KO UT**	-0.08286	0.04659	P>0.05	ns
WT T vs. **KO T**	-1.433	0.8322	P>0.05	ns
KO UT vs. **KO T**	-1.35	0.7841	P>0.05	ns

Table 4A (Cont): SS mitochondrial State 3 Respiration (n atoms O2/mg protein/ min)

SS Respiration State 3				
N	**WT UT**	**WT T**	**KO UT**	**KO T**
1	22.06	17.66	31.69	27.66
2	25.12	24.27	30.55	27.51
3		23.33	21.11	34.31
4	24.15	24.48	16.25	29.44
5	11.89	26.95		30.98
6	20.48	32.73	19.24	11.32
7	15.55	25.7	16.85	20.31
8				20.34
9				
10				
AVG	**19.88**	**25.02**	**22.62**	**25.23**
SEM	**2.11**	**1.70**	**2.79**	**2.63**

ANOVA				
ANOVA TABLE	**SS**	**df**	**MS**	**P-value**
Between	265.3	3	88.42	0.6142
Within	1191	25	47.64	
Total	1456	28		

POST-HOC TEST				
Bonferroni	**Mean Diff.**	**t-value**	**P-value**	**Summary**
WT UT vs. **WT T**	-6.89	1.868	P>0.05	ns
WT UT vs. **KO UT**	-2.366	0.6412	P>0.05	ns
WT UT vs. **KO T**	-7.107	1.989	P>0.05	ns
WT T vs. **KO UT**	4.524	1.226	P>0.05	ns
WT T vs. **KO T**	-0.2166	0.06064	P>0.05	ns
KO UT vs. **KO T**	-4.741	1.327	P>0.05	ns

Table 4B: IMF mitochondrial State 4 Respiration (n atoms O2/mg protein/ min)

IMF State 4 Respiration				
N	**WT UT**	**WT T**	**KO UT**	**KO T**
1	13.62	15.73	6.12	16.79
2	9.71	13.87	6.22	5.67
3	10.77	18.97	10.19	15.54
4	19.6	12.68	7.58	19.04
5	20.51	20.68	11.55	21.04
6	16.35	24.86	14.02	10.64
7	12.4	19.78	13.41	17.02
8	19.49	19.18	6.56	24.62
9	11.16	12.19	7.33	20.29
10	18.97	21.46	9.17	10.57
AVG	**15.26**	**17.55**	**9.46**	**16.12**
SEM	**1.32**	**1.41**	**1.16**	**1.81**

ANOVA				
ANOVA TABLE	**SS**	**df**	**MS**	**P-value**
Between	429	3	143	0.0005
Within	686.8	36	19.08	
Total	1116	39		

POST-HOC TEST				
Bonferroni	**Mean Diff.**	**t-value**	**P-value**	**Summary**
WT UT vs. **WT T**	-2.682	1.373	P>0.05	ns
WT UT vs. **KO UT**	6.043	3.094	P<0.05	*
WT UT vs. **KO T**	-0.864	0.4423	P>0.05	ns
WT T vs. **KO UT**	8.725	4.467	P<0.05	***
WT T vs. **KO T**	1.818	0.9307	P>0.05	ns
KO UT vs. **KO T**	-6.907	3.536	P<0.05	**

Table 4B (Cont): IMF mitochondrial State 3 Respiration (n atoms O2/mg protein/ min)

IMF State 3 Respiration				
N	**WT UT**	**WT T**	**KO UT**	**KO T**
1	56.78	60.41	49.03	43.87
2	41.49	73.22	40.44	67.34
3	48.82	56.04	45.61	67.45
4	64.21	75.84	40.68	65.75
5	63.47	73.93	62.68	63.04
6	62.63	76.11	71.09	58.85
7	41.11	72.51	65.42	63.58
8	51.05	76.63	33.41	79.63
9	52.17	56.78	20.09	61.39
10	56.04	65.92	45.6	58.85
AVG	**53.78**	**69.05**	**51.05**	**62.98**
SEM	**2.67**	**2.89**	**4.83**	**2.84**

ANOVA				
ANOVA TABLE	**SS**	**df**	**MS**	**P-value**
Between	2700	3	899.9	0.0004
Within	4141	36	115	
Total	6841	39		

POST-HOC TEST				
Bonferroni	**Mean Diff.**	**t-value**	**P-value**	**Summary**
WT UT vs. **WT T**	-14.96	3.119	P<0.05	*
WT UT vs. **KO UT**	6.372	1.329	P>0.05	ns
WT UT vs. **KO T**	-9.198	1.918	P>0.05	ns
WT T vs. **KO UT**	21.33	4.448	P<0.05	***
WT T vs. **KO T**	5.764	1.202	P>0.05	ns
KO UT vs. **KO T**	-15.57	3.246	P<0.05	*

Table 4C: SS Mitochondrial State 4 ROS production (ROS/n atoms O2/min)

SS ROS State 4				
N	**WT UT**	**WT T**	**KO UT**	**KO T**
1	5518.55	9513.23	12240.9	3632.1
2	4236.03	7679.32	4855.01	4862.4
3	13419.1	9954.88	5263.31	5377.39
4	5788.87	5409.09	5464.9	7089.41
5	7699.18	12881.2	4512.4	3086.08
6		2474.03		5104.54
7				4343.21
8				
9				
10				
AVG	**7332.34**	**7985.29**	**6467.30**	**4785.02**
SEM	**1619.29**	**1497.65**	**1452.75**	**492.32**

ANOVA				
ANOVA TABLE	**SS**	**df**	**MS**	**P-value**
Between	34850000	3	11620000	0.9241
Within	1482000000	20	74090000	
Total	1517000000	23		

POST-HOC TEST				
Bonferroni	**Mean Diff.**	**t-value**	**P-value**	**Summary**
WT UT vs. **WT T**	-653	0.1253	P>0.05	ns
WT UT vs. **KO UT**	865	0.1589	P>0.05	ns
WT UT vs. **KO T**	-2289	0.4664	P>0.05	ns
WT T vs. **KO UT**	1518	0.2912	P>0.05	ns
WT T vs. **KO T**	-1636	0.3519	P>0.05	ns
KO UT vs. **KO T**	-3154	0.6427	P>0.05	ns

Table 4C (Cont): SS Mitochondrial State 3 ROS production (ROS/n atoms O2/min)

SS ROS State 3				
N	**WT UT**	**WT T**	**KO UT**	**KO T**
1	2928.62	3488	1851.09	2151.72
2	2678.59	2525.53	1635.03	1558.5
3	7474.3	2403.39	2252.56	1226.89
4	2172.28	1905.11	2743.68	1741.79
5	1827.38	1976.26	7064.88	1651.59
6		1361.06		5042.31
7				1922.34
8				2348.62
9				
10				
AVG	**3416.23**	**2276.56**	**3109.45**	**2205.47**
SEM	**1032.51**	**295.07**	**1006.75**	**423.61**

ANOVA				
ANOVA TABLE	**SS**	**df**	**MS**	**P-value**
Between	6404000	3	2135000	0.5153
Within	54250000	20	2713000	
Total	60660000	23		

POST-HOC TEST				
Bonferroni	**Mean Diff.**	**t-value**	**P-value**	**Summary**
WT UT vs. **WT T**	1140	1.143	P>0.05	ns
WT UT vs. **KO UT**	306.8	0.2945	P>0.05	ns
WT UT vs. **KO T**	1211	1.289	P>0.05	ns
WT T vs. **KO UT**	-832.9	0.8351	P>0.05	ns
WT T vs. **KO T**	71.09	0.07992	P>0.05	ns
KO UT vs. **KO T**	904	0.9628	P>0.05	ns

Table 4D: IMF Mitochondrial State 4 ROS production (ROS/n atoms O2/min)

IMF State 4 ROS				
N	**WT UT**	**WT T**	**KO UT**	**KO T**
1	1797.83	1333.3	3383.73	1416.28
2	2167.44	1841.06	3638.13	3467.04
3	2277.78	1168.57	2162.4	1867.51
4	1572.01	2164.89	3556.15	1329.1
5	1800.88	1309.54	2862.86	1324.51
6	1753.74	945.8	2164.88	2747.92
7	1296.61	1287.01	2348.71	1369.96
8	2944.6	1370.88	3688.68	636.55
9	2061.99	1168.38	5920.34	1062.03
10	1168.57	1228.14		1448.37
AVG	**1884.15**	**1398.83**	**2975.69**	**1666.93**
SEM	**162.53**	**124.68**	**238.12**	**264.72**

ANOVA				
ANOVA TABLE	**SS**	**df**	**MS**	**P-value**
Between	20310000	3	6772000	< 0.0001
Within	20710000	35	591793	
Total	41030000	38		

POST-HOC TEST				
Bonferroni	**Mean Diff.**	**t-value**	**P-value**	**Summary**
WT UT vs. **WT T**	502.4	1.46	P>0.05	ns
WT UT vs. **KO UT**	-1419	4.014	P<0.05	**
WT UT vs. **KO T**	217.2	0.6314	P>0.05	ns
WT T vs. **KO UT**	-1921	5.435	P<0.05	****
WT T vs. **KO T**	-285.2	0.8289	P>0.05	ns
KO UT vs. **KO T**	1636	4.628	P<0.05	***

Table 4D (Cont): IMF Mitochondrial State 3 ROS production (ROS/n atoms O2/min)

IMF State 3 ROS				
N	**WT UT**	**WT T**	**KO UT**	**KO T**
1	672.37	357.72	622.03	980.86
2	704.16	329.13	782.34	285.08
3	632.42	559.21	815.26	427.37
4	635.86	465.53	855.12	555.98
5	619.72	538.39	727.01	706
6	669.55	297.81	568.65	964.07
7	480.2	377.92	725.15	416.49
8	643.98	351.13	1372.52	263.16
9	706.68	486.32	770.26	446.96
10	559.21	220.25		220.66
AVG	**632.42**	**418.13**	**808.51**	**526.66**
SEM	**21.72**	**31.93**	**87.31**	**86.95**

ANOVA				
ANOVA TABLE	**SS**	**df**	**MS**	**P-value**
Between	837606	3	279202	0.0004
Within	1260000	35	35993	
Total	2097000	38		

POST-HOC TEST				
Bonferroni	**Mean Diff.**	**t-value**	**P-value**	**Summary**
WT UT vs. **WT T**	234.1	2.759	P>0.05	ns
WT UT vs. **KO UT**	-171.8	1.971	P>0.05	ns
WT UT vs. **KO T**	105.8	1.246	P>0.05	ns
WT T vs. **KO UT**	-405.9	4.657	P<0.05	***
WT T vs. **KO T**	-128.3	1.512	P>0.05	ns
KO UT vs. **KO T**	277.6	3.185	P<0.05	*

Table 5A: NQO1 Protein expression in WT and KO mice (UT vs. T)

NQO1				
N	**WT UT**	**WT T**	**KO UT**	**KO T**
1	2.39	1.41	1.51	1.25
2	1.74	1.52	0.82	0.86
3	1.83	1.34	0.84	0.95
4	1.38	1.17	0.33	0.34
5	1.55	1.37	0.33	0.35
6	1.34	1.19	0.32	0.28
AVG	1.71	1.33	0.69	0.67
SEM	0.16	0.06	0.19	0.17

2-WAY ANOVA			
Source of Variation	**P value**	**P value summary**	**Significant?**
Interaction	0.26	ns	No
Genotype	< 0.0001	****	Yes
Training	0.2114	ns	No

	POST-HOC TEST			
Bonferroni	**Mean Diff.**	**t-value**	**P-value**	**Summary**
WT:UT vs. WT:T	0.3717	1.733	P>0.05	ns
WT:UT vs. KO:UT	1.013	4.724	P<0.05	***
WT:UT vs. KO:T	1.033	4.818	P<0.05	***
WT:T vs. KO:UT	0.6417	2.992	P<0.05	*
WT:T vs. KO:T	0.6617	3.085	P<0.05	*
KO:UT vs. KO:T	0.02	0.09324	P>0.05	ns

Table 5B: HO-1 Protein expression in WT and KO mice (UT vs. T)

HO-1				
N	**WT UT**	**WT T**	**KO UT**	**KO T**
1	0.91	1.75	3.64	3.18
2	4.58	3.56	3.53	8.23
3	5.55	6.70	3.00	6.57
4	8.02	3.77	3.07	2.12
5	2.58	2.73	3.74	4.53
6	2.73	4.58	5.00	7.32
7	3.29	4.26	2.72	7.35
AVG	3.95	3.91	3.53	5.62
SEM	0.88	0.59	0.28	0.89

2-WAY ANOVA			
Source of Variation	**P value**	**P value summary**	**Significant?**
Interaction	0.1439	ns	No
Genotype	0.3714	ns	No
Training	0.1605	ns	No

POST-HOC TEST				
Bonferroni	**Mean Diff.**	**t-value**	**P-value**	**Summary**
WT:UT vs. WT:T	0.04429	0.04443	P>0.05	ns
WT:UT vs. KO:UT	0.4229	0.4242	P>0.05	ns
WT:UT vs. KO:T	-1.663	1.668	P>0.05	ns
WT:T vs. KO:UT	0.3786	0.3798	P>0.05	ns
WT:T vs. KO:T	-1.707	1.713	P>0.05	ns
KO:UT vs. KO:T	-2.086	2.092	P>0.05	ns

Table 5C: G6PD Protein expression in WT and KO mice (UT vs. T)

G6PD				
N	**WT UT**	**WT T**	**KO UT**	**KO T**
1	1.62	2.21	1.74	3.66
2	3.37	3.22	1.47	2.16
3	0.80	3.22	0.68	0.81
4	0.75	3.11	0.57	0.93
5	1.48	3.83	3.36	2.02
6	4.26	5.32	3.37	5.74
7	4.21	4.18	3.17	2.02
8	2.20	1.46	2.99	5.48
9	4.63	5.11	5.66	6.11
AVG	**2.05**	**3.49**	**1.87**	**2.55**
SEM	**0.59**	**0.42**	**0.51**	**0.76**

2-WAY ANOVA			
Source of Variation	**P value**	**P value summary**	**Significant?**
Interaction	0.8089	ns	No
Genotype	0.7614	ns	No
Training	0.1605	ns	No

POST-HOC TEST				
Bonferroni	**Mean Diff.**	**t-value**	**P-value**	**Summary**
WT:UT vs. WT:T	-0.9267	1.188	P>0.05	ns
WT:UT vs. KO:UT	0.03444	0.04417	P>0.05	ns
WT:UT vs. KO:T	-0.6233	0.7993	P>0.05	ns
WT:T vs. KO:UT	0.9611	1.232	P>0.05	ns
WT:T vs. KO:T	0.3033	0.3889	P>0.05	ns
KO:UT vs. KO:T	-0.6578	0.8434	P>0.05	ns

Table 5D: GPx1 Protein expression in WT and KO mice (UT vs. T)

GPx1				
N	**WT UT**	**WT T**	**KO UT**	**KO T**
1	1.95	1.97	2.58	5.57
2	4.64	4.15	3.13	4.23
3	1.97	4.17	4.61	4.00
4	4.18	6.37	2.85	2.11
5	3.59	8.58	5.82	4.19
6	6.98	9.19	7.91	
7	3.18	3.42	4.71	2.24
8	2.75	2.85	4.04	7.44
9	5.40	5.58	4.78	4.61
AVG	**3.85**	**5.14**	**4.49**	**4.30**
SEM	**0.55**	**0.84**	**0.55**	**0.61**

2-WAY ANOVA			
Source of Variation	**P value**	**P value summary**	**Significant?**
Interaction	0.2622	ns	No
Genotype	0.8788	ns	No
Training	0.4047	ns	No

POST-HOC TEST				
Bonferroni	**Mean Diff.**	**t-value**	**P-value**	**Summary**
WT:UT vs. WT:T	-1.293	1.427	P>0.05	ns
WT:UT vs. KO:UT	-0.6433	0.7097	P>0.05	ns
WT:UT vs. KO:T	-0.4499	0.4814	P>0.05	ns
WT:T vs. KO:UT	0.65	0.717	P>0.05	ns
WT:T vs. KO:T	0.8435	0.9027	P>0.05	ns
KO:UT vs. KO:T	0.1935	0.2071	P>0.05	ns

Table 6A: NQO1 Protein Expression WT and KO (Young vs. Older mice)

NQO1 Young vs. Older Mice			
N	**WT Y**	**WT A**	**KO A**
1	5.36	7.06	0.79
2	4.14	7.8	1.06
3	4.29	4.65	1.19
4	3.93	6.01	0.9
5	3.54	4.56	0.69
6	4.65	10.46	2.2
7	7.54	8.06	
AVG	**4.78**	**6.94**	**1.14**
SEM	**0.51**	**0.79**	**0.22**

ANOVA				
ANOVA TABLE	**SS**	**df**	**MS**	**P-value**
Between	110.1	2	55.03	< 0.0001
Within	38.57	17	2.269	
Total	148.6	19		

POST-HOC TEST				
Bonferroni	**Mean Diff.**	**t-value**	**P-value**	**Summary**
WT Y vs. WT A	-2.164	2.688	P<0.05	*
WT Y vs. KO A	3.64	4.344	P<0.05	**
WT A vs. KO A	5.805	6.927	P<0.05	****

Table 6B: HO-1 Protein Expression WT and KO (Young vs. Older mice)

HO-1 Young vs. Older Mice			
N	**WT Y**	**WT A**	**KO A**
1	3.81	9.31	7.47
2	1.92	10.24	11.72
3	3.68	4.02	7.52
4	7.8	5.01	4.74
5	5.68	6.13	9.88
6		7.17	13.65
7		8.98	
AVG	**4.58**	**7.27**	**9.16**
SEM	**1.00**	**0.88**	**1.32**

ANOVA				
ANOVA TABLE	**SS**	**df**	**MS**	**P-value**
Between	57.49	2	28.75	0.0381
Within	105.3	15	7.017	
Total	162.7	17		

POST-HOC TEST				
Bonferroni	**Mean Diff.**	**t-value**	**P-value**	**Summary**
WT Y vs. WT A	-2.688	1.733	P>0.05	ns
WT Y vs. KO A	-4.585	2.859	P<0.05	*
WT A vs. KO A	-1.898	1.288	P>0.05	ns

Table 6C: G6PD Protein Expression WT and KO (Young vs. Older mice)

G6PD Young vs. Older Mice			
N	**WT Y**	**WT A**	**KO A**
1	2.23	6.06	4.2
2	3.8	5.35	4.01
3	6.74	2.04	3.18
4	1.06	3.93	3.86
5	2.17	2.6	1.86
6		4.21	5.24
7		6.03	
AVG	**3.46**	**4.32**	**3.73**
SEM	**1.23**	**0.60**	**0.46**

ANOVA				
ANOVA TABLE	**SS**	**df**	**MS**	**P-value**
Between	57.49	2	28.75	0.0381
Within	105.3	15	7.017	
Total	162.7	17		

POST-HOC TEST				
Bonferroni	**Mean Diff.**	**t-value**	**P-value**	**Summary**
WT Y vs. WT A	-1.117	1.151	P>0.05	ns
WT Y vs. KO A	-0.525	0.5231	P>0.05	ns
WT A vs. KO A	0.5921	0.6422	P>0.05	ns

Table 6D: GPx1 Protein Expression WT and KO (Young vs. Older mice)

GPx1 Young vs. Older Mice			
N	**WT Y**	**WT A**	**KO A**
1	8.34	8.19	7.05
2	6.75	6.74	8.98
3	6.07	3.54	4.99
4	3.55	3.73	3.27
5	4.43	5.94	7.09
6	9.14	10.45	6.72
7		12.53	
AVG	**7.05**	**7.30**	**6.35**
SEM	**0.67**	**1.26**	**0.80**

ANOVA				
ANOVA TABLE	**SS**	**df**	**MS**	**P-value**
Between	3.891	2	1.946	0.378
Within	110	16	6.878	
Total	113.9	18		

POST-HOC TEST				
Bonferroni	**Mean Diff.**	**t-value**	**P-value**	**Summary**
WT Y vs. WT A	-0.9229	0.6325	P>0.05	ns
WT Y vs. KO A	0.03	0.01981	P>0.05	ns
WT A vs. KO A	0.9529	0.6531	P>0.05	ns

Table 7: Maximum TET per mg of muscle

Maximum TET per mg of muscle (mN/mg)				
N	**WT UT**	**WT T**	**KO UT**	**KO T**
1	7.00	5.46	6.21	6.63
2	6.47	3.69	7.27	4.15
3	6.69	9.03	4.12	7.10
4	5.31	7.44	7.05	4.79
5	4.81	6.53	2.01	7.49
6	3.74	5.94	3.37	6.47
7	8.48	5.27	5.64	9.56
8	4.68	7.76	6.10	9.18
9	6.23	7.30	7.51	6.84
10	4.55	7.19	5.02	
AVG	**5.80**	**6.56**	**5.43**	**6.91**
SEM	**0.45**	**0.48**	**0.57**	**0.59**

2-WAY ANOVA			
Source of Variation	**P value**	**P value summary**	**Significant?**
Interaction	0.4977	ns	No
Genotype	0.9888	ns	No
Training	0.0388	*	Yes

POST-HOC TEST				
Bonferroni	**Mean Diff.**	**t-value**	**P-value**	**Summary**
WT:UT vs. WT:T	-0.765	1.048	No	ns
WT:UT vs. KO:UT	0.366	0.5013	No	ns
WT:UT vs. KO:T	-1.116	1.488	No	ns
WT:T vs. KO:UT	1.131	1.549	No	ns
WT:T vs. KO:T	-0.3512	0.4682	No	ns
KO:UT vs. KO:T	-1.482	1.976	No	ns

Appendix B – Supplementary Figures

Supplementary 1

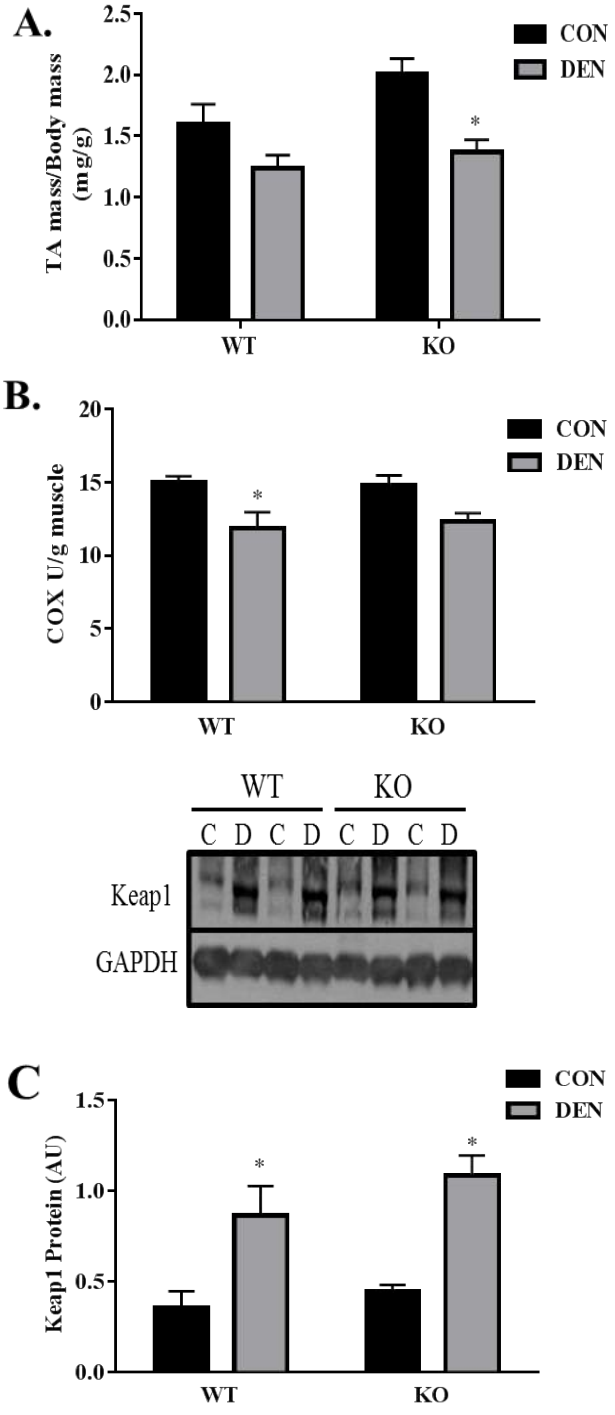

Figure S1. Following 7 days of denervation **(A)** TA mass **(B)** COX activity and the **(C)** protein expression of keap1 were measured. **P*<0.05 Den vs. Con. Data are expressed as means ± SEM.

Supplementary 2

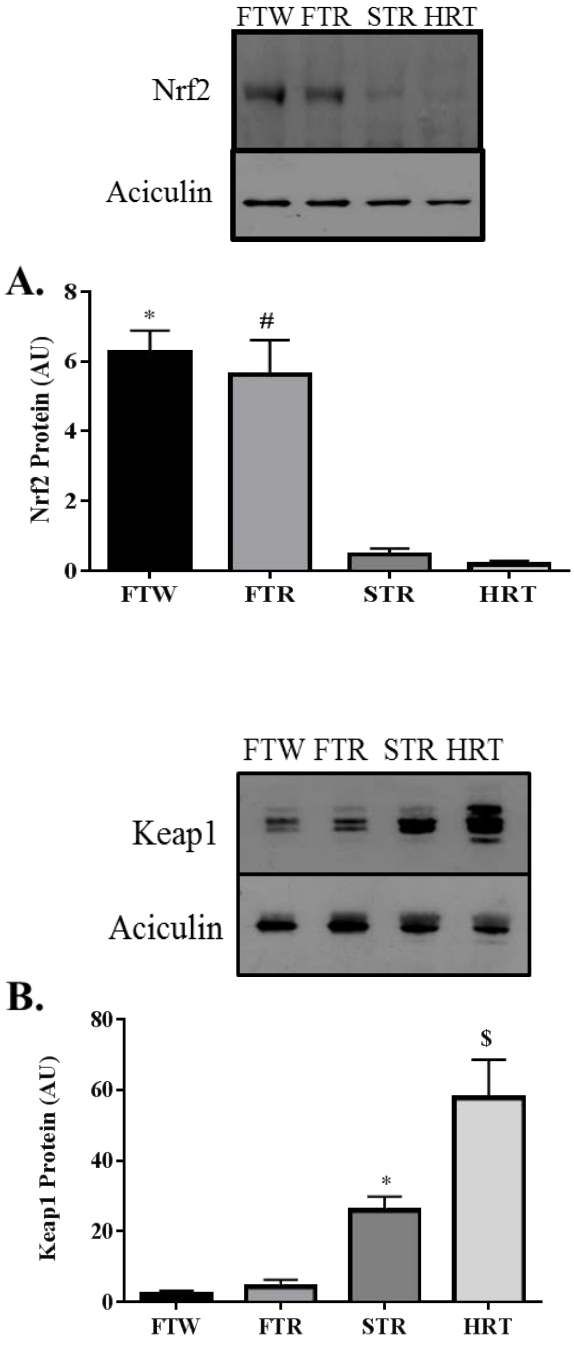

Figure S2. Protein expression for (A) Nrf2 and (B) Keap1 were examined in different fibre types in order to determine if there was any correlation between the Nrf2-Keap1 pathway and mitochondrial content. The ratio of Keap1:Nrf2 protein was highest in the most oxidative muscle types, suggesting that the pathway is relatively inactive when mitochondrial content is high. The opposite ratio was observed in the low oxidative FTW muscle. Data are expressed as means ± SEM; ANOVA was used for analysis; Nrf2 **P*<0.05 FTW vs. STR and HRT, #*P*<0.05 FTR vs. STR and HRT; keap1 **P*<0.05 STR vs. Fast twitch fibres; $*P*<0.05 HRT vs. all fibre types.

Supplementary 3

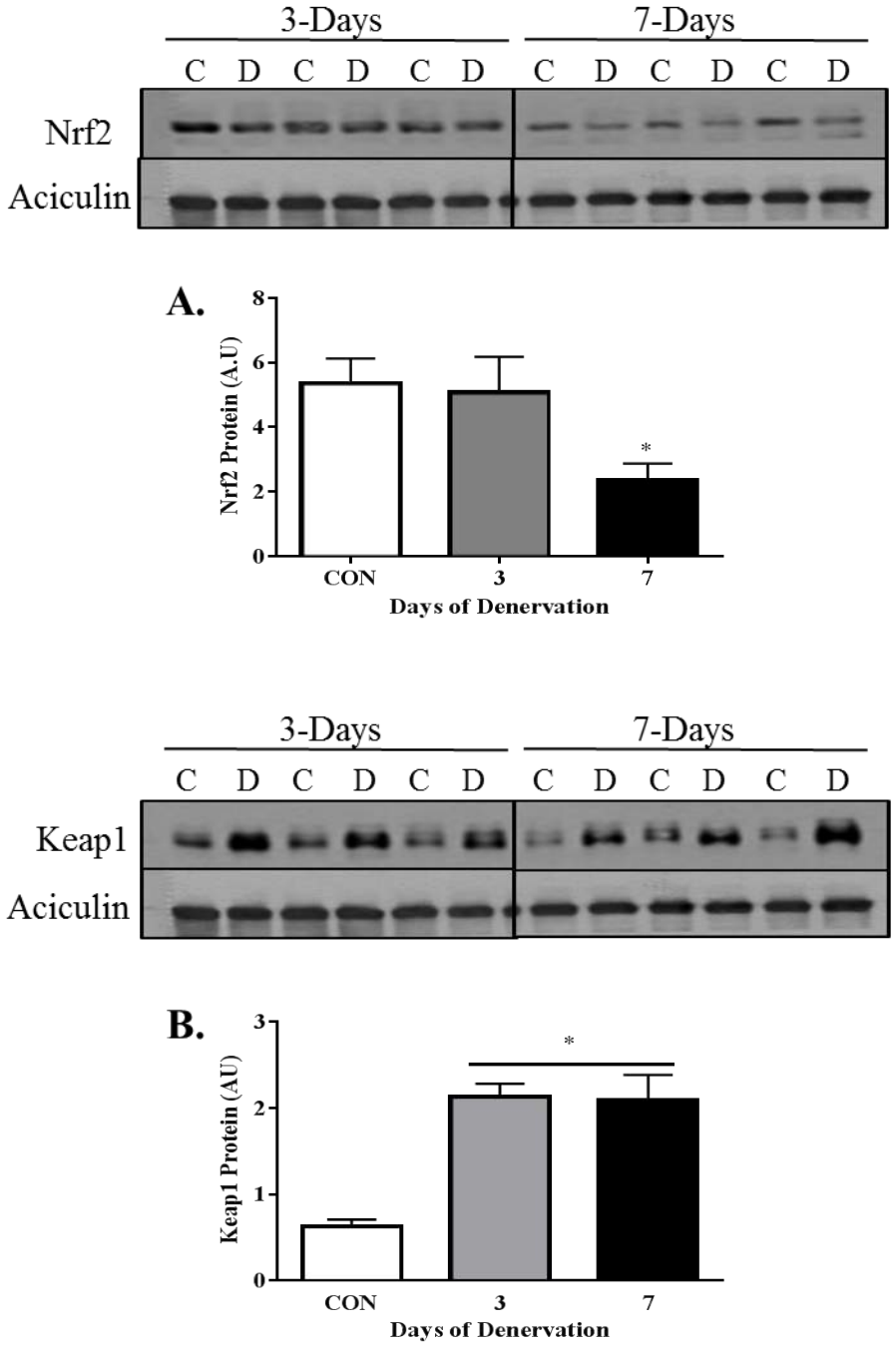

Figure S3. Male Sprague-Dawley rats were subjected to 3 and 7 days of denervation. Nrf2 **(A)** and Keap1 **(B)** protein levels were examined. Nrf2 protein was reduced at day 7, however, Keap1 protein was significantly increased following 3 and 7 days of denervation. **P*<0.05 Den vs. Con. Data are expressed as means ± SEM.

APPENDIX C – Protocols

CYTOCHROME C OXIDASE ASSAY FOR MICROPLATE READER

J. Biol. Chem. 189:665, 1951,
Meth. Biochem. Anal. 2:427, 1955,
Meth. Enzymol. 10:245, 1967.

THEORY:

Tissue extract containing cytochrome c oxidase is added to the test solution containing fully reduced cytochrome c. The rate of cytochrome c oxidation is measured over time as a reduction in absorbance at 550 nm. The reaction is carried out at 30^{o} C.

REAGENTS:

1. 20 mM KCN; MW= 65.12, 13.02 mg/10 ml dH_2O

2. 100 mM K-Phosphate Buffer

- make up 0.1 M KH_2PO_4; MW= 136.09
  = 13.6 g/1000 ml
  (pH approx. 5)
  (rm. temp)
- make up 0.1 M $K_2HPO_4.3H_2O$; MW= 174.18
  = 17.4 g/1000 ml
  (pH approx. 8)
  (rm. temp)
- mix in equal proportions, pH to 7.0

3. 10 mM K-Phosphate Buffer

- dilute 0.1 M KPO_4 Buffer prepared above 1:10 with ddH_2O (eg. 10 ml buffer + 90 ml ddH_2O)

4. Extraction Buffer (100 mM Na-K-Phosphate, 2 mM EDTA; pH 7.2)

- 500 ml 0.1 M $Na_2HPO_4.\ 2H_2O$;

Combine 8.9 g sodium phosphate with 0.372 g EDTA up to 500 ml.

- 200 ml 0.1 M KH_2PO_4;

Combine 2.7 g potassium phosphate with 0.149 g EDTA up to 200 ml.

- combine both solutions and pH to 7.2

5. Test Solution (reduced cytochrome c, 2 mg/ml), for 10 ml (enough for 36 microplate wells);

- weigh out 20 mg of horse heart cytochrome c (Sigma, C-2506) in a scintillation vial

- add 1 ml of 10 mM KPO_4 buffer and dissolve cytochrome c

- make up a small volume of 10 mg/ml sodium dithionite-10 mM KPO_4 stock solution (make fresh each experiment and use within twenty minutes)

- add 40 μl of the dithionite stock solution to the test solution and observe red-orange colour change

- add 8 ml of ddH_2O

- add 1 ml of 100 mM KPO_4 buffer.

PROCEDURE:

1. Place powdered muscle samples in liquid N_2.

2. Add 50 μl of extraction Buffer to 1.5 ml Eppendorf tubes in the aluminum block on ice. (One Eppendorf per sample).

3. Add 5-7.5 mg tissue to each tube, recording exact tissue mass. Mix by tapping.

4. Add the volume of Extraction Buffer required to obtain a 20-fold dilution.

5. Add a stir bar and mix for 15 min. Make up Test Solution during this time and wrap in foil.

6. Sonicate each tube 3 x 3 seconds, cleaning the probe between samples.

7. Pipette some of 20-fold sample extract into new Eppendorf tube and add volume of Extraction Buffer required to obtain an 80-fold dilution. (eg. 50 μl of 20-fold extract + 150 μl Ext. Buffer = 200 μl of 80-fold sample extract). Keep 80-fold sample extract tube on ice for duration of experiment

8. Add 270 μl of Test Solution into 4-8 wells of 96-well microplate and incubate at 30°C for 10 minutes to stabilize the temperature and absorbance.

9. Open KC4 plate reader program (on Triton). Select CONTROL icon, then PRE-HEATING tab, enter 30°C and select ON. (Do not run assay until KC4 temperature has reached 30°C.)

10. Select WIZARD icon, then READING PARAMETERS icon.

- Select Kinetic for Reading Type.
- Select Absorbance for Reader and 550 nm for wavelength (drop-down menu).
- Select Sweep for Read Mode.
- Select 96 Well Plate (default) for Plate Type.
- Enter first and last well to be read (eg. A1 and A4 if reading 4 samples simultaneously).
- Select Yes and Pre-heating and enter 30 for Temperature Control.
- For Shaking enter 0 for both intensity and duration (shaking is not necessary and it will delay the first reading).
- Do not select either of the two options for Pre-reading.
- Click on the KINETIC… rectangular tile to open the Kinetic window.
- Enter run time (1 minute is recommended) and select MINIMUM for Interval time (under these conditions the minimum Interval time should be 3 seconds).
- Select Allow Well Zoom During Read to see data in real time (optional).
- Under Scales, checkmarks should appear for both Auto check boxes. Do not select Individual Well Auto Scaling.
- Press OK to return to Reading Parameters window. Press OK to return to Wizard window. Press OK. Do not save the protocol.

11. Set the multipipette to 250 μl and secure 4-8 yellow tips on the white projections (make sure they are on tight and all at the same height).

12. In a second, clean 96 well plate, pipette samples into 4-8 empty wells (start with A1). Recommended volumes: 30 μl of 80-fold extract for Mixed Gastroc, 10 μl for Heart. Adjust volumes according to oxidative capacity of the tissue. (eg. 25 μl for Red Gastrocnemius and 35 μl for White Gastrocnemius).

13. Remove microplate with Test Solution in 4-8 wells from the incubator (as long as it has been incubating for 10 minutes). Place this plate beside the plate with the sample extracts in it.

14. On KC4 program, select the READ icon and press the START READING icon, then press the READ PLATE button. A box will appear that says, “Insert plate and start reading”. Do not press OK yet, but move the mouse so that the cursor hovers over the OK button.

15. Using the multipipette (set to 250 μl) carefully draw up the Test Solution. Make sure the volume is equal in all the pipette tips, and that no significant air bubbles have entered any of the tips.

16. Pipette the Test Solution into the wells with the sample extracts (the second plate). As soon as all the Test Solution has been expelled from the tips (do not wait for the second push from the multipipette), place the plate onto the tray of the

plate reader and with the other hand on the mouse, press the OK button. (Speed at this point is paramount, as there is an unavoidable latency period between the time of pressing the OK button and the time of the first reading.)

17. If desired, add 5 μl KCN to one of the wells to measure any absorbance changes in the presence of the CYTOX inhibitor.

18. Once reading is complete, hold the CTRL key on the keyboard, and use the mouse to click once on each of the squares corresponding to a well that had sample in it. Once all the desired wells have been highlighted by a black square (up to a maximum of 8 wells), let go of the CTRL key and a large graph will appear with lines on it representing each sample.

19. To obtain the rate of change of absorbance over different time periods, select Options and enter the amount of time for which you would like a rate of change of absorbance to be calculated. The graph, along with one rate (at whichever time interval is selected) for each sample can be printed on a single sheet of paper, and the results can be saved.

20. The delta absorbance will appear in units of mOD/min and the number given will be negative. Convert this to OD/min by dividing by 1000 and omit the negative sign in the calculation. (eg. if Mean V: -394.8 mOD/mn, then use 0.395 OD/min)

CALCULATION: CYTOX activity (μmole/min/g tissue)

$$= \frac{\text{delta absorbance/min x total volume (ml) x 80 (dilution)}}{\text{18.5 } (\mu\text{mol/ml extinction coeff.) x sample vol (ml)}}$$

Example Calculation:

30 μl of 80-fold sample extract
250 μl of Test Solution
Mean V: -284.2 mOD/mn

$$\text{COX activity} = \frac{(.284)(.280)(80)}{(18.5)(.030)}$$

= 11.5 μmol/min/g tissue

= 11.5 U/g tissue

Filename: COX ASSAY MICROPLATE

Tissue	Heart	Mixed Gastroc
Weight (mg)	5 mg	7.5 mg
Vol. for 20-fold	100 μl	150 μl
Remove, put in new Eppendorf	50 μl	75 μl
Vol. needed for 80-fold	Add 150 μl of extract. buffer	Add 225 μl of extract. buffer
Final Volume of 80-fold	200 μl	300 μl
Vol. of 80-fold per well	10 μl	30 μl

PROTOCOL: GENOTYPING MICE USING PCR

***Background*:** This protocol is designed to detect sequences in the murine genome that differ between wild-type and null animals using polymerase chain reaction amplification. PCR is a rapid, inexpensive and simple way of copying specific DNA fragments from minute quantities of source DNA material. There are basically 3 procedural steps involved in PCR:

1) Denaturation: DNA is heated to high temperature to separate the DNA double helix to single strands making them accessible to primers. During denaturation (94° C, 30sec), the DNA strands separate to form single strands.

2) Annealing: The reaction mixture is cooled down. Primers anneal to the complementary regions in the DNA template strands, and double strands are formed again between primers and complementary sequences. During annealing (60°C, 30sec) one primer binds to one DNA strand and another binds to the complementary strand. The annealing sites of the primers are chosen so that they will prime DNA synthesis in the region of interest during extension.

3) Extension: The DNA polymerase synthesizes a complementary strand. The enzyme reads the opposing strand sequence and extends the primers by adding nucleotides in the order in which they can pair. During extension (72°C, 45sec), DNA synthesis proceeds through the target region and for variable distances into the flanking region, giving rise to long fragments of variable lengths. The whole process is repeated over and over.

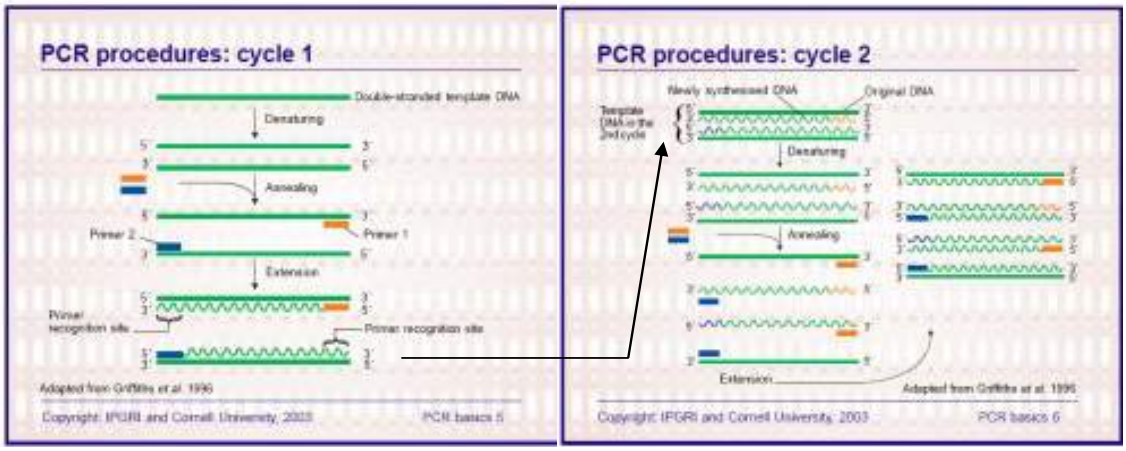

Fig.1: Schematic of basic PCR procedures.

The DNA polymerase, known as Taq polymerase, is named after the hot-spring bacterium *Thermus aquaticus* from which it was originally isolated. The enzyme can withstand the high temperature needed for DNA-strand separation. The cycle of heating and cooling is repeated over and over, stimulating the primers to bind to the original sequences and to newly synthesized sequences. The enzyme will continue to extend

primer sequences. This cycling of temperatures results in copying and then copying of copies, leading to an exponential increase in the number of copies of specific sequences. Because the amount of DNA placed in the tube at the beginning is very small, almost all the DNA at the end of the reaction cycles are copied sequences.

The reaction products are then separated by gel electrophoresis and visualized with the use of ethidium bromide.

Reagents

Lysis Buffer (pH=8.0)

10 mM Tris HCl (0.121g/100ml)
150 mM NaCl (0.8766g/100ml)
20 mM EDTA (0.744g/100ml)
Autoclave for 30min and store at room temperature.

Supermix

Sigma Jumpstart REDtaq Ready Mix PCR Reaction Mix (P0982)
Product contains 20 mM Tris-HCl, pH 8.3, 100mM KCl, 4 mM MgCl2, 0.002% gelatin, 0.4 mM each dNTP (dATP, dCTP, dGTP, TTP), inert dye, stabilizers, 0.06 unit/µl Taq DNA polymerase, JumpStart Taq antibody.

Primers

Forward and Reverse for WT and Null Stock Concentration 500 pmol/µl
Working Concentration of Primers (10X dilution): 50 pmol/ul
To make up 50 pmol/µl: use 5 µl of 500 pmol/µl stock and add 45µl of sterile water

Proteinase K
ProK- concentration of 1mg/ml

Reagents for Agarose Gel Electrophoresis of PCR product

Agarose
50 X TAE
1X TAE (dilute 50X TAE with stH_2O)
10mg/ml EtBr
Sterile water

50XTAE
242 g TRIS
500ml dH_2O
100ml 0.5M EDTA (pH 8.0)
57.1ml Glacial Acetic Acid
Make up to 1L and autoclave

DNA EXTRACTION FROM EAR CLIPPINGS

1. Make **(fresh)** 10:1 mixture of lysis buffer to ProK (@concentration of 1mg/ml-**fresh**)
2. Add 20 µl of this mixture to a 1.5 ml sterile eppendorf tube.
3. Obtain ear clipping from animal, add to tube and vortex (ensure ear clipping is immersed in solution).
4. Incubate in a 55 °C water bath (no higher than 60 °C) for 30min, vortexing every 15 minutes.
5. Add 180 µl sterile distilled water.
6. Place in boiling water for 5 minutes (use hot plate) and then vortex.
7. Store at -20°C, or use immediately for PCR

PCR method

1. Make mastermix for each of the primers you will be using.
   Mastermix contains: 25 µl of Supermix sample
   1 µl of Forward Primer per sample
   1 µl of Reverse Primer per sample
   Enough sterile distilled water for a volume per sample of 50 µl.

2. For each sample use 48 µl of mastermix and 2 µl of template DNA extracted from procedure described above. Add 1 drop of mineral oil to each PCR tube to prevent evaporation of sample during cycling.

3. Cycling times:	Initial Denaturation	94°C	2min
	35 cycles: Denaturation	94°C	30sec
	Annealing	60°C	30sec
	Extension	72°C	45sec
	Final Extension	72°C	5min
	Hold	4°C	

Running PCR product on gel

1. Loading buffer is already included in Supermix.

2. Preparation of a 1.2% agarose gel. ***For large gel system***: 3.6g Agarose, 6 ml 50X TAE and volumed up to 300 ml with sterile H_2O. Mix solution and note weight followed by boiling in microwave. Remove periodically to mix during boiling procedure in microwave. Upon complete dissolving of agarose and a homogenous and releatively clear agarose solution, weigh solution and replace lost amount of evaporated H_2O. Add 25µl of EtBr (10mg/ml), slightly cool solution in room temperature (5-10min), then pour into caster.
For small gel system: 1.92g Agarose, 3.2 ml 50X TAE, and 156.8ml st H_2O; follow same procedure as noted above. Only add 8 µl of EtBr (10mg/ml).

Electrophoresis Running Buffer: 1X TAE: 40 ml of 50X TAE made up to 2L with H_2O.

3. Run 10 µl of PCR product reaction on either a small or large 1.2% agarose gel for 1hr @ approximately 90V.

Example of Experimental Setup/Procedure for PCR Genotyping (15 mice)

1. Make up mastermix for both wild-type and null primers for the number of animals required for genotyping.

Mastermix(proportions)

A) WT Mastermix

25µl Supermix
1µl Forward Primer WT
1µl Reverse Primer WT
23µl Sterile Water
50µl Total

B) Null Mastermix

25µl Supermix
1µl Forward Primer Null
1µl Reverse Primer Null
23µl Sterile Water
50µl Total

X 17 reactions (over estimate, since 15 animals required)

Total Mastermix

A) WT Mastermix

425µl Supermix
17µl Forward Primer WT
17µl Reverse Primer WT
391µl Sterile Water
850µl Total

B) Null Mastermix

425µl Supermix
17µl Forward Primer Null
17µl Reverse Primer Null
391µl Sterile Water
850µl Total

1. Label PCR tubes with 1N and 1W to represent each animal and each mastermix, respectively.

2. Place 48 µl of null mastermix in PCR tubes with N designation and 48 µl of wild-type mastermix in PCR tubes with W designation.

3. Add 2µl of DNA template from animals into the appropriate PCR tubes i.e. DNA isolated from animal #1 into 1 N and 1W.

4. Include negative controls using dH_2O instead of DNA template with both Null and wild-type mastermix i.e. 2 µl of dH_2O into PCR tubes with 48 µl of WT mastermix and 2 µl of dH_2O into PCR tubes with 48 µl of Null mastermix.

5. Add 1 drop of mineral oil to each tube and place tubes into thermocycler for 35 cycles. Use file # 29 on thermocycler for the initial 2 min denaturation then STOP this program. Use file # 30 for repeated cycles. Scroll through the settings in File # 29 and change the settings to achieve:

Denaturation	94°C	30sec
Annealing	60°C	30sec
Extension	72 °C	45sec

Then link this file (#29) to file #33 which is the final extension of 72°C for 10min (protocol states 5min but 10min does not make a difference). This will be followed by a hold cycle at 4°C. Samples can be left holding overnight if necessary.

6. Prepare either large gel or small gel or both depending on number of samples. Load PCR products onto gel and run for 1-1.5 hours.

7. Visualize PCR products using UV lightbox in the molecular core facility. Null PCR product should be about 600bp whereas WT PCR product will be about 300bp. If animal #1 displays a band for both the Null and the WT, the animal is a **heterozygote**. If animal #1 exhibits only a Null band but no WT band then the animal is a **homozygous null**. If the animal displays a wild-type but no Null band then the animal is **homozygous wild-type.**

Fig.2: Typical agarose gel displaying PCR products and animal genotypes.

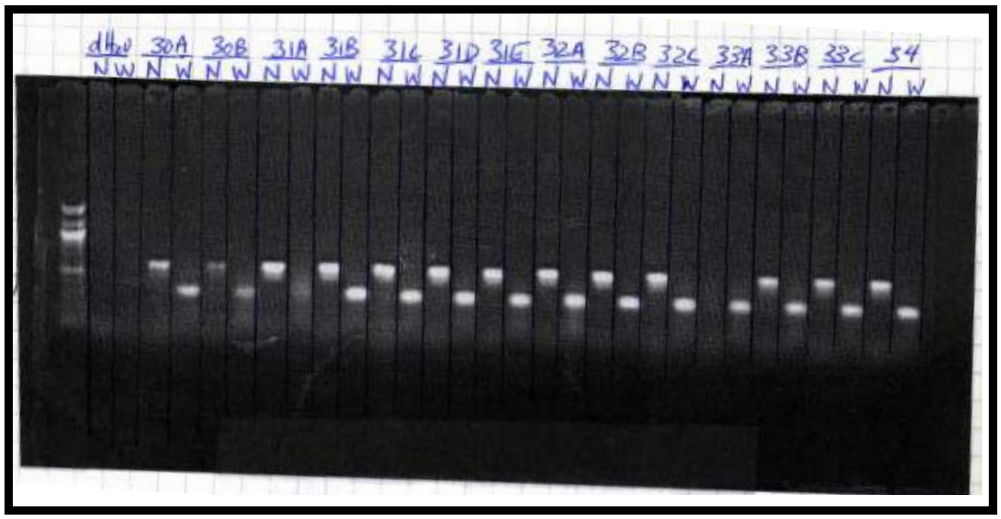

Genotype

30A-hetero	31E-hetero	33C-hetero
30B-hetero	32A-hetero	34-hetero
31A-null	32B-hetero	
31B-hetero	32C-hetero	
31C-hetero	33A-wild-type	

IN SITU STIMULATION

Animals are anesthetized (60 mg/kg) and prepared for in situ stimulation according to the following procedure:

A. Surgical Preparation:

Hindlimb Muscles

1. The right hindlimb was skinned, and prepared for electrical stimulation.

2. A hole is made with forceps under the achilles tendon. This is used to start the incision for the removal of the hamstring muscles medially and laterally. Vessels are cauterized to prevent blood loss.

3. The sciatic nerve is carefully isolated to prevent irritation. It is tied off and cut proximally, leaving a nerve stump 2-3 cm long for stimulation.

4. A string is tied around the achilles tendon through the hole (step 2) and used to secure a pin attaching the cut achilles (and thus the gastrocnemius-plantaris-soleus muscle group) to a strain gauge.

B. Stimulation:

1. The animal is placed ventral side down in the in situ preparation with the stabilization pin positioned in a brass block, and the achilles tendon attached to the strain gauge via the metal pin.

2. Body temperature is maintained using a heating pad. Muscle temperature is maintained at 37^{o}C with a heat lamp, and monitored with a surface thermometer (Yellow Springs Instrument Co., Inc. Ohio). The muscle belly is covered with Saran wrap over the temperature probe to prevent tissue dehydration. It is periodically squirted with 0.9% NaCl.

3. The appropriate resting tension of the muscle is established by generating a length-tension curve.

4. The voltage required to produce maximum tension can be determined with either indirect nerve stimulation or direct muscle stimulation. Muscles are stimulated directly with platinum wire electrodes inserted parallel to the long axis of muscle fibers, or indirectly by attaching the nerve to the coiled platinum electrodes being careful not to stretch it.

5. The time to peak tension and 1/2 relaxation time can be determined from single twitches, elicited using supramaximal voltage.

6. Muscle endurance performance is evaluated using continuous stimulation of the muscle over 5-15 minutes at, for example, 1 Hz stimulation frequency, using supramaximal voltage and 0.1 ms duration.

7. Gastrocnemius muscle can then be removed and freeze clamped for biochemical analysis.

MITOCHONDRIAL ISOLATION FROM SKELETAL MUSCLE

References: Cogswell et al. Am J Physiol, 1993, 264: C388-C389
Krieger et al. J Appl Physiol, 1980, 48: 23-28

Reagents
All buffers are set to pH 7.4 and stored at 4 °C

- Buffer 1
  100 mM KCl
  5 mM MgSO4
  5 mM EDTA
  50 mM Tris base

- Buffer 1 + ATP
  Add 1 mM ATP to Buffer 1

- Buffer 2
  100 mM KCl
  5 mM MgSO4
  5 mM EGTA
  50 mM Tris base
  1 mM ATP

- Resuspension medium
  100 mM KCl
  10 mM MOPS
  0.2% BSA

- Nagarse protease (Sigma, P-4789)
  10 mg/ml in Buffer 2
  Make fresh for each isolation, keep on ice

Procedure

1. Remove the tibialis anterior (TA) muscle from the rat, and put it in a beaker containing 5 ml Buffer 1, on ice immediately.
2. Place TA on a watch glass that is also on ice and trim away fat and connective tissue. Proceed to thoroughly mince the muscle sample with forceps and scissors, until no large pieces are remaining.
3. Place the minced tissue in a plastic centrifuge tube and record the exact weight of tissue.
4. Add a 10-fold dilution of Buffer 1 + ATP to the tube.

5. Homogenize the samples using the Ultra-Turrax polytron with 40% power output and 10 s exposure time. Rinse the shaft with 0.5 ml of Buffer 1 + ATP to help minimize sample loss.
6. Using a Beckman JA 25.50 rotor, spin the homogenate at a centrifuge setting of 800 g for 10 min. This step divides the IMF and SS mitochondrial subfractions. The supernate will contain the SS mitochondria and the pellet will contain the IMF mitochondria.

SS mitochondrial isolation:

7. Filter the supernate through a single layer of cheesecloth into a second set of 50 ml plastic centrifuge tubes.
8. Spin tubes at 9000 g for 10 min. Upon completion of the spin discard the supernate and gently resuspend the pellet in 3.5 ml of Buffer 1 + ATP. Since the mitochondria are easily damaged, it is important that the resuspension of the pellet is done carefully.
9. Repeat the centifugation of the previous step (9000 g for 10 min) and discard the supernate.
10. Resuspend the pellet in 200 µl of Resuspension medium, being gentle so as to prevent damage to the SS mitochondria. Some extra time is needed during this final resuspension to ensure the SS pellet is completely resuspended.
11. Keep the SS samples on ice while proceeding to islolate the IMF subfraction.

IMF mitochondrial isolation:

7. Gently resuspend the pellet (from step 6) in a 10-fold dilution of Buffer 1 + ATP using a teflon pestle.
8. Using the Ultra-Turrax polytron set at 40% power output, polytron the resuspended pellet for 10 s. Rinse the shaft with 0.5 ml of Buffer 1 + ATP.
9. Spin at 800 g for 10 min and discard the resulting supernate.
10. Resuspend the pellet in a 10-fold dilution of Buffer 2 using a teflon pestle.
11. Add the appropriate amount of nagarse. The calculation for the appropriate volume is 0.025 ml/g of tissue. Mix gently and let stand exactly 5 min.
12. Dilute the nagarse by adding 20 ml of Buffer 2.
13. Spin the diluted samples at 5000 g for 5 min and discard the resulting supernate.
14. Resuspend the pellet in a 10-fold dilution of Buffer 2. Gentle resuspension is with a teflon pestle.
15. Spin the samples at 800 g for 10 min. Upon the completion of the spin, the supernate is poured into another set of 50 ml plastic tubes (on ice), and the pellet is discarded.
16. Spin the supernate at 9000 g for 10 min. The supernate is discarded and the pellet is resuspended in 3.5 ml of Buffer 2.
17. Spin samples at 9000 g for 10 min and discard the supernate.
18. Gently resuspend the pellet in 300 µl of Resuspension medium.

Background: Mitochondria are the primary source of reactive oxygen species (ROS) to the cell. It is estimated that about 2% of total cellular oxygen is converted ROS by the inappropriate reduction of molecular oxygen by intermediate members of the electron transport chain (ETC). ROS are damaging molecules that are capable of compromising

the integrity of macromolecules within the mitochondria and may lead to overall organelle dysfunction. In particular, mtDNA may be prone to attack by ROS because 1) mtDNA is located in close proximity to the ETC, 2) mtDNA lacks the protective sheath of histones compared to nuclear DNA and, 3) mitochondria have an insufficient repair system for mtDNA mutations. ROS can exist in a variety of molecular permutations such as superoxide (O_2^-), hydroxyl radical (OH^-) and hydrogen peroxide (H_2O_2).

DCF (2,7,-dichloro-fluorescein; Fig.1) is a reagent that is non-fluorescent until the acetate groups are removed by intracellular esterases and oxidation occurs within the mitochondria (Fig.1). DCF is oxidized by all of the different forms of ROS and this can be detected by monitoring the increase in fluorescence with a fluorometric plate reader. The appropriate plate reader filter settings for fluorescein are the following: **Excitation 485/20 and Emission 528/20** (Fig.2).

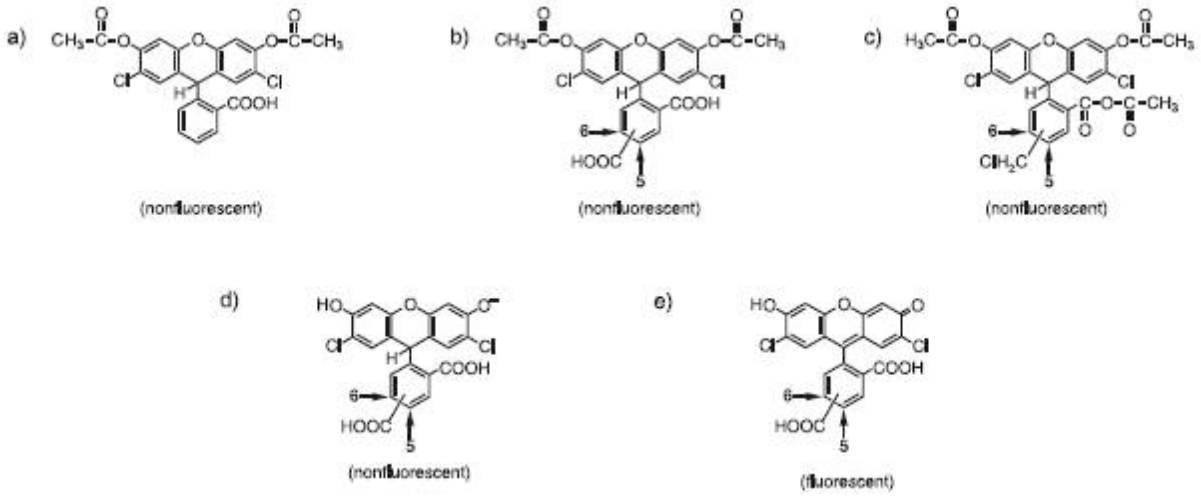

Fig.1-DCF molecule and oxidation of DCF resulting in fluorescence

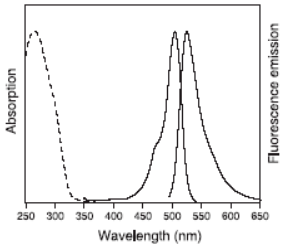

Figure 1. Absorption spectrum of reduced dye (---) and absorption/emission spectra of oxidized dye (—).

Fig.2-Absorption and Emission Spectra of oxidized dye \

KC4 Software Settings: The Settings icon in the upper left corner allows the alteration of various parameters. Once clicked, another window appears, click on the Wizard Icon. In this window there will be a variety of components that can be altered. The following are the parameters that need to be changed in order to utilize the DCF and measure time-dependent ROS production from isolated mitochondria:

1) Top Middle Panel- Absorbance, Fluorescence, Luminescence- choose **Fluorescence**
2) Top Left Panel- End Point, Kinetic, Spectrum- choose **Kinetic**
3) Top Middle Panel- Click on larger box labeled Kinetic to set parameters- **Run Time 1:20:00, Interval 5:00 (takes a measure every 5 minutes),** click on box labeled **Allow Well Zoom during Read,** and also click on box labeled **Individual Well Auto Scaling**- The Well Zoom and Auto scaling allows for monitoring each individual well during the experiment and scales it appropriately.
4) Middle Panel-***Filter Set***- Choose #1, then set the **excitation to 485/20**, and **emission to 528/20** as described above. The optics position should be set to the **TOP** (i.e. readings are taken from the top of the well) and the sensitivity is set at **50** (depending upon the amount and/or nature of the sample).
5) Plate-Type-choose **96-well plate**, choose which wells are to be read i.e. **A1-C12.**
6) Shaking-**Intensity** set at **1, Duration** set at **15s** and then click the box that is labeled **before every reading** (it shakes the samples for 15 s before every reading).
7) Temperature Control- Click on the box indicating **YES ,** also click on box labeled pre-heating, and put 37°C into the temperature box.

DCF Reagent and VO_2 Buffer

DCF (2,7,-dichlorodihydrofluorescein diacetate) reagent MW=487.29 (Molecular Probes D-399/ 100mg)

1°STOCK- Make up **50mM** Stock Solution in EtOH- 24 mg/ml- only make about 500ul i.e. 14 mg per 500ul EtOH. Wrap stock solution in aluminum foil and limit exposure to light since DCF is light-sensitive.

Working Stock Solution-2° STOCK- Dilute 50mM by 100-fold by taking 10ul and adding 990 ul of EtOH to attain a **500uM DCF Stock Solution**. This will be the DCF concentration used to add to the reaction mixture.

VO_2 Buffer- refer to mitochondrial respiration protocol

Procedure

1. SS and IMF mitochondria are isolated as described in the mitochondrial isolation protocol. Alternatively, frozen mitochondrial extracts can also be used.

2. Determine the volume necessary for 50ug of mitochondria. Typical volumes should range between 5-40ul depending upon concentration of mitochondrial extracts.

3. Final concentration of DCF is 50uM. The total volume of the reaction mixture is 250ul. Thus, 25ul of DCF is used in the reaction mixture since this represents a 10-fold dilution. Set up table (***as shown below***) and determine the amount of VO_2 buffer necessary to make each of the reaction mixtures equal to 250 ul. (Remember to include a ***control*** with only VO2 buffer and DCF reagent as in Well #1 shown below)

	SS			
	Control	Mar.23	Mar.25	Mar.29
	Well #1	Well #2	Well #3	Well #4
ug mito	0	50	50	50
ul mito	0.00	11.77	9.80	17.24
VO2 Buff	225.00	213.23	215.20	207.76
DCF (50uM)	25	25	25	25
Total Volume	250	250	250	250

4. Once table is complete and volumes for all samples have been determined, place the frozen (already thawed) or fresh mitochondria, VO_2 buffer and DCF (500uM) into a 37°C circulating water bath for 5-10 min.

5. Pipette the volume of VO_2 buffer required for each of the samples followed by the mitochondrial samples into the appropriate wells of a 96-well plate. In addition, include a well (usually in the corner well) with only 250 ul of VO_2 buffer to monitor temperature (see below). Place the 96-well plate with the VO_2 buffer and mitochondria into a 37°C incubator. Using the YSI temperature probe, place the recording electrode into the well with buffer only and monitor the temperature until 37°C is reached. During this time, be sure that the KC4 software is set up and that the Biotek plate reader is pre-heating to 37°C.

6. Once mitochondria and buffer have reached temperature (37°C), take the DCF out of the circulating water bath (37°C) and quickly add the DCF to each of the reaction mixtures. Following addition of DCF, promptly place the plate into the Biotek plate reader for fluorescence measurement and start the KC4 program by pressing **READ** plate on the upper left portion of the computer screen. Kinetic program will operate for 1 h and 20 min.

IN VIVO TREADMILL RUN

DAY 1: Acclimatize

1. Place the mice on the treadmill and allow them to sit idle for 5 minutes. Also ensure that the treadmill is set to a 10% incline.
2. Adjust the speed to 5m/min for 5 minutes
3. Stop the treadmill and place the mice back in their respective cages

DAY 2: Acclimate

1. If lactate is required, collect blood samples prior to beginning the second day of treadmill acclimatization.

2. Place the mice on the treadmill and allow them to sit idle for 5 minutes
3. Adjust the speed to 5m/min for 5 minutes, followed by 10m/min for 10 minutes
4. Stop the treadmill and place the mice back in their respective cages

DAY 3: Exhaustive Run

1. Exhaustive run is outlined as follows:

DAY 1	DAY 2	DAY 3
5 min at 0m/min	5 min at 0m/min	5 min at 0m/min
5 min at 5m/min	5 min at 5m/min	5 min at 5m/min
	10 min at 10m/min	10 min at 10m/min
		15 min at 15m/min
		20 min at 20m/min
		2m/min every 2 minutes until exhaustion

NRF2 ACTIVATION ASSAY

Company: Active Motif, Carlsbad, CA, USA
Product: Trans AM Nrf2
Cat #: 50296

Note: All buffers and reagents are provided and prepared according to the manufacturers protocol. Adapted protocol is listed below--

---

Step 1: Binding of Nrf2 to its consensus sequence

1. Add 40µl complete binding buffer to each well to be used
2. **Sample wells:** Add 10µl of sample diluted in complete lysis buffer per well. Manufacturer recommends using 5-20µg of nuclear extract diluted in complete lysis buffer per well
3. **Positive control wells:** Add 5µg of the provided positive control extract diluted in 10µl of complete lysis buffer per well (2µl of control extract in 8µl of complete lysis buffer per well)
4. **Blank wells:** Add 10µl complete lysis buffer only per well
5. Use the provided adhesive cover to seal the plate. Incubate for 1 hour at room temperature with mild agitation (100 rpm on a rocking platform)

6. Wash each well 3 times with 200µl 1X washing buffer. For each wash, flick the plate over a sink to empty the wells, then tap the inverted plate on absorbent paper towels

Step 2: Binding of primary antibody

1. Add 100µl of diluted Nrf2 antibody (1:1000 dilution in 1X antibody binding buffer) to each well being used
2. Cover the plate and incubate for 1 hour at room temp. without agitation
3. Wash the well 3 times as described above.

Step 3: Binding of secondary antibody

1. Add 100µl of diluted HRP-conjugated antibody (1:1000 dilution in 1X antibody binding buffer) to all wells being used
2. Cover the plate and incubate for 1 hour at room temperature without agitation
3. During this incubation, place the developing solution at room temperature
4. Wash the wells 4 times as described above.

Step 4: Colorimetric reaction

1. Add 100µl developing solution to all wells being used
2. Incubate 2-15 minutes at room temperature protected from direct light. Monitor the blue colour development in the sample and positive control wells until it turns medium to dark blue. Do not overdevelop.
3. Add 100 µl stop solution. In presence of the acid, the blue colour turns yellow.
4. Read absorbance on a spectrophotometer within 5 minutes at 450nm with a reference wavelength of 655nm.

References

1. Pi, J. et al. (2007) *Free Radical Biol Med* 42(12): 1797-1806.
2. Lee, O-H, et al. (2007) *J Biol Chem* 282(50): 36412-36420
3. Theodore, M. et al. (2008) *J Biol Chem* 283(14): 8984-8994
4. Kobayashi, A., et al. (2006) *Mol Cell Biol* 26(1): 221-229.

SDS POLYACRYLAMIDE GEL ELECTROPHORESIS (SDS-PAGE)
PROTEAN BIO-RAD SYSTEM

Reagents

1. Acrylamide/Bis-Acrylamide, 30% Solution 37.5:1 (BioShop 10.502)
    a. Store at 4°C
2. Under Tris Buffer
    a. 1M Tris-HCl, pH 8.8 (60.5g/500ml)
    b. Store at 4°C
3. Over Tris Buffer
    a. 1M Tris-HCl, pH 6.8 (12.1g/100ml)
    b. Bromophenol Blue (for colour)
    c. Store at 4°C
4. Ammonium Persulfate (APS)
    a. 10% (w/v) APS in ddH_20 (1g/10ml)
    b. Stored at 4°C
5. Sodium Dodecyl Sulfate (SDS)
    a. 10% (w/v) in ddH_20 (1g/10ml)
    b. Store at room temperature
6. TEMED (Sigma T-9281)
7. Electrophoresis Buffer, pH 8.3 (10L)
    a. 25mM Tris 30.34g, 192mM Glycine 144g, 0.1% SDS 10g
    b. Volume to 10L with ddH_20
    c. Store at room temperature
8. 6X SDS
    a. Warm 100% glycerol in water bath at 65°C for 30 minutes
    b. Combine 1.2g SDS, 0.06g Bromophenol Blue, 3mls of 1M Tris, pH 6.8 and 1ml of ddH_20 and stir at 4°C for 5 minutes
    c. Add 3mls of 100% glycerol, stir and aliquot mixture.
    d. Store at -20°C
    e. Add 5% (v/v) ß-mercaptoethanol (Sigma M6250) to 6X SDS <u>just prior</u> to use
9. *tert*-Amyl alcohol ReagentPLus, 99% (Sigma 152463)

Procedure

1. **Prepare electrophoresis rack:**
    a. Clean glass plates thoroughly with soap followed by 95% ethanol then ddH_20.
    b. Dry carefully with a kimwipe.
    c. Assemble glass plates as shown below:

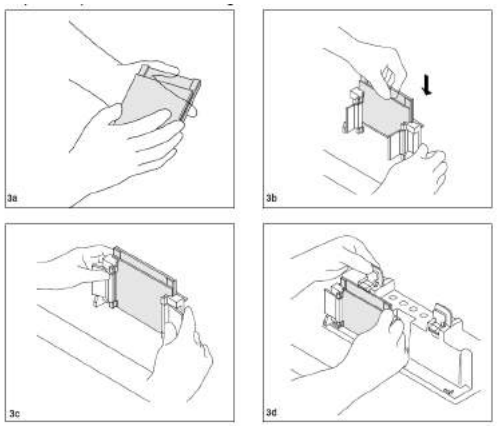

d. Check the seal y adding a small volume of ddH_20 then pour off and let dry.

2. **Prepare separating gels:**
   a. Mini Protean 3 Bio-Rad System volumes:

	8%	**10%**	**12%**	**15%**	**18%**
Acrylamide	2.7 ml	3.3 ml	4.0 ml	5.0 ml	6.0 ml
ddH_20	4.1 ml	3.5 ml	2.8 ml	1.8 ml	0.8 ml
Under Tris	3.0 ml	3.0 ml	3.0 ml	3.0 ml	3.0 ml
SDS	100µl	100µl	100µl	100µl	100µl
APS	100µl	100µl	100µl	100µl	100µl
TEMED	10µl	10µl	10µl	10µl	10µl

   b. Mix the contents of the separating gel without adding APS or TEMED. Stir.
   c. Add APS and TEMED. Stir.
   d. Slowly pour the entire volume of the solution into the space between the two plates while keeping plates tilted to prevent bubble formation.
   e. Add *tert*-Amyl alcohol to coat top surface of gel solution.
   f. Allow 30 minutes for gel polymerization.
   g. Remove *tert*-Amyl alcohol by pouring it off and remove any remainder with a kimwipe. Rinse with ddH_20.

3. **Prepare stacking gel:**
   a. For a single mini gel use the following volumes:

Acrylamide	500 µl
Over Tris	625 µl
ddH_20	3.75 ml
SDS	50 µl
APS	50 µl
TEMED	7.5 µl

   b. Mix the contents of the stacking gel without adding APS or TEMED. Stir.

c. Add APS and TEMED. Stir.
d. Using a Pasteur pipette slowly add the entire volume from the beaker in between the plates.
e. Add comb for desired number of wells.
f. Allow 30 minutes for gel polymerization.

4. Prepare samples:

a. Turn of the block heater to 95ºC.
b. Pipette required volume of sample into new eppendorf with 6X SDS (1 volume of sample to 1/6 sample volume of 6X SDS). Keep samples on ice until all samples are prepared.
c. Briefly spin each sample to bring volume to the bottom of the eppendorf.
d. Incubate each sample at 95 ºC for 5 minutes in the heating block to denature the proteins.
e. Briefly spin again to return volume to the bottom of the eppendorf.

5. Assemble Mini-PROTEAN gel caster system:

a. See images below:

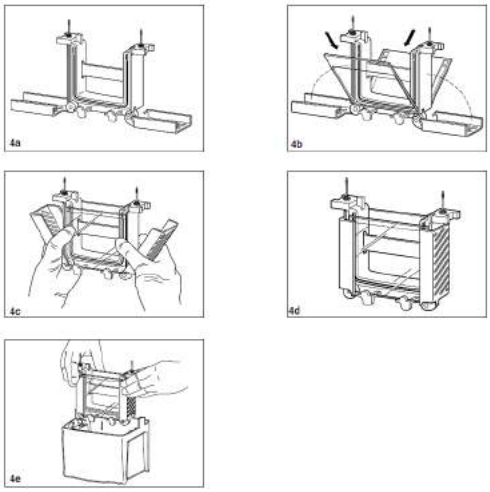

b. If you are only running one gel a plastic rectangular pseudo plate must be clamped on the other side of the caster.
c. Fill with electrophoresis buffer between the plates and outside of the plates in the chamber.
d. Slowly remove the comb using both hands (one on each side) by pulling the comb straight upwards.
e. Fix any wells that are deformed using a small spatula.
f. Clean out the wells using a syringe filled with electrophoresis buffer.
g. Withdraw the entire volume of the sample using a Hamilton syringe. Inject volume slowly into the bottom of the well.

6. Gel electrophoresis

a. Immediately after all samples are loaded place the lid on the gel chamber.

b. Place positive and negative plugs into the power supply and turn on power supply.
c. Set power supply to 120V. Gel will run for ~2 hours depending on percent gel made.
d. When the bromophenol blue has run off the bottom of the gel turn off the power supply. Remove plugs from power supply and remove lid.
e. Prepare for electrotransfer of proteins from the gel to nitrocellulose membrane.

WESTERN BLOTTING AND IMMUNODETECTION

Reagents

1. Transfer Buffer
    a. 0.025M Tris-HCl pH 8.3 12.14g
    b. 0.15M Glycine 45.05g
    c. 20% Methanol 800ml
    d. make up to 4L with ddH_20
    e. store at 4°C
2. Ponceau S stain
    a. 0.1% (w/v) Ponceau S
    b. 0.5% (v/v) Acetic Acid
    c. Store at room temperature
3. Wash Buffer
    a. Tris-HCl pH 7.5 12g
    b. NaCl 58.5g
    c. 0.1% Tween 10ml
    d. Store at room temperature
4. Blocking Solution
    a. 5% (w/v) skim milk power in wash buffer OR
    b. 5% (w/v) BSA in wash buffer
5. Enhanced Chemiluminescence Fluid (ECL; Santa Cruz sc-2048)
6. Film/Developer/Fixer

Procedure

1. Transfer Procedure
    a. Remove electrophoresis plates from chamber and separate the plates.
    b. Cut away unnecessary parts of the gel using a spatula and measure remaining gel size.
    c. Using a paper cutter cut 6 pieces of Whatman paper per gel to the same size as the gel. Wearing gloves cut nitrocellulose membrane (GE Healthcare RPN303D) to the dimensions of the gel.

d. Assemble Whatman paper, nitrocellulose memebrane and gel as shown below:

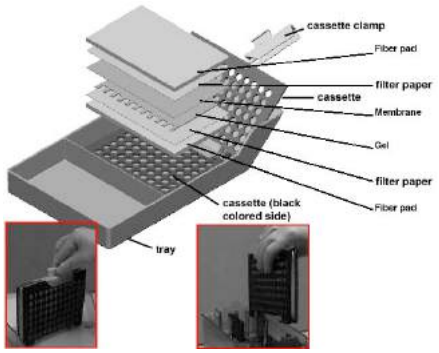

e. Close the cassette and place in the transfer chamber with the black side of the cassette facing the back side of the chamber.
f. Place ice pack in the chamber.
g. Place lid on the chamber and connect the leads to the power supply.
h. Turn on the power supply and run at 120V for 2 hours. This can vary depending on the size of the protein of interest.

2. Removal of transfer membrane:

a. Turn off the power supply and disconnect leads from the power supply then remove the lid from the chamber.
b. Remove the cassette from the chamber.
c. With gloves on, remove the Whatman paper and gel and place the nitrocellulose membrane in a plastic dish.
d. Add Ponceau S stain on the membrane and gently swirl.
e. Drain off the remaining Ponceau S and save for reuse.
f. Rinse the membrane with ddH_20 to reduce the red background. Wrap membrane in saran wrap and scan image.
g. Cut the membrane while protein bands are still visible at the desired molecular weight.
h. Rotate membrane at room temperature in wash buffer until remaining Ponceau S has been removed.
i. Incubate membrane for 1 hour with rotation in blocking solution.
j. Incubate membrane with desired antibody diluted in blocking solution overnight at 4ºC. Membrane is placed face down into the solution on a glass plate covered in parafilm. To maintain a moist environment overnight, wet a small kimwipe and form it into a ball and place in each corner of the dish. Cover the dish with saran wrap.

3. Immunodetection

a. Wash the blots in wash buffer with gentle rotation for 5 minutes 3X.
b. Incubate the blots for 1-2 hours with the appropriate secondary antibody diluted in blocking solution.
c. Membrane is placed face down in solution on a glass plate covered with parafilm. Place moist kimwipes in each corner of the dish and cover the dish with saran wrap.
d. Following the incubation, wash the membrane 3X for 5 minutes with wash buffer.

4. **Enhanced Chemiluminescence Detection**
    a. Mix ECl fluids “A” and “B” in a 1:1 ratio in a disposable Rohr tube.
    b. Place blots on saran wrap face up and apply ECL solution for 2 minutes.
    c. Dab off excess ECL on a kimwipe and place blots face down on a fresh piece of saran wrap and wrap tightly.
    d. Expose blot to film (time will vary depending on protein and antibody).
    e. Place film into developer (time will vary).
    f. Once image appears place film into fixer for 2 minutes. Wash with fresh water when complete.

Appendix D – Other Contributions to the Literature

Other Contributions to the Literature

Published refereed papers

1. Tryon LD, **Crilly MJ**, Hood DA. Effect of denervation on the regulation of mitochondrial transcription factor A expression in skeletal muscle. *Am J Physiol Cell Physiol.* 309(4): C228-38, 2015.
2. Tryon L, Vainshtein A, Memme JM, **Crilly MJ**, Hood DA. Recent advances in mitochondrial turnover during chronic muscle disuse. *Integrative Medicine Research*. 3(4): 161-171, 2014.

Contribution to book chapter

1. Hood DA, Tryon LD, Vainshtein A, Memme JM, Chen CW, Pauly M, **Crilly MJ**, Carter H. Exercise and the regulation of mitochondrial turnover. *Prog Mol Biol Transl Sci.* 135 (chapter 5): 99-127.

Review paper (in preparation)

1. Erlich AT, Tryon D, **Crilly MJ**, Memme JM, Moosavi Z, Oliveira A, Beyfuss K, Hood DA. Function of specialized regulatory proteins and signaling pathways in exercise-induced muscle mitochondrial biogenesis. *Integrative Medicine Research* [unpublished].

Conference Proceedings and Presentations:

1. **Crilly MJ**, Hood DA. The role of Nrf2 in the maintenance of mitochondrial content and running performance. Poster and abstract. (CSEP Annual Meeting, 2015, Hamilton, Ontario).
2. **Crilly MJ,** Hood DA. The influence of the Nrf2-Keap1 pathway on skeletal muscle and mitochondrial function. Poster and abstract. (MHAD, 2015, Toronto, Ontario)
3. **Crilly MJ,** Hood DA. The role of Nrf2 in muscle phenotype and mitochondrial function. Poster and abstract. (Experimental Biology, 2015, Boston, MA)
4. Tryon L, **Crilly MJ**, Hood DA. Mitochondrial transcription factor A regulation in response to rat skeletal muscle denervation. Poster and abstract. (CSEP Annual Meeting, 2014, St. Johns, Newfoundland)
5. **Crilly MJ**, Carter HN, Tryon L and Hood DA. Relationship of muscle mitochondrial content and the Keap1-Nrf2 pathway. (CSEP Annual Meeting, 2014, St. Johns, Newfoundland)
6. **Crilly MJ**, Hood DA. Role of ROS in mediating denervation-induced muscle atrophy. Oral presentation and abstract. (OEP Annual Meeting, 2014, Barrie, Ontario)
7. Carter HN, **Crilly MJ**, O'Leary MFN, Vainshtein A, Ostojic O, Hood DA. Chronic contractile activity induces a transcriptional profile to restore muscle mitochondrial homeostasis with age. Oral presentation and abstract. (CSEP Annual Meeting, 2013, Toronto, Ontario)

8. Memme JM, **Crilly MJ**, Tryon L, Iqbal S, Hood DA. Denervation-induced adapti ons in autophagy and mitochondrial morphology protiens. Poster and abstract. (MHAD, 2013, Toronto, ON)
9. **Crilly MJ**, Memme JM, Pastore SP, Hood DA. Circadian regulation of mitochon drial content in skeletal muscle. Poster and abstract. (MHAD, 2013, Toronto, ON)